X-611-69-413
PREPRINT

CONTRIBUTIONS TO THE 1969 BUDAPEST CONFERENCE ON COSMIC RAYS

BY THE

HIGH-ENERGY ASTROPHYSICS BRANCH

SEPTEMBER 1969

GSFC
GODDARD SPACE FLIGHT CENTER
GREENBELT, MARYLAND

X-611-69-413

CONTRIBUTIONS TO THE 1969 BUDAPEST CONFERENCE ON COSMIC RAYS

by the

High-Energy Astrophysics Branch

September 1969

GODDARD SPACE FLIGHT CENTER

Greenbelt, Maryland

CONTENTS

OG-18

GAMMA-RAY ASTRONOMY RESULTS AT BALLOON ALTITUDES

D. A. Kniffen, C. E. Fichtel and H. B. Ogelman*

NASA/Goddard Space Flight Center
Greenbelt, Maryland 20771 U.S.A.

Abstract:

Results of several balloon flights of a digitized gamma-ray spark chamber have failed to detect a point source of gamma-rays greater than 30 MeV. Upper limits to the fluxes emitted by possible discrete sources are presented. A scan of the galactic center region gives a line intensity of $(2.3 \pm 1.2) \times 10^{-4} \gamma (cm^2 sec\ rad)^{-1}$ above 100 MeV for galactic latitudes of -3° to +3°. Although this result does not justify a claim of a positive result, it is consistent with the OSO-III measurement of $4.1 \pm 0.7 \times 10^{-4} \gamma (cm^2 sec\ rad)^{-1}$ (1).

The intensity, energy spectrum and zenith angle dependence of the atmospheric gamma-rays were also measured. The observed downward intensity is in reasonable agreement with other measurements; however, the upward moving intensity > 100 MeV is a factor of about 3 lower than the OSO-3 result.

Preliminary results from a July 1969 balloon flight of a new 50 cm by 50 cm spark chamber gamma-ray telescope are presented. The results do not indicate a detectable line intensity in the galactic longitude interval $142.5° \leq l^{II} \leq 194.0°$ with a 95 percent confidence limit of $2.3 \times 10^{-4} \gamma (cm^2 sec\ rad)^{-1}$ for $-3° \leq b^{II} \leq 3°$ and 5.4×10^{-4}

*NAS/NASA Postdoctoral Research Associate

$\gamma(cm^2 sec\ rad)^{-1}$ for $-15° \leq b^{II} \leq 15°$ for gamma rays with energies above an estimated 100 MeV. The detector sensitivity should have been sufficient to measure the line intensity in this region at the reported OSO-III level (1) though the disagreement is only one standard deviation.

Introduction:

It has been over a decade since Morrison (3) first suggested the important astrophysical information obtainable by studying the gamma-ray emission of discrete sources. A number of more recent calculations based on later astrophysical information have better defined the fluxes and spectra which might be expected.

Based on the earlier rather optimistic flux predictions (3),(4) a number of experimental balloon investigations were undertaken (e.g. (5),(6),(7),(8),(9),(10),(11),(12). As more refined calculations yielded increasingly pessimistic predictions(13),(14),(15),(16), larger and more advanced detectors were developed (10), (18), (19), (20), (21) and satellite experiments flown (1), (22), (23) to search for the predicted diffuse gamma radiation. Though these experiments have all failed to establish the existence of a > 30 MeV discrete gamma-ray source, Clark, Garmire and Kraushaar (1) have obtained positive evidence for a diffuse galactic γ-ray line intensity which peaks in the direction of the galactic center.

In 1962, gamma-ray investigations were begun at the Goddard Space Flight Center with a nuclear emulsion experiment designed

to search for gamma-rays with energies in excess of 10 MeV (7). To improve sensitivity, and provide time discrimination, development of a digitized spark chamber detector was begun in January 1964. This detector, with a 15.2 cm x 15.2 cm active area, has been flown by balloons many times, beginning in 1966. Some of the more recent results obtained with this detector will be reported in this paper. As the need for additional sensitivity became apparent, a 50 cm x 50 cm detector was developed and flown by balloon from Palestine, Texas in July 1969.

Detector:

The discussion of the detector system will be limited to the 50 cm x 50 cm spark chamber, since the 15.2 cm x 15.2 cm detector has been described in detail elsewhere (24).

The larger detector is depicted schematically in Figure 1. Functionally, the instrument consists of the spark chamber, the triggering telescope and the support electronics.

The triggering telescope contains three basic elements; the anticoincidence plastic scintillator dome, A, surrounding the entire spark chamber, and the charged particle telescope consisting of the nine element B scintillator array and the nine element Cerenkov counter matrix. In the gamma-ray mode each element of the B array B_i is placed in coincidence with the corresponding element of the C matrix C_i, giving nine telescopes operating in the $\bar{A}\, B_i C_i$ mode. Thus this mode requires a neutral which converts into one or more charged particles within the detector volume and actuates one or

more of the nine charged particle telescopes. This logic is chosen to most efficiently accept gamma-rays converting to negatron-positron pairs within the chamber volume, while rejecting to the greatest extent possible masquerading events.

The spark chambers consist of 32 modules each with two orthogonal sets of 400 parallel wires, one set on either side of the module, with 4.0 mm separation between the planes, and 1.25 mm separation between parallel wires. Each wire threads a ferrite core and is attached to a common buss. A coincidence pulse causes high voltage to be applied across the grids, and the resultant spark current "sets" the cores threaded by the affected wires. In this manner, an x and y coordinate are obtained for each module or z level. Figure 2 represents a computer printout of a typical gamma-ray pair production event.

A stainless steel plate, 0.03 radiation lengths thick, is placed between each of the 11 modules above the central scintillator, and serves as the pair conversion target, giving a pair conversion probability of .2 at high energies. Plates with a thickness of .02 radiation lengths of stainless steel are placed between the lower 22 modules to provide information on the energy of each of the converted electrons and hence of the gamma-ray by analyzing their multiple coulomb deflections. The scattering data combined with the balloon gondola aspect data also allow a determination of the most probable

arrival direction of the gamma-ray. A more thorough discussion of the detector and support electronics is given by Ross et al. (25).

An additional feature of the coincidence system allows a test of the prediction of a very short pulse of energetic photons associated with the explosive phase of a supernova (2). A detailed discussion of this mode of the experiment is given by Fichtel and Ogelman (26).

Analysis:

The data is obtained during flight by means of a telemetry link to a ground station which records the data, together with time, accurate to milliseconds, and aspect and housekeeping data on magnetic tape. From this data, a microfilm record, as shown in Figure 2, is obtained for each event. The events are each examined and possible gamma-ray events are selected for further analysis. The coordinates of each track at each modular level are recorded and the data are reentered into the computer where the energy and arrival direction with respect to chamber coordinates are calculated for each gamma-ray. This data is merged with aspect data to obtain the celestial arrival direction.

A more detailed discussion of the analysis procedures used with the 15.2 x 15.2 cm chamber is given in a paper by Fichtel, Kniffen and Ogelman (27). The preliminary 50 cm x 50 cm chamber results reported here use similar techniques, although eventually the analysis of at least 80% of the events will be done completely by computer.

Results:

1. Discrete Sources: A number of possible discrete source objects expected to be more likely emitters of gamma-rays with energies above 30 MeV have been examined. 95% confidence limits on gamma-rays with energies in excess of 100 MeV of 4 to $6 \times 10^{-5} \gamma (cm^2 sec)^{-1}$ have been obtained for the Crab nebula, Centaurus A, the Quiet Sun, Sco XR-1 and X-1, the Galactic Center as a point source, Oph XR-1 and XR-2 and the Moon. A limit of $2.2 \times 10^{-4} \gamma (cm^2 sec)^{-1}$ was obtained for Virgo (M-87). Limits on the 30-100 MeV flux are slightly higher.

2. Diffuse Sources: Following the observation by Clark et al. (1) of a line emission of > 100 MeV gamma-rays from the galactic plane with a peak intensity from the galactic center, the data from the balloon flight which examined this region of the sky was re-examined for a possible line intensity of energetic gamma-rays.

The region examined includes the galactic longitude interval $-10° \leq l^{II} \leq 25°$. For gamma-rays with energies > 100 MeV, a line intensity of $(2.3 \pm 1.2) \times 10^{-4} \gamma (cm^2 sec\ rad)^{-1}$ is obtained for a latitude interval of $-3° \leq b^{II} \leq 3°$. While this result is consistent with no galactic line emission, it is not in disagreement with the line intensity of $(4.1 \pm 0.7) \times 10^{-4} \gamma (cm^2 sec\ rad)^{-1}$ detected on OSO-III (1). Recent results of other experimenters (19), (21), (28) also fail to provide unambiguous evidence for galactic plane emission though each of these experiments observe excess intensities at the 2σ level.

3. Albedo Intensities: In 1968, the small spark chamber was flown in an inverted position to study the intensity and energy spectrum of upward moving albedo gamma-rays. This data should be useful as a relatively constant source for calibration of satellite-borne gamma-ray detectors. Figure 3 displays the energy spectrum obtained together with the downward moving spectrum observed previously. It is apparent that the upward moving spectrum is considerably softer and more intense at the low energies.

A comparison of the > 100 MeV albedo intensity with that measured by the OSO-III experiment (1) indicates the latter to be higher by a factor of about 3.0 above the intensity of $3.7 \pm 0.8 \times 10^{-3}$ $\gamma(cm^2 sr\ sec)^{-1}$ measured in this experiment over the same angular interval. This is possibly a geometric effect due to the much higher altitude of the satellite experiment, which for the opening angle, causes it to cover a much wider range of zenith angles (angle with respect to the downward vertical). Our albedo measurements indicate the spectrum becomes harder and more intense toward the horizon, as seen from balloon altitudes. The problem is currently being studied quantitatively. It is also planned that both detectors shall be recalibrated.

4. 50 cm x 50 cm Chamber Results: On July 15, 1969, the new large spark chamber was launched on an 18 million cubic foot balloon from Palestine, Texas, in a flight timed to search for a discrete source of gamma rays from the Crab nebula and line emission from the galactic plane in the region of the anticenter. An electronic failure resulted in a premature termination of data acquisition, with about

40 percent of the expected data received; 2.5 hours of useful data were obtained at a float depth of 2.9 g/cm^2.

A preliminary analysis of the data has indicated no evidence for a line intensity of gamma-rays within the galactic longitude interval $142.5° \leq l^{II} \leq 194.0°$. The 95 percent coincidence upper limits obtained are $2.3 \times 10^{-4}\gamma(\text{cm}^2\text{sec rad})^{-1}$ for $-3° \leq b^{II} \leq 3°$ and $5.4 \times 10^{-4}\gamma(\text{cm}^2 \text{ sec rad})^{-1}$ for $-15° \leq b^{II} \leq 15°$. This result is based on an examination of unambiguous gamma-ray produced electron pair events. Though the exact energy threshold has not been determined, based on an examination of the pair opening angles and previous experience, it is estimated that these limits apply to gamma-rays with energies in excess of 100 MeV.

For comparison, it is noted that the OSO-III (1) experiment observed an average line intensity of about $1.3 \pm .2\gamma(\text{cm}^2\text{sec rad})^{-1}$ over the same longitude interval. If the line intensity is confined to $-3° \leq b^{II} \leq 3°$, this intensity should have been observable within the sensitivity of the detector, though the disagreement is only about one standard deviation. However, taken together with the two standard deviation disagreement in the galactic center region, there is mounting evidence that either (1) the calibration of one or both of the detectors is not correct (though our background intensities appear in reasonable agreement with those of other observers [27]), or (2) the line intensity extends over a wider galactic latitude interval. The angular resolution of the OSO-III detector does not allow a definite exclusion of the latter possibility, though it is not likely on theoretical grounds. As mentioned previously, a calibration is currently being planned to investigate the first possibility.

Acknowledgement:

The outstanding efforts of the Project Manager, Mr. R. W. Ross, are gratefully acknowledged. For their outstanding engineering and technical support, we are also indebted to S. R. Allison, V. P. Cogan, W. J. Cruickshank, S. M. Derdeyn, C. H. Ehrmann, L. J. Horning, A. M. Marshall, A. F. Mascaro, J. W. O'Connor and R. L. Smith, Jr. We should also like to thank Mr. H. Demboski and Cmdr. D. Sumner of the Office of Naval Research for arranging the flights, and the members of the Balloon Launch Facility of the National Center for Atmospheric Research for an excellent balloon launch.

References

1. G. W. Clark, G. P. Garmire and W. L. Kraushaar, Ap. J., 153, L203, 1968.
2. S. A. Colgate, Can. J. Phys, 46, S476, 1968.
3. P. Morrison, Il Nuovo Cimento, 7, 858, 1958.
4. M. P. Savedoff, Il Nuovo Cimento, 13, 12, 1959.
5. A. Bracessi, M. Ceccarelli and S. Salandin, Il Nuovo Cimento, 17, 691, 1960.
6. T. L. Cline, Phys. Rev. Letters, 7, 109, 1969.
7. C. E. Fichtel and D. A. Kniffen, J. Geophys. Res., 70, 4227, 1965.
8. R. Cobb, J. G. Duthie and J. Stewart, Phys. Rev. Letters, 14, 507, 1965.
9. G. M. Frye, Jr., F. Reines, and A. H. Armstrong, J. Geophys. Res., 71, 3119, 1966.
10. G. M. Frye, Jr. and L. H. Smith, Phys. Rev. Letters, 17, 733, 1966.
11. J. G. Duthie, R. Cobb, and J. Stewart, Phys. Rev. Letters, 17, 263, 1966.
12. C. E. Fichtel, T. L. Cline, C. H. Ehrmann, D. A. Kniffen and R. W. Ross, Can. J. Phys., 46, S419, 1968.
13. G. Garmire and W. L. Kraushaar, Space Sci. Rev., 4, 123, 1965.
14. V. L.Ginsburg and S. I. Syrovatskii, Soviet Phys.-Uspekhi, 7, 696, 1965.
15. R. J. Gould and G. R. Burbidge, Annales d'Astrophys., 28, 171, 1965.
16. G. C. Fazio, Annual Rev. Astron. and Astrophys., 5,(ed. L. Goldberg), 481, 1967.

17. G. M. Frye, Jr. and C. P. Wang, Can. J. Phys., 46, S448, 1968.

18. G. C. Fazio, H. F. Helmken, S. J. Cavrak, and D. R. Hearn, Can. J. Phys., 46, 1968.

19. J. P. Delvaille, P. Albats, K. I. Greisen, and H. B. Ogelman, Can. J. Phys., 46, S425, 1968.

20. T. C. May and C. J. Waddington, Ap. J., 156, 437, 1969.

21. J. V. Valdez and C. J. Waddington, Ap. J., 156, L85, 1969.

22. W. L. Kraushaar, G. W. Clark, G. Garmire, H. Helmken, P. Higbie and M. Agogino, Ap. J., 141, 845, 1965.

23. G. C. Fazio and E. M. Hafner, J. Geophys. Res., 72, 2542, 1967.

24. C. H. Ehrmann, C. E. Fichtel, D. A. Kniffen, and R. W. Ross, Nuc. Instr. and Methods, 56, 109, 1967.

25. R. W. Ross, C. H. Ehrmann, C. E. Fichtel, D. A. Kniffen, and H. B. Ogelman, IEEE Trans. Nuc. Sci., NS-16, 304, 1969.

26. C. E. Fichtel and H. B. Ogelman, NASA TND-4732, 1968.

27. C. E. Fichtel, D. A. Kniffen and H. B. Ogelman, Ap. J., 157, In press, 1969.

28. G. M. Frye, Jr. and C. P. Wang, Case-Western Reserve Preprint, 1969.

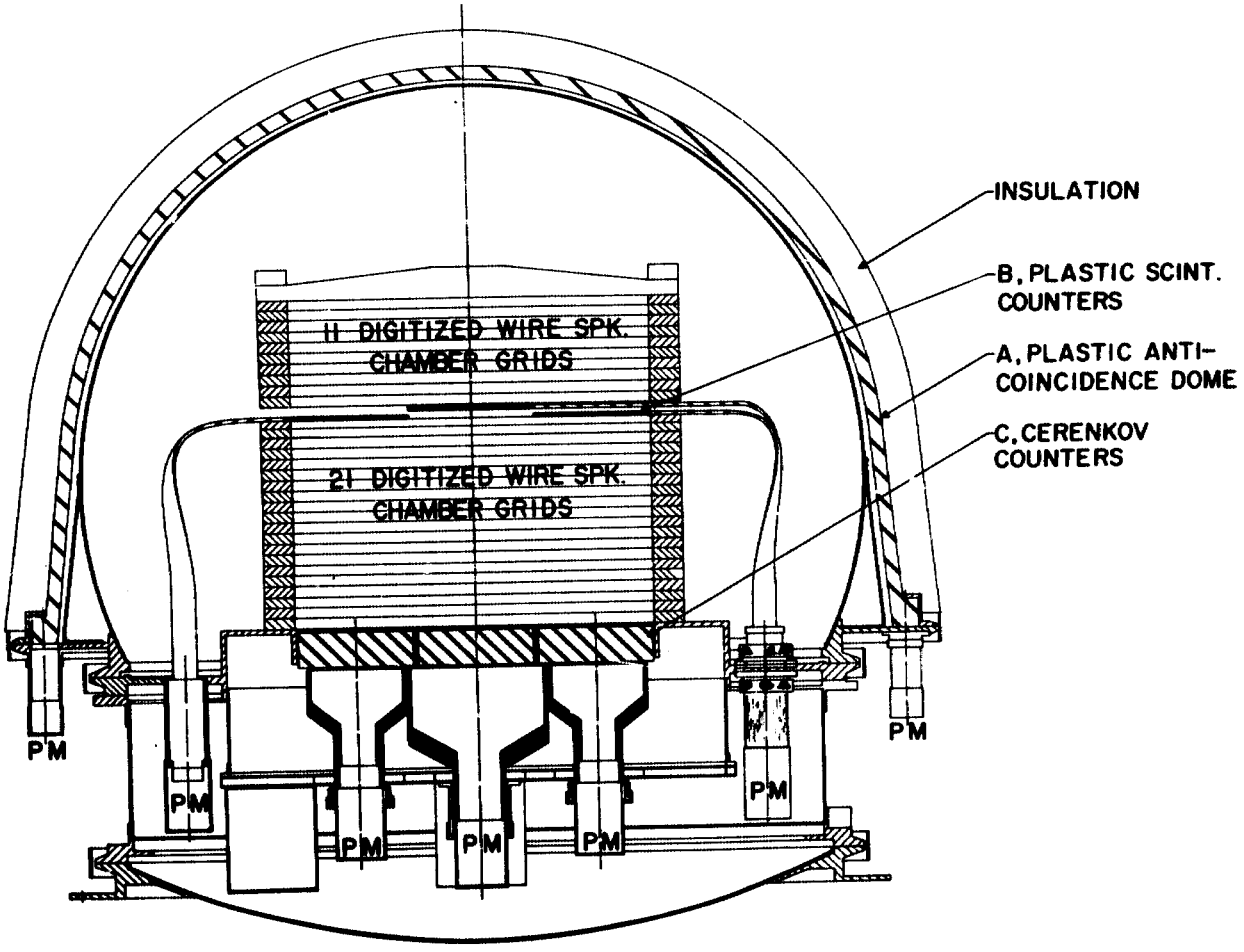

SCHEMATIC OF 1/2 x 1/2 M. DIGITIZED SPARK CHAMBER GAMMA RAY TELESCOPE

Figure 1. A schematic diagram of the 50 cm x 50 cm area detector.

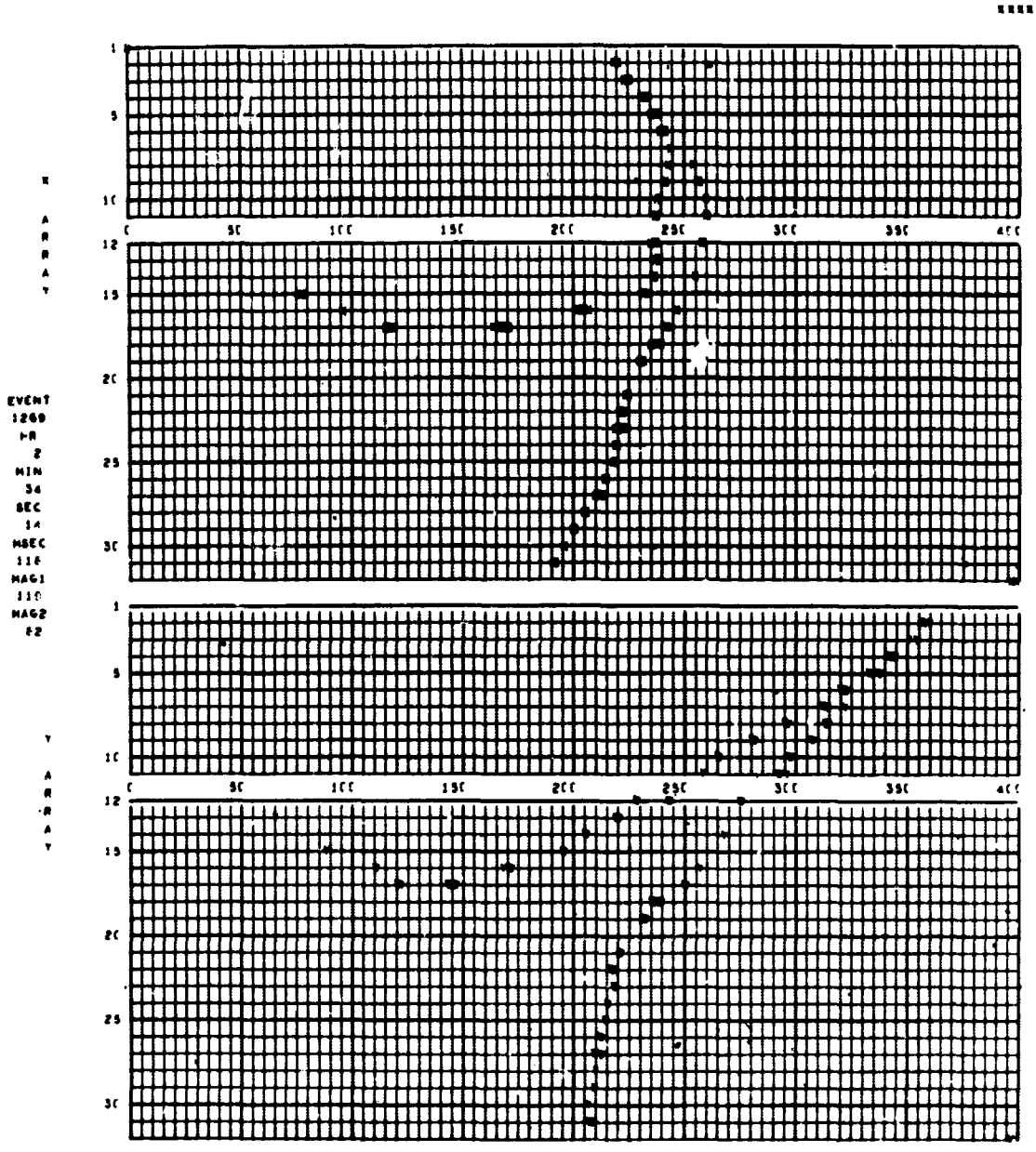

Figure 2. Computer printout of 50 cm x 50 cm chamber gamma-ray event. The X array and Y array refer to orthogonal views of the event in the X-Z and Y-Z planes, with alphabetic characters indicating set cores. The vertical scale has been compressed by a factor of about 1.5 with respect to the horizontal axis.

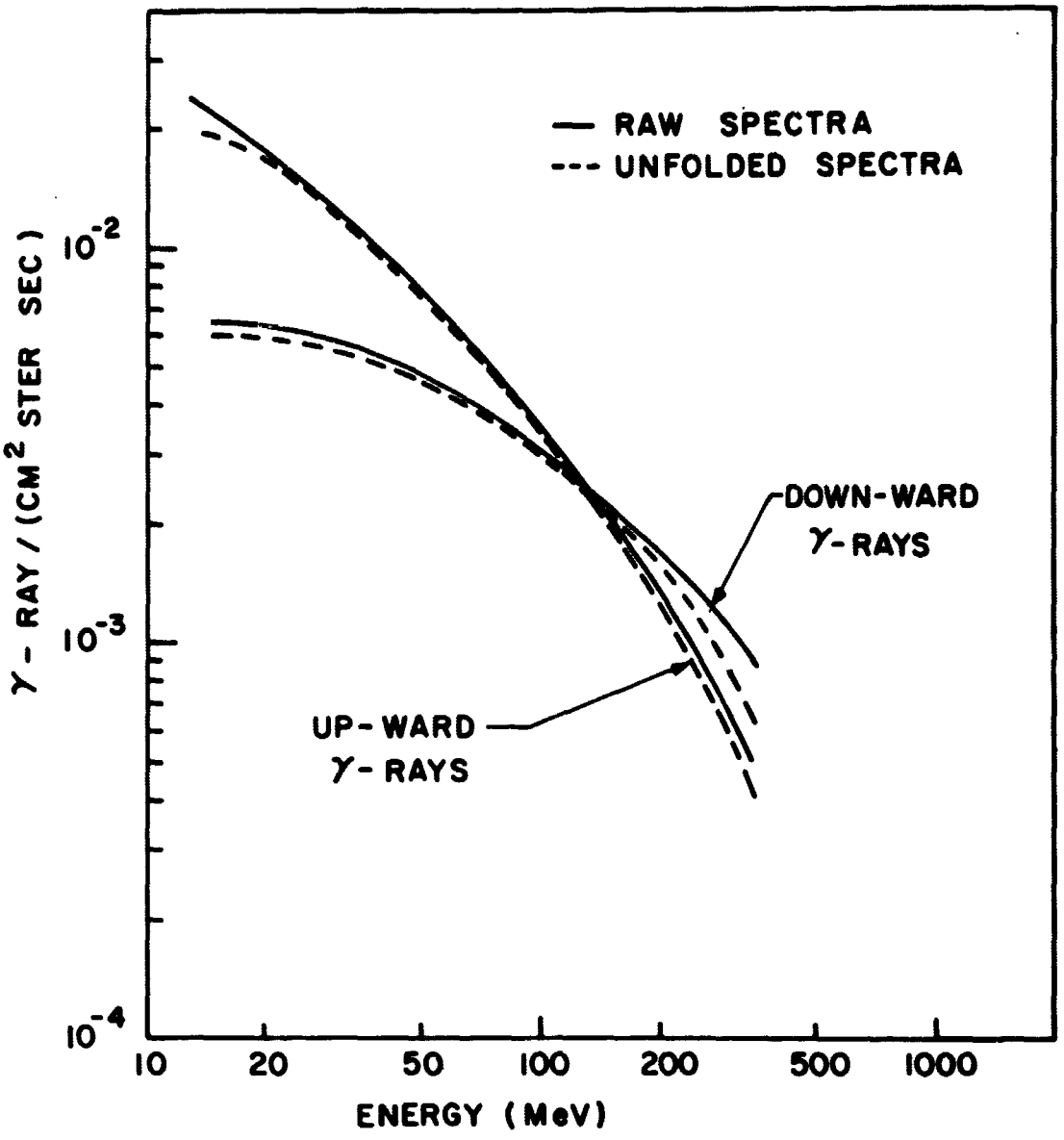

Figure 3. The atmospheric gamma-ray energy spectra, both uncorrected and corrected for the energy resolution of the detector. Both downward moving and albedo spectra are presented.

SEARCH FOR SHORT PULSES OF ENERGETIC PHOTONS FROM * SUPERNOVAE USING THE ATMOSPHERIC FLUORESCENCE

H. Ögelman+ and D. Bertsch

NASA/Goddard Space Flight Center
Greenbelt, Maryland

SUMMARY:

Recent theories on supernova explosion and subsequent neutron star formation indicate that during gravitational collapse when the outer shells of the star might be accelerated to cosmic ray velocities, a short time-scale (~microseconds) burst of energetic photons should also be generated. A wave front of energetic photons passing the Earth would be absorbed in the atmosphere and would induce fluorescence emission. In this paper, a photomultiplier system designed to observe the secondary fluorescence light is described. This system has been in operation since September 1968. An upper limit to the rate of supernova like events is given as one per 86 hours at sensitivity levels discussed in the text. A second system was put into operation in June 1969. The two stations are now operating in coincidence over a baseline of 175km to remove local noise sources. In 45 hours of observation only lightning like events have been observed in coincidence.

* Presented at the XIth International Conference on Cosmic Rays, Budapest, Hungary.

+ NAS/NASA Resident Postdoctoral Research Associate.

INTRODUCTION:

Today, one-half century after the discovery of cosmic rays, the origin of these particles remains unknown. For many years, mechanisms such as that proposed by Fermi (1) were thought to be the most likely sources of cosmic ray acceleration. These mechanisms provide for a gradual statistical increase in cosmic ray energies through collisions with large, moving regions of plasma. With the discovery of cosmic synchrotron radiation and its interpretation in terms of high energy electrons trapped in the magnetic fields of exceptional objects like the supernovae remnants, attention has been shifted from slow statistical mechanisms to violent coherent acceleration processes that might take place in discrete sources such as supernovae explosions (2) or pulsars (3), (4).

While detailed calculations of acceleration processes in supernovae explosions and in pulsars are lacking because of insufficient data, both phenomena must be regarded as plausible cosmic ray sources on the basis of available energy. Supernovae, with energy outputs of 10^{49} to 10^{52} ergs, constitute the most energetic discrete events in our galaxy (5), (6). Pulsars, which now appear to be neutron stars formed in the core of supernovae, evidently have an energy content comparable to that of the supernova explosion (3), (4).

One of the most detailed and plausible mechanisms for cosmic ray acceleration in supernova events is furnished by a theory due to Colgate and Johnson (2). In this hydromagnetic shock wave theory, Colgate (7) subsequently predicted that a microsecond time scale

burst of energetic photons should accompany the cosmic ray acceleration. Irregardless of the details of mechanism, it seems evident that relativistically exploding stellar plasma shells would emit short time scale electromagnetic radiation.

In the case of pulsars, the energy released in a single pulse is many orders of magnitude smaller than a supernova explosion. Besides the regular pulses, pulsars might undergo exceptional changes, such as the abrupt increase in the frequency of the Vela pulsar around the end of February 1969 (8), (9). Dyson's volcano theory of pulsars indicates such occurrences should take place every few years or so (10). He speculates that the event should be accompanied by some enhancement or other unusual behavior.

Because of these theories and the importance of their implications, it is extremely attractive to have an experimental arrangement capable of observing wide regions of the sky in order to search for short time-scale events (7), (11). These monitors could further provide an early-warning system for a variety of other rocket or balloon experiments which might examine other channels of information in these rare phenomena.

A detector system has been designed to detect fluorescence light produced in the atmosphere when an energetic photon pulse is absorbed. This system has been in operation since September 1968.

GENERAL DESIGN CONSIDERATION

Work done on the phenomenon of atmospheric fluorescence (12), (13), (14) shows that the emission consists almost entirely of the N_2 second positive and the N_2^+ first negative band system of molecular nitrogen

and that the bulk of the light that reaches sea level is in the wavelength band from 3200 Å to 4500 Å.

Atmospheric fluorescence will be induced by a wide band incident photon energies, ranging from high energy photons produced in cascade showers down to soft X-rays and ultraviolet photons. The primary photons deposit their energy at different altitudes, depending on their energy. In addition, fluorescence efficiency is a function of pressure and consequently different energy photons will have a different fluorescence yield.

Figure 1 shows the fluorescence efficiency and the absorption coefficient in air as a function of incident photon energy. For photons above 100 keV, the Compton and pair production processes dominate, depositing most of the energy around 20 to 30km in altitude where the fluorescence efficiency is around 5×10^{-4}. For photons below 10 keV the photoelectric process dominates, causing the photons to deposit their energy at altitudes where the fluorescence efficiency is close to its limiting zero pressure value of 5×10^{-3}.

A wide-angle photomultiplier system, aimed toward the zenith, would collect fluorescence photons coming from a large region of the atmosphere. Consequently, the pulse shape observed by such a system would be broadened by the propagation time difference between various parts of the source region. Effectively the shape of the fluorescence light pulse would be approximated by the integrated output of the energetic photon pulse profile with a time constant of $\sim h/c$, where h is the average altitude of fluorescence emission and c is the speed of light.

The maximum sensible energy range to search for such a pulse is between keV X-rays and a few GeV gamma rays. Below this range, the interstellar absorption limits the observable flux and above this range, Cerenkov light detectors or actual particle counters would be more efficient. Consequently, the interesting region of altitudes for fluorescence emission lies between 100km and 30km implying time scales of 300to 100 microseconds, even for very short incident primary pulses. Figure 2 shows sample calculations of the expected pulse shapes for the photomultiplier system used in this experiment.

To detect a pulse just described against the night sky background, the threshold for detection should be such as to have the signal greater than the background noise fluctuations during the integration time τ_i of the detector electronics. Assuming that $\tau_i \geq \tau$, where τ is the length of the incident primary pulse, the total number of photoelectrons, S, produced in the photomultiplier is approximately

$$S \simeq \frac{AW\epsilon_{fl}\epsilon_{pm}\epsilon_t}{8\pi R^2 E_\upsilon} \cdots\cdots$$

where

A = area of photomultiplier

W = energy in the primary pulse

ϵ_{fl} = fluorescence efficiency of air

ϵ_{pm} = photoelectron efficiency of the photocathode

ϵ_t = total transmission efficiency

R = distance to the source of primary pulse

E_υ = average energy of the fluorescence photons

The total noise N due to the omnidirectional night-sky background flux B during the integration time τ_i is:

$$N \simeq BA\tau_i\epsilon_{pm}$$

and the signal-to-noise ratio is:

$$\frac{S}{\sqrt{N}} \simeq \left(\frac{A\epsilon_{pm}}{B\tau_i}\right)^{1/2} \frac{W\epsilon_{fl}\epsilon_t}{8\pi R^2 E_\upsilon}$$

An estimate of the rate n of supernova events can be made by requiring that the signal-to-noise ratio exceed at least 5 for good confidence, and by assuming that galaxies are uniformly distributed with a density ρ_g, each with f supernova per unit time of energy W in energetic photons. The rate is then

$$n \simeq 10^{-3}\rho_g f \left(\frac{A\epsilon_{pm}}{B\tau_i}\right)^{3/4} \left(\frac{W\epsilon_{fl}\epsilon_t}{E_\upsilon}\right)^{3/2}$$

Using the following estimated values:

ρ_g = 5×10^{-75} galaxies $(\text{cm})^{-3}$

f = 1 supernova $(\text{galaxy})^{-1}$ $(100 \text{ years})^{-1}$

$(3.2 \times 10^{-10} \text{sec}^{-1}\text{galaxy}^{-1})$

A = 500 cm^2

ϵ_{pm} = 0.1

$B = 5 \times 10^{7}$ photons/cm^{2}-sec

$\tau_i = 10^{-4}$ sec

$W = 5 \times 10^{47}$ ergs (Ref. 7)

$\epsilon_{fl} = 10^{-3}$ (Figure 1)

$\epsilon_t = 0.3$

$E_U = 5 \times 10^{-12}$ ergs

gives a rate of one event per 18 hours which should be easily observed.

Besides the night sky background fluctuations, there are other sources of real light pulses in the atmosphere such as lightning, meteors, aurora, Cerenkov light from air showers as well as man-made signals including airplanes, airport beacons, etc. Although there are ways of discriminating against such pulses locally, one of the most effective ways of eliminating this noise is to have an array of detectors separated by a few hundred kilometers and have accurate timing information. By demanding a coincidence between widely separated events, local noise is eliminated. Furthermore, accurate timing of the relative arrival time of signals at separated stations can be used to determine the direction of the source.

DETECTION SYSTEM

In the present pilot program, two independent stations separated by 175km are being maintained. One is located near Greenbelt, Maryland at the Goddard Space Flight Center's Optical Site and the other is at the Fan Mountain Observatory of the University of Virginia in Charlottesville, Virginia.

Each station consists of the following equipment, illustrated in the block diagram of Figure 3. Three 12-inch EMI, type 9545-B photomultiplier tubes are housed in a weatherproof container with an automatic dome system to protect the tubes during daylight periods. The tubes are all pointed in the zenith direction. Collimators are used to restrict the opening angles to a maximum of 70° from the vertical; FWHM being 86°. Two of the tubes have transmission filters covering the useful fluorescence region between wavelengths of 3200 Å and 4300 Å and are denoted by V_1 and V_2 (violet) in the subsequent discussions. The third tube has a filter with a lower wavelength cutoff of about 4300 Å which is effectively above the fluorescence emission bands. This tube is denoted by Y_3 (yellow). The relative response characteristics of these tubes, including the filter and atmospheric transmission is shown in Figure 4. This two level spectroscopic information provides an extremely useful means of distinguishing various noise pulses from the type of pulses of interest.

The direct anode output of each tube is connected to an ammeter-relay system which turns off the high voltage to the photomultiplier tubes in the event that the anode current exceeds the safe limit. Also, the anode current of one or more tubes is monitored by means of a chart recorder to determine the background sky conditions throughout the night. In addition, each anode is capacitively coupled to a 100 microsecond delay line. The delay lines are tapped at 5 micro-second intervals. On each delay line, the first ten taps are resistively added to give a pulse height which is proportional to the output of

the light pulse integrated over the first 50 microseconds. This integrated signal from each tube is fed into preamp-discriminators which test to see if the signals exceed a preset level. The outputs of the discriminator modules in turn go to a coincidence unit. In the usual mode of operation, only a coincidence of outputs from the V_1 and V_2 tubes is required to denote an event. However, due to airport lights in the vicinity of the Goddard site, we have been forced to operate about 80% of the time with the added requirement that the Y_3 tube output be in anticoincidence with the other two in order to avoid excessive dead time produced by recording such lights.

When acceptable triggering criteria are met, both beams of a dual beam oscilloscope are triggered. One beam, operated at a sweep rate of 100 μsec/cm is chopped between three inputs displaying the light pulse shape from the 100 microsecond delayed output of each photomultiplier. The second beam of the oscilloscope is operated at a sweep of 0.1 sec/cm and contains a 36 bit NASA time code that gives the days, hours, minutes, and seconds in a serial code frame of one second. Using this time code, the time of the event can be read to a 10 millisecond absolute accuracy.

A Beattie Coleman 35mm camera with an open shutter records the oscilloscope traces as they are swept. Peripheral data including frame number, a clock reading, and a date are superimposed on each frame of film. At the conclusion of the oscilloscope trace, the camera advances the film in preparation for the next event. A dead-time generator used in anticoincidence prevents further triggers from occurring during a two second interval, permitting the system to recycle.

The entire system is turned on and off automatically by a programmed timer that is set to avoid running during intolerable sun and moon lighting conditions.

RESULTS

A pilot station at the Goddard Space Flight Center Optical Site has been in operation since September 1968. In June 1969, a second station was set up at the Fan Mountain Observatory of the University of Virginia. The data reported here includes times up to August 1969. The total clear sky observation time for the periods in question amount to 410 hours at the Goddard Station, 80 hours at the Fan Mountain Station and 45 hours of mutually clear sky conditions at both stations. During this operation time, over 20,000 events were recorded. The events could roughly be classified in five categories:

1. Cerenkov light from air showers.
2. Lightning.
3. Airplane and airport beacons.
4. Unexplained events, unlike the expected supernova pulse.
5. Possible supernova type pulses with time scales around 100 to 500 microseconds and having less than 10% amplitude in the wavelength channel above 4300 Å.

Figure 5 shows a typical example of each case. The majority of events fall within the first three categories. In the category of possible supernova pulses a total of six events have been recorded. Of this number, five were seen when only one station was in operation. One event was recorded at Fan Mountain station, but was not seen at the Goddard station.

The average triggering threshold sensitivity for the stations in terms of photons/cm^2 in the violet filter region (3400 Å to 4300 Å), integrated over 50 microseconds, was about 200 photons/cm^2 at the Goddard station and 70 photons/cm^2 at the Fan Mountain station. With the values of fluorescence efficiency and supernova distribution, frequency, and explosion parameters used previously the rate of such events should be one per 96 hours at Goddard and one per 21 hours at Fan Mountain. The coincidence rate should be one per 96 hours as dictated by the Goddard station. If all supernovae-like events were due to supernova, this rate would be one per 83 hours, which is close to the expected value.

During period of operation of the two stations together, 34 lightning events were recorded in coincidence, indicating that lightning effects can propagate over large distances. Figure 6 shows a pair of these events as recorded by each station. The large amplitude in the $\lambda > 4300$ Å Y_3 tube points out the non-fluorescence nature of these pulses. Also, on the night of July 17, 1969, five coincidences were observed within the time period, 0715 to 1030 UT. Although these pulses do not look like the typical lightning events, they most likely are scattered light from distant lightning activity. Figure 7 shows a pair of these events.

CONCLUSIONS

With the present data we cannot claim the positive detection of a fast supernova pulse of energetic photons. The upper limit, at a 95% confidence level, using the coincidence data is less than one per

15 hours which is consistent with one per 96 hour expected rate. On the basis of single station runs, the supernova-like events give a rate of one per 83 hours, again within the uncertainties of the expected rate. We wish to emphasize, however, that single station data might include a variety of local phenomena and should be regarded with caution.

Although the detection of supernovae bursts have been the primary objective in this experiment, the present setup is sensitive also to other phenomena that may release electromagnetic radiation in the optical to gamma ray regions with time scales from one to several hundred microseconds. For example, if a source at a distance of one kiloparsec releases 10^{35} ergs in the optical band or 10^{38} ergs of X and gamma rays in short time scales, it should be detected by the present system.

In the next stage of development of the experiment, we are planning to increase the number of stations and to improve the timing accuracy of each event. Using LORAN-C navigational radio pulses, a timing accuracy of 10 microseconds can be achieved, and this accuracy at each station in a triangular array would enable the arrival direction of the incident pulse to be calculated with a few degrees. A less precise measure of arrival direction can be obtained at each station by increasing the number of violet-filtered photomultiplier tubes at each station, and aiming them at different regions of the sky. Comparison of pulse heights and shapes should provide a rough measure (within 20°) of arrival direction. The latter scheme is much

easier and cheaper than the accurate timing scheme and we expect to institute it in the near future. Needless to say, the few degrees of accuracy, although more difficult, is far more preferable since it would make it feasible for optical telescopes to search for the object in order to study the long time-scale phases of the supernova evolution.

ACKNOWLEDGEMENTS

The authors would like to thank Dr. Carl Fichtel for his support during this experiment. Also, they recognize W. Pusey, J. Shifman and D. Thompson of the Goddard Space Flight Center and A. Miller of the University of Virginia for invaluable assistance. They are grateful to Professor L. Frederick of the University of Virginia for providing the use of the Fan Mountain facilities of the Astronomy Department, and Dr. S. Maran of Goddard Space Flight Center for initiating the arrangement.

References

1. E. Fermi, Phys. Rev., 75, 1169 (1949).
2. S. A. Colgate and H. J. Johnson, Phys. Rev. letters, 5, 235 (1960).
3. T. Gold, Nature, 221, 5175 (1969).
4. T. Gold, Nature, 221, 25 (1969).
5. V. L. Ginzburg and S. I. Syrovatskii, "The Origin of Cosmic Rays", New York, Pergamon Press, Macmillan Co. (1964).
6. R. L. Minkowski, Annual Review of Astro. and Astrophysics, 2, 247 (1964).
7. S. A. Colgate, Can. J. Phys., 46, 5476 (1968)
8. V. Radhakrishnan and R. N. Manchester, Nature, 222, 228 (1969).
9. P. E. Reichley and G. S. Downs, Nature, 222, 229 (1969).
10. F. J. Dyson, Nature, 223, 486 (1969).
11. C. E. Fichtel and H. B. Ögelman, "Experimental Tests of the Supernovae Origin of Cosmic Rays", NASA TN D-4732, Sept. 1968.
12. P. Hartman, "Luminescence Efficiency of Air on Electron Bombardment", Los Alamos Report (1963).
13. K. Greisen, "Proceedings Ninth International Conference on Cosmic Rays", London, 609 (1965)
14. A. N. Bunner, "Cosmic Ray Detection by Atmospheric Fluorescence", Ph.D. Thesis, Cornell University (1966).

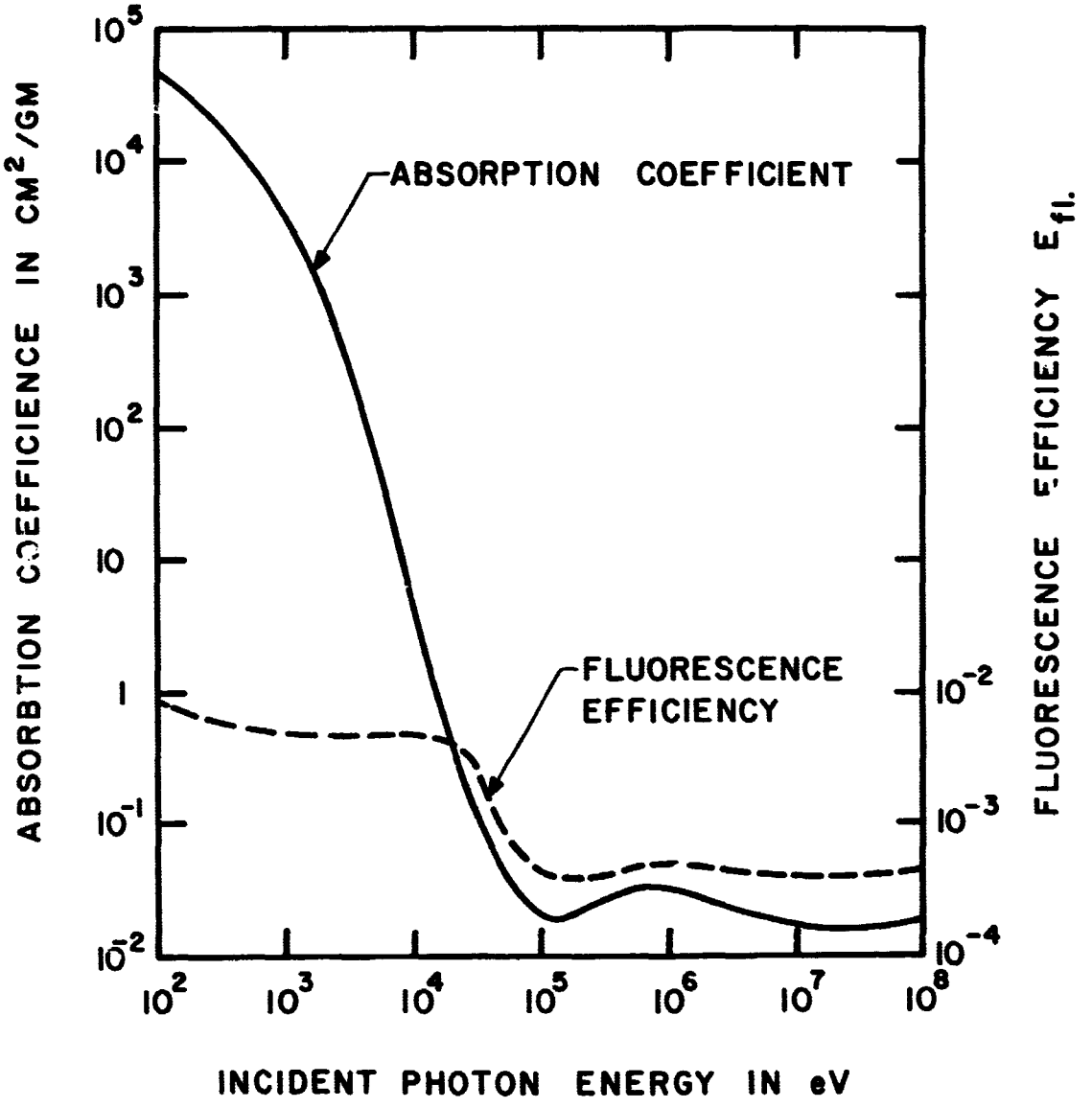

Figure 1. Absorption coefficient and fluorescence efficiency in the atmosphere as a function of the incident photon energy

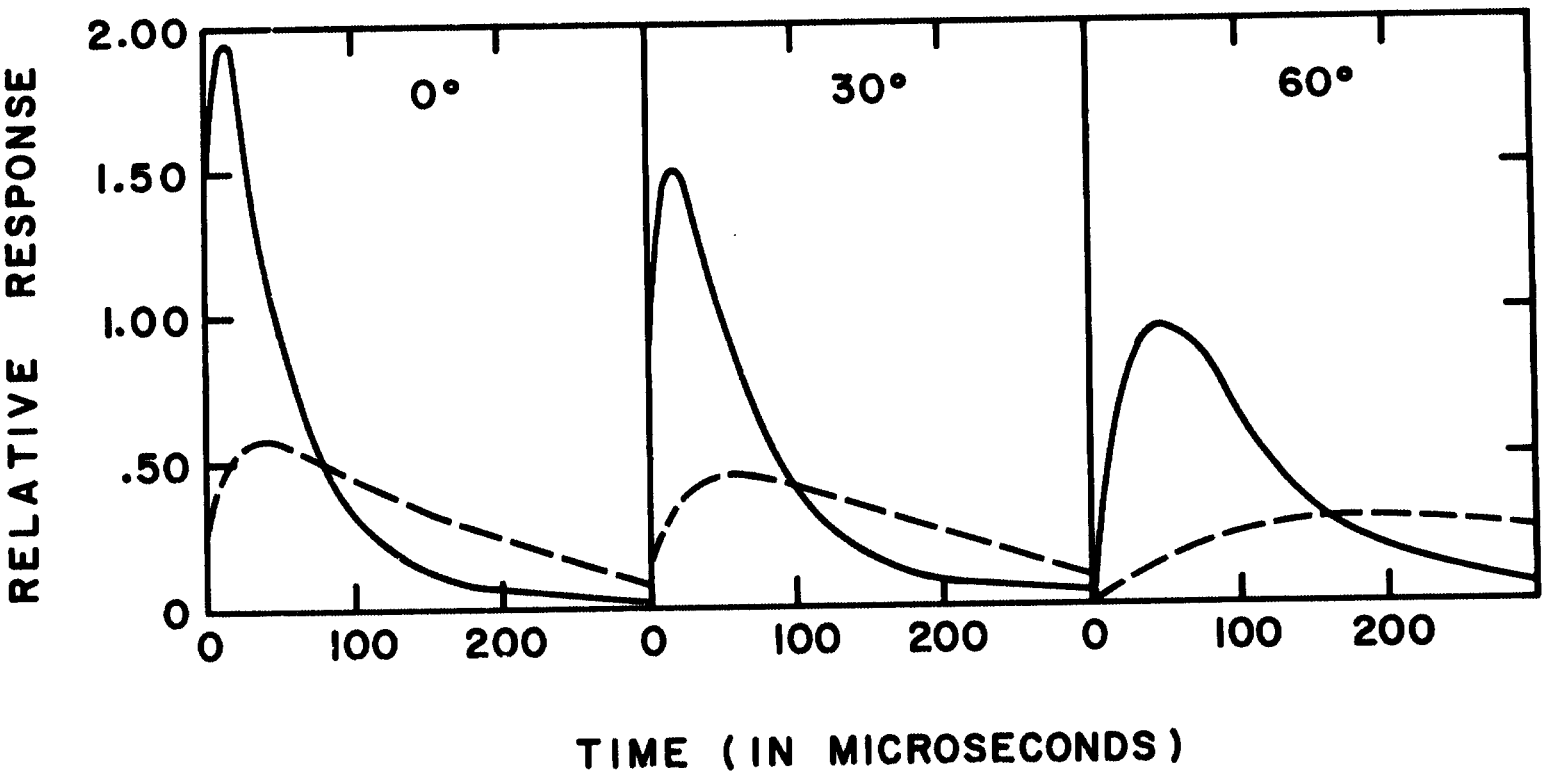

Figure 2. Relative response of the present photomultiplier system calculated for a delta function excitation pulse incident at 0°, 30° and 60° from the zenith. The solid curves represent energy deposition altitude of 30 km and the dashed curves for 100 km

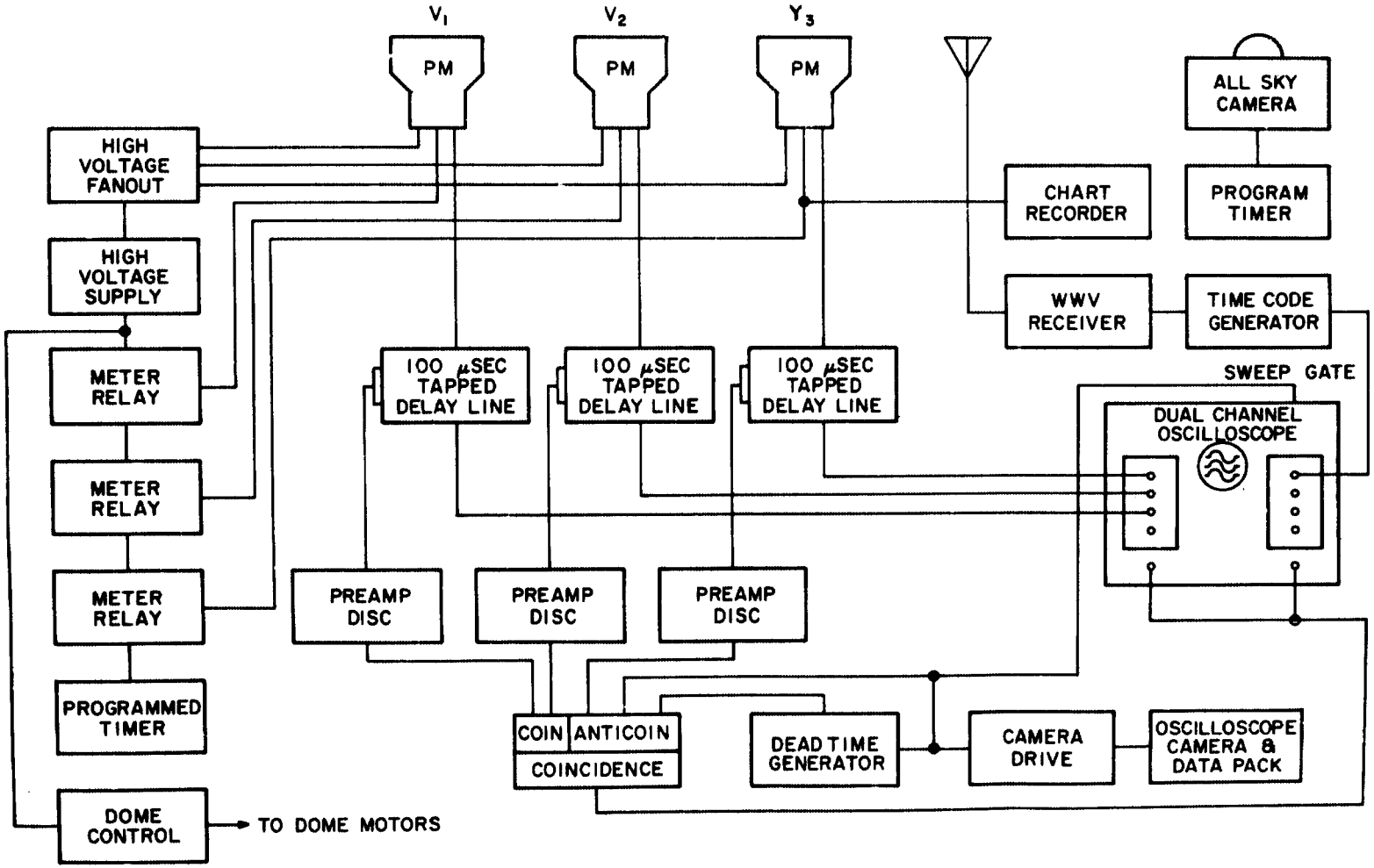

Figure 3. Block diagram of the experimental arrangement for a single station

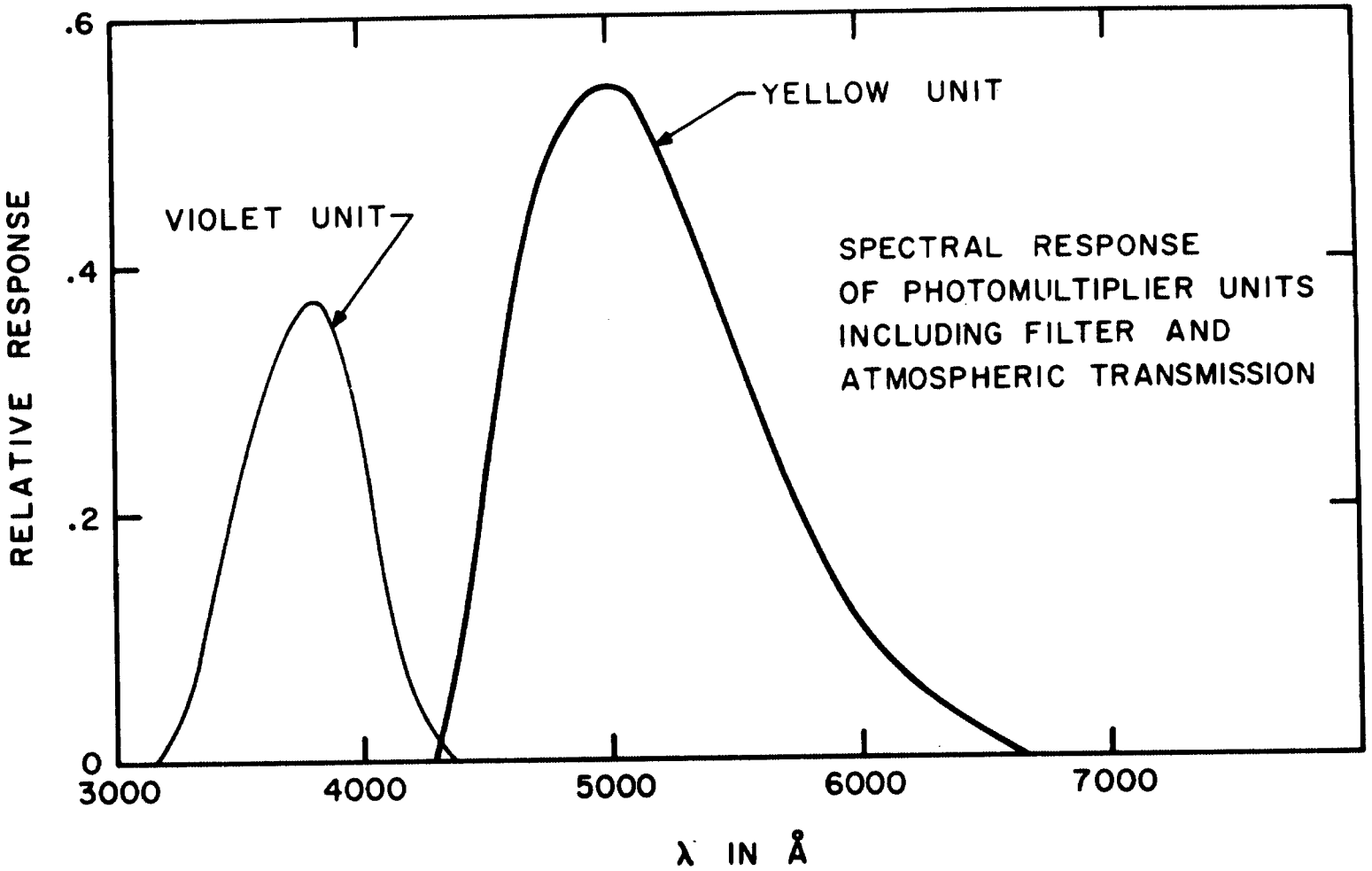

Figure 4. Spectral response of the two-color photomultiplier system including filter and atmospheric transmission

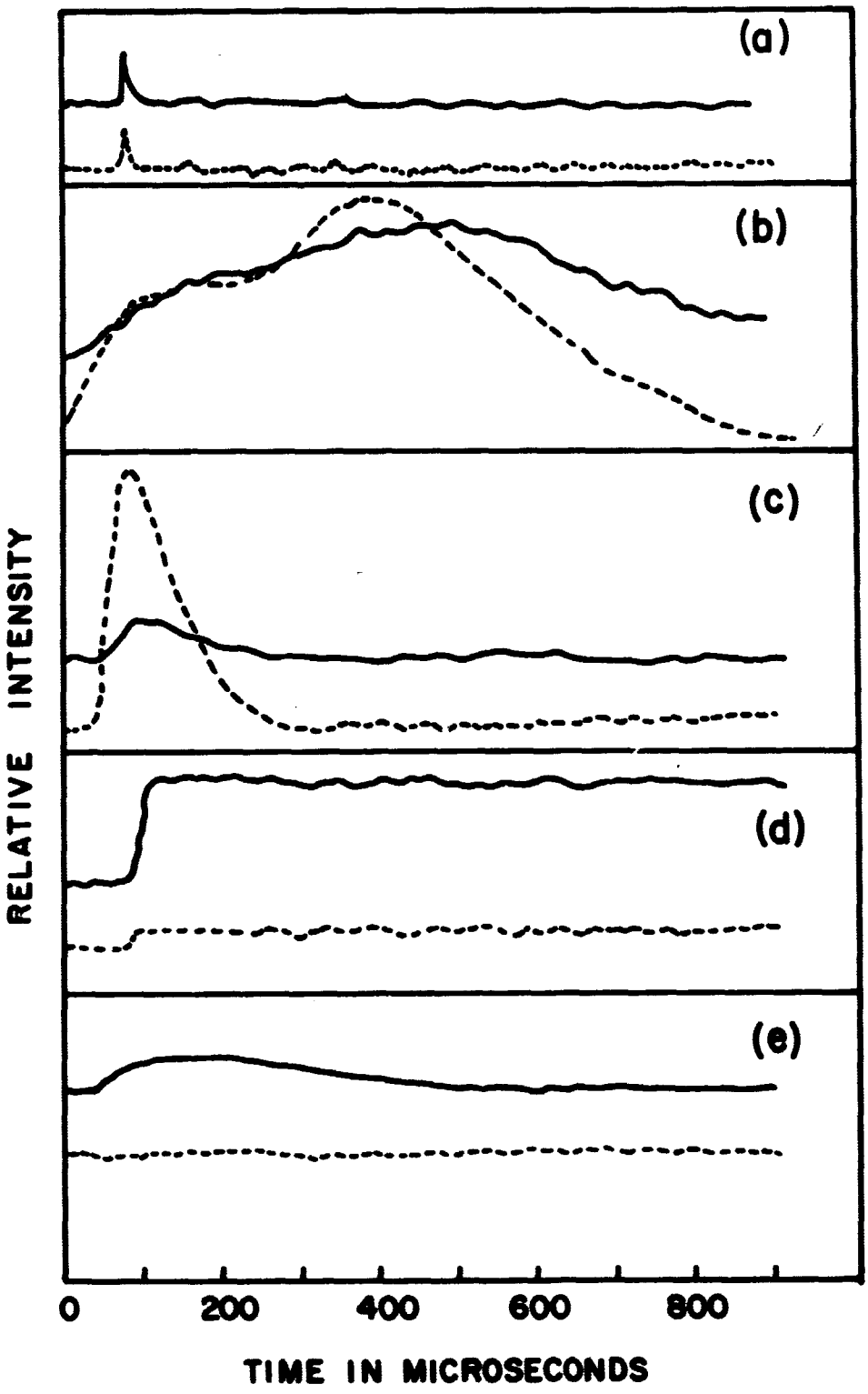

Figure 5. Representative samples of observed light pulses. Solid lines are the responses of the violet unit (3200 Å to 4300 Å), dashed lines are that of the yellow unit (above 4300 Å). (a) Cerenkov pulse from an air shower. (b) Lightning. (c) Airport runway approach flashers. (d) An event of unknown origin. (e) An event like that expected from supernova

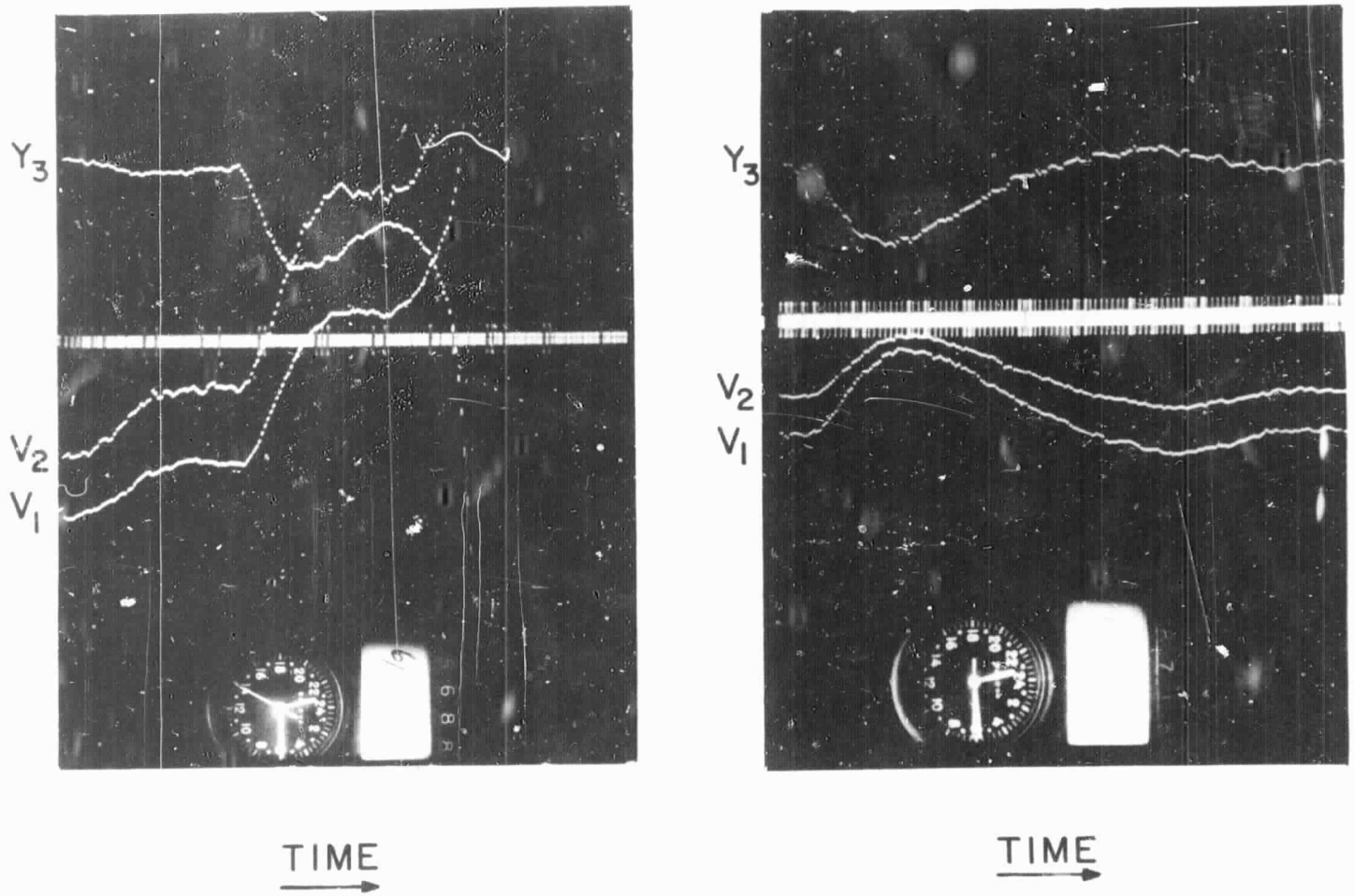

Figure 6. A lightning pulse observed in coincidence over a baseline of 175 km. Y_3 unit response is inverted in the pictures. Full scale of time axis is 900 microseconds. The NASA 36-bit serial time code format is displayed in the center. The left hand picture is from the Fan Mountain Station and the right hand picture is from the Goddard Station

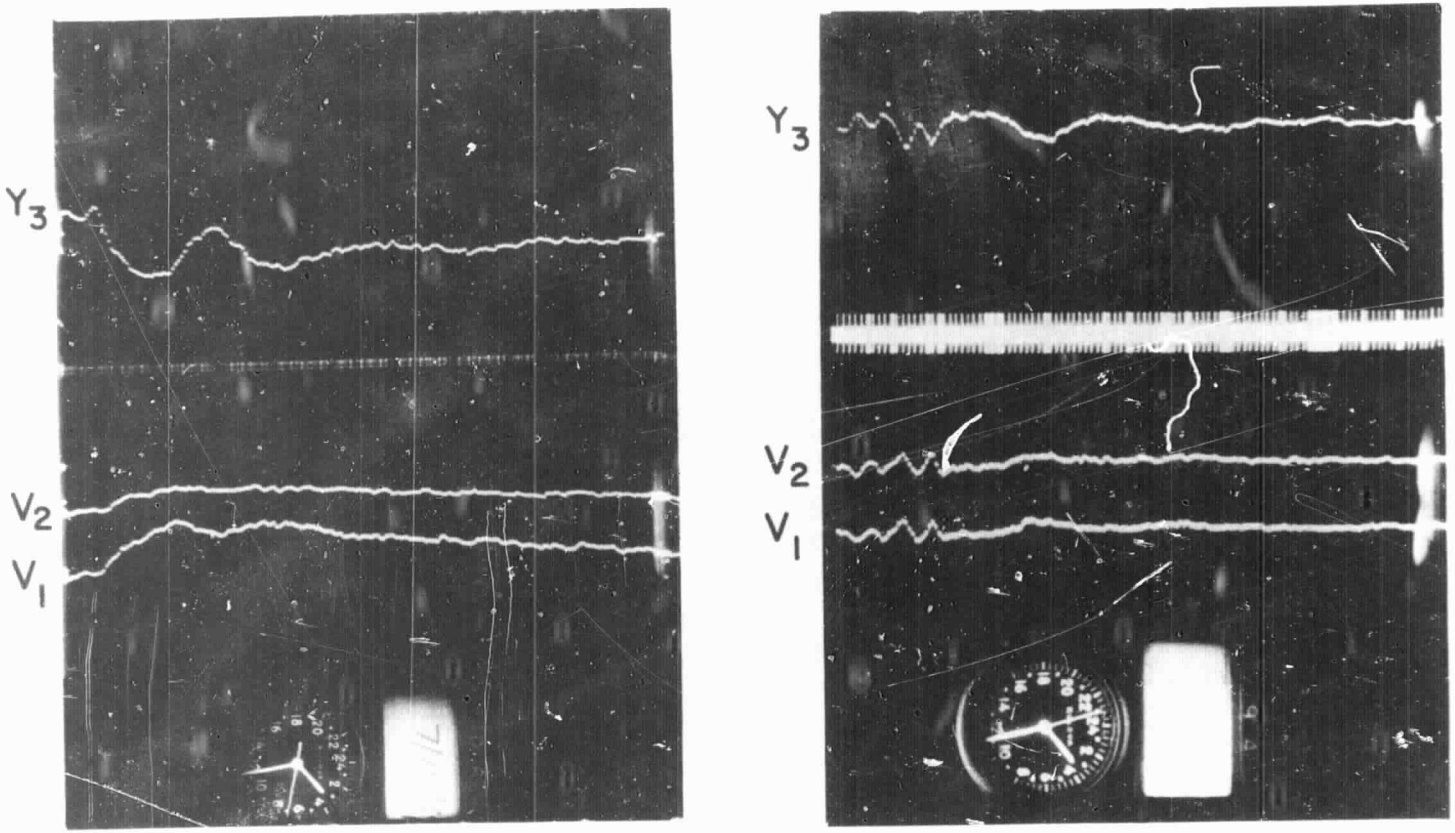

Figure 7. A coincidence event over a baseline of 175 km; origin is most likely distant lightning. The format is identical to that explained in Figure 6, except Fan Mountain V_2 trace gain is reduced by a factor of 2.5

COSMIC-RAY ELECTRONS AND POSITRONS OF ENERGIES 2 TO 9.5 MeV OBSERVED IN INTERPLANETARY SPACE

T. L. Cline and G. Porreca

NASA/Goddard Space Flight Center
Greenbelt, Maryland 20771, U.S.A.

ABSTRACT

The differential energy spectra of electrons and positrons in the 2 to 9.5 MeV interval have been studied in interplanetary space during solar quiet times following March 1968 with the OGO-5 satellite. The detector flown was designed to separately identify cosmic-ray and solar electrons, positrons, protons and alphas, and solar x-rays; it used new techniques to minimize its background and to determine directly the background encountered. The observed quiet-time electron spectrum, approximately of the form 90 $E^{-1.5}$ m^{-2} sec^{-1} $ster^{-1}$ MeV^{-1} from 2 to 9.5 MeV, roughly agrees with the expected unmodulated cosmic-ray knock-on electron spectrum. The positron to electron ratio, totalled for this energy interval, is only 1.8 percent. This is the lowest e^+/e ratio measured in any energy region; it also suggests that this electron component is of knock-on or directly-accelerated origin, rather than of meson-decay of soft-shower origin. The resulting average positron intensity, near 0.2 m^{-2} sec^{-1} $ster^{-1}$ MeV^{-1}, compares with the balloon data above 10 MeV such that all points or upper limits are below the predicted spectrum of cosmic-ray electrons from pion decay by a factor of up to ten. This result indicates a moderate modulation of the positron intensity in the medium-energy region, having a detailed energy dependence yet to be determined.

The differential spectrum of low-energy, relativistic electrons* in interplanetary space and the related positron to electron ratio have been measured with a new detector on the OGO-5 satellite. This observation, made during selected solar quiet-times from March to October, 1968, represents the only search for interplanetary cosmic-ray positrons in the region from 3- to 12-MeV and incorporates the lowest-energy threshold (2 MeV) used to date for the detection of cosmic-ray electrons. It is also the only interplanetary measurement of the electron spectrum below 12 MeV made using an instrument different in design from that employed on the IMP-1, when an unexpected new spectral component was found at low energies (1), indicating that cosmic-ray electrons other than of high-energy origin, such as meson decay, may exist in interplanetary space. Calculations of the expected intensity of galactic knock-on electrons were later found to provide at least a partial explanation for the low-energy component (2), depending on assumptions of acceleration or solar modulation (3, 4). Recent observations of interplanetary flare electrons in the same, few-MeV energy region indicate that brief, large intensity increases may occur following solar microwave flares (5), but it is unknown whether low-level solar electron production may occur during apparent quiet-times, as discussed in an accompanying paper (6). Thus, because of the lack of confirmation of, and

*"Electron intensity" defines $n(e^-) + n(e^+)$.

elaboration on, the IMP-1 results using different apparatus, it is still of definite interest to carry out some independent electron measurements. The existence of interplanetary positrons from sources other than cosmic-ray pion production is another question; the first result from an earlier search with OGO's 1 and 3 (7) in the >0.5-MeV region gave an intensity value too high to be compatible with that process. This was a genuine identification of positrons, but in the absence of any fix on the background production, the detected intensity was initially set as an upper limit, as discussed in another accompanying paper (8). Continued studies of positrons as well as electrons are therefore needed to describe the very low-energy cosmic radiation.

The satellite used for this experiment is the OGO-5; it was launched on March 4, 1968, has an orbit with about a 62.5-hour period and a roughly 150,000-kilometer apogee. The solar quiet-time data reported here were taken starting with the line of apsides about 40 degrees from the sun-earth line; the region of space sampled was thus both towards the sun and in front of the magnetosphere. The detector aperture sweeps out during one orbit a band at a varying orientation to the ecliptic; assuming isotropy, all apogee data were summed in this first study regardless of aspect.

The detector, shown in Figure 1, was developed primarily for the purposes of studying cosmic-ray and solar electrons and positrons in the few-MeV region; it can also observe solar electrons of > several hundred-keV energy, >80-keV solar x-rays, and medium-energy galactic and solar protons and alpha particles.

It employs the energy-loss vs. energy scheme of particle identification, as does the IMP device, but differs in that it is flown on a boom well outside the satellite body, it has more in the way of active shielding, and it is constructed using plastic ΔE and E scintillators rather than CsI. Thus, any background in an apparent electron intensity, due to cosmic-ray-produced secondaries in or near the detector, should be minimized for this arrangement. In addition, a new in-flight technique is used for the direct determination of the contribution of such background, described below.

In one of several modes of detector operation, a $\Delta E \cdot E \cdot \bar{P}$ coincidence is required to transmit the gated, 256-channel pulse heights from each of the ΔE and E scintillators, and from the CsI crystal 'C', unaccompanied by a pulse from the plastic-scintillator guard counter 'P'. The C and P outputs from the same tube are separated electronically by pulse-shape analysis. In this mode, the electron and proton lines are distinct and clearly identifiable. Positrons are separated from electrons by analysis of the gamma radiation in the C crystal coincident with a stopping electron. A half-MeV line would be created with a few-percent efficiency by stopping positrons, superimposed on the continuum. In a second mode of operation, a $\Delta\bar{E} \cdot E \cdot \bar{P}$ trigger is required to transmit the gated ΔE, E and C signals. This technique makes it possible to evaluate the in-flight background by using the spectrum of electrons created in and stopping in the total-energy scintillator to infer the spectrum of background electrons which produce a $\Delta E \cdot E$ coincidence, masquerading as incident cosmic-ray

particles. The positron background is similarly deduced since the coincident gamma-ray events are also monitored with this scheme. Calibration of the detector was initiated prior to flight with the use of radioactive sources and sea-level mu mesons, and with a mono-energetic 3-MeV positron beam. In-flight calibration is continuously maintained using telescoped cosmic rays, stopping protons, the minimum-ionizing electron line and the background annihilation line to fix the gains of the three PM-tube systems.

The quiet-time electron and positron energy spectra were obtained as follows. The data represented by the selected minimum-ionizing line were used to obtain a pulse-height distribution vs. apparent energy; histograms of incident particle intensities were then determined by using an energy-dependent factor, varying near 1.4 MeV, which represents the energy loss of an incident electron required for it to create a $\Delta E \cdot E$ coincidence. The geometric factor for stopping electrons, which varies between 7.6 and 13. cm^2 steradian, was then used to create the raw spectrum. Finally, background effects were evaluated as follows.

First, estimates were made of the knock-on and compton-electron production local to the detector; these are spectrally like the observations, but provide at most about 1 percent of the rate. The upper limit to the local beta-decay electron rate (in particular from N^{12}, created by interactions from the carbon in the detector) involves a nearly flat spectrum, but is well under one percent the observed rate. Other processes including inefficiency of the guard counter and the bremsstrahlung of high- into low energy electrons, also contribute a small

background only towards the highest energies. Second, the background electron spectrum was determined in flight by inference from the E pulse-height spectrum, taken with the $\Delta\bar{E} \cdot E \cdot \bar{P}$ trigger requirement. The result is that such background is indeed a negligible input, as was anticipated. A very small, flat background rate was subtracted to produce the corrected electron spectrum. Daily averages of electron intensity were plotted and found to vary, but always return to a constant, low value. Data from periods of more than twice this daily minimum were then rejected, and a final, average quiet-time spectrum was produced. This result is shown plotted in Figure 2 together with the IMP-1 results (1), a newer IMP-4 spectrum for which detailed correction and recalibration was made (9), and some balloon results (10, 11). The IMP-4 measurement was made one year before these observations; it is seen that the two recent interplanetary spectra agree. The observed spectrum above 2 MeV is also a relatively good fit to the predicted galactic knock-on spectrum; because of possible solar modulation, this result may be coincidental, but it does suggest that interplanetary electrons in the 2 to 10 MeV interval are mostly of knock-on origin if there is little solar modulation at these electron energies.

The positron to electron ratio was obtained by examining the spectrum of detected gamma rays coincident with stopping electrons. A half-MeV component superimposed over background with the expected line shape did present itself with statistical significance; the corresponding e^+/e ratio, totalled over the entire energy interval, was 1.8 ± 0.2 percent. This corresponding positron

intensity is plotted in Figure 3 as a dashed line of appropriate slope; it is alternatively shown broken into differential energy bins as three points with reduced statistical significance. This preliminary positron intensity curve may be revised downward by further analysis, but we contend that it represents the intensity rather than its upper limit. It is also seen to be well below a smooth connection between the OGO-3 result near 1 MeV (7) and the various balloon values above 10 MeV (12, 13, 14), suggesting independent origins for the two components.

In conclusion, the observed e^+/e ratio in the 2 to 9.5 MeV interval is compatible only with a directly accelerated or knock-on origin, not soft-shower or meson-decay origin, for most of the electrons. Also, the 2 to 9.5-MeV positron intensity, if averaged at one value of 0.2 intensity units, together with the higher-energy values and limits are compatible with a smooth spectrum of about the same shape as that calculated for pion decay (15, 16) but less intense by an amount up to a factor of ten. The shape of the modulation factor needed to fit the data to the calculations will require much more accurate measurements, however. Of course, one cannot have simultaneous agreement with the galactic knock-on spectrum and a large modulation of the electron intensity at the lowest energies. Finally, the observed low positron intensity above 2 MeV may not be inconsistent with a much higher intensity in the lower energies appropriate to beta decay. Ramaty, Stecker, and Misra show that a high positron intensity below 2 MeV from secondary, galactic beta-decays may exist, depending on the intensity of local, low-energy cosmic rays (17);

such a mechanism may account for the value at >0.5 MeV (7, 8), providing such a cut-off that the component is unobservable in the >2 MeV region.

We wish to thank H. Costlow for his assistance with the detector preparation and calibration, W. Andersen, T. Funkhauser, Mrs. J. Holloway and P. Yu for their assistance with the data processing, and the OGO-5 Project for the successful flight.

REFERENCES

1. T. L. Cline, C. H. Ludwig and F. B. McDonald, Phys. Rev. Letters, 13, 786-789, 1964.
2. K. A. Brunstein, Phys. Rev., 137, B757-759, 1965.
3. P. B. Abraham, K. A. Brunstein and T. L. Cline, Phys. Rev., 150, 1088-1103, 1966.
4. K. A. Brunstein and T. L. Cline, Nature, 209, 1186-1188, 1966.
5. T. L Cline and F. B McDonald, Solar Physics, 5, 507-530, 1968.
6. G. M. Simnett, T. L. Cline and F. B. McDonald, Budapest Conf., (1969).
7. T. L. Cline and E. W. Hones, Jr., Can. J. Phys., 46, S527-529, 1968.
8. T. L. Cline and E. W. Hones, Jr., Budapest Conf., (1969).
9. G. M. Simnett and F. B. McDonald, to be published in Astrophys. J. (GSFC Preprint X-611-68-450).
10. W. R. Webber, J. Geophys. Res., 73, 4905-4914, 1968.
11. R. E. Beedle and W. R. Webber, Can. J. Phys., 46, S1014-1019, 1968.
12. K. P. Beuermann, C.J.Rice, E. C. Stone and R. E. Vogt, Phys. Rev. Letters, 22, 412-415, 1969.
13. C E. Fichtel, T. L. Cline, and D. A. Kniffen, Budapest Conf., (1969).
14. J. Fanselow, R. C. Hartman, R. H. Hildebrand, and P. Meyer, to be published in Ap. J.
15. R. Ramaty and R. E. Lingenfelter, J. Geophys. Res., 71, 3687-3703, 1966.

16. R. Ramaty and R. E. Lingenfelter, Phys. Rev. Letters, 20, 120-124, 1968.

17. R. Ramaty, F. W. Stecker and D. Misra, Budapest Conf., (1969).

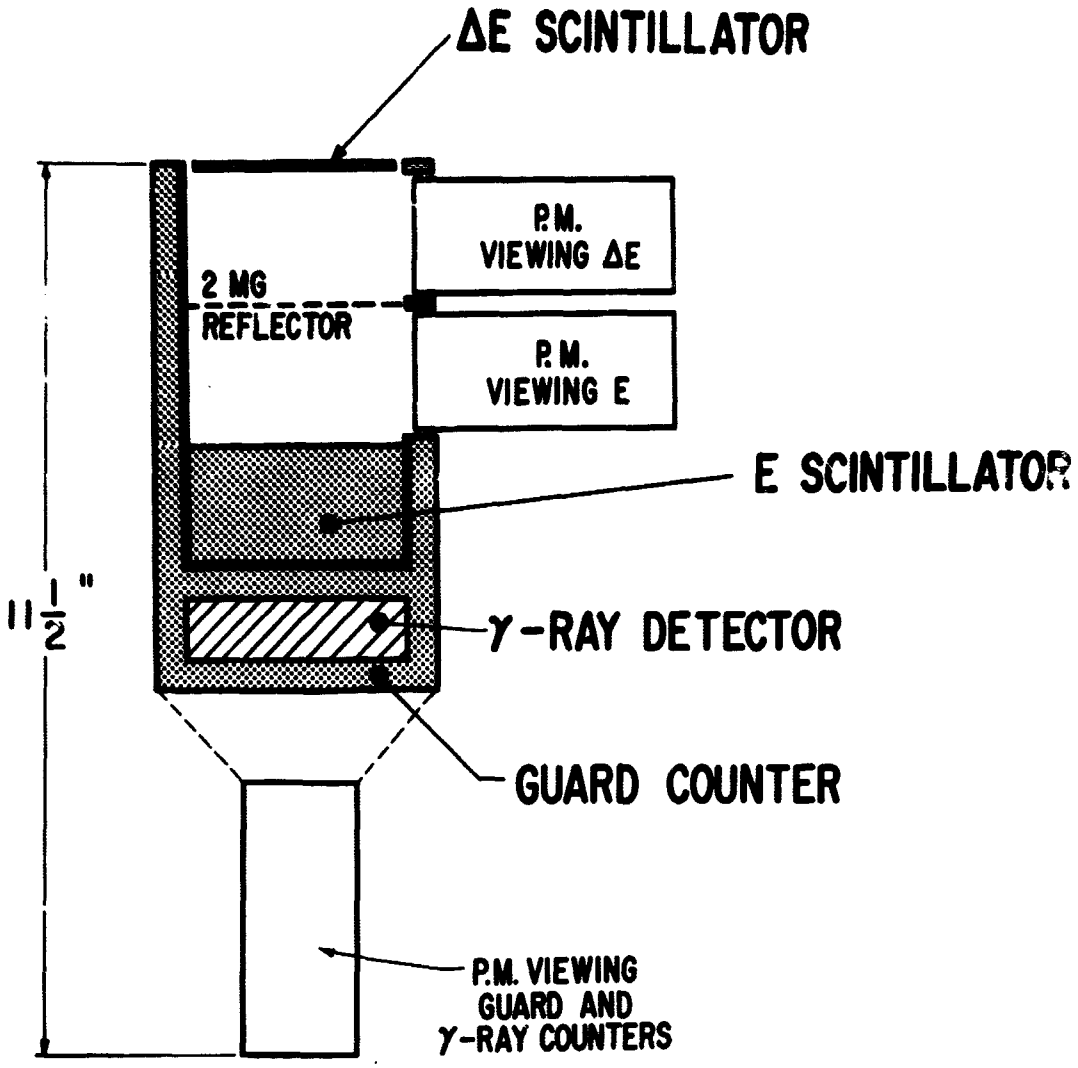

Figure 1. Cross section of the detector

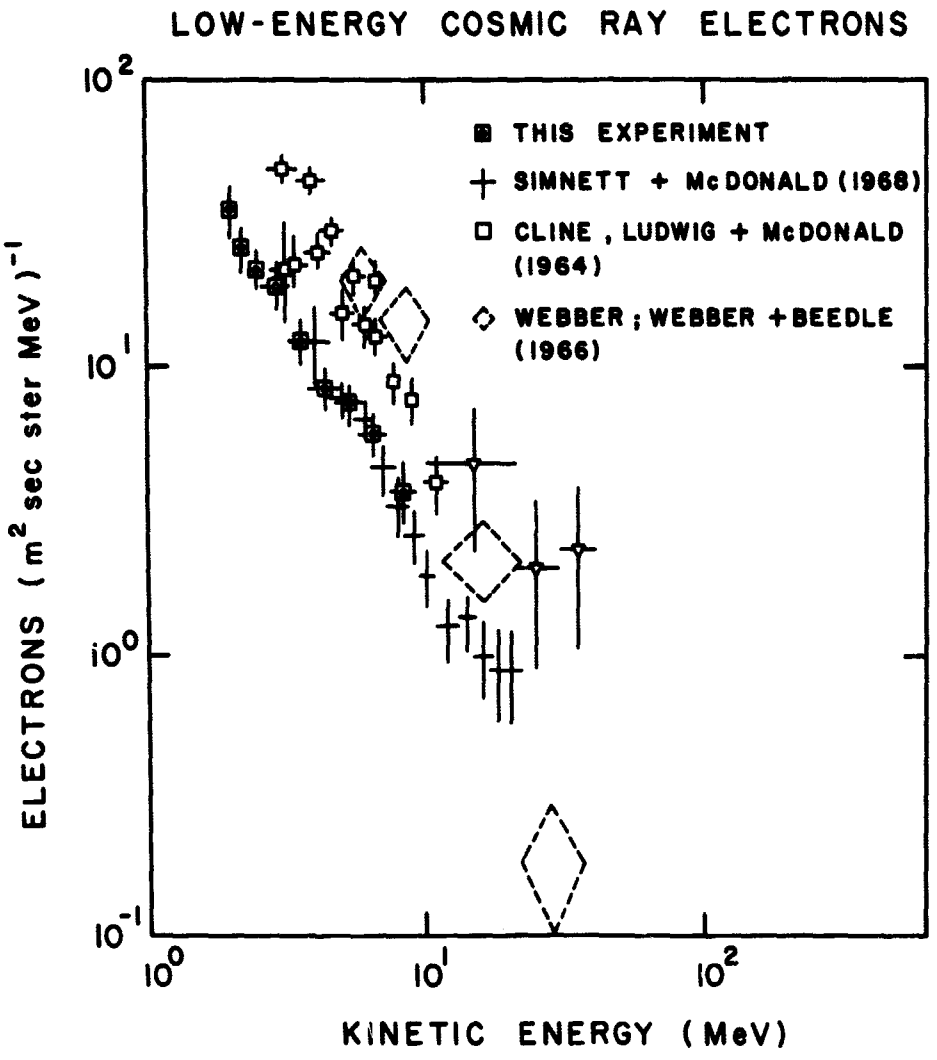

Figure 2. Electron intensity observations below ≈20 MeV

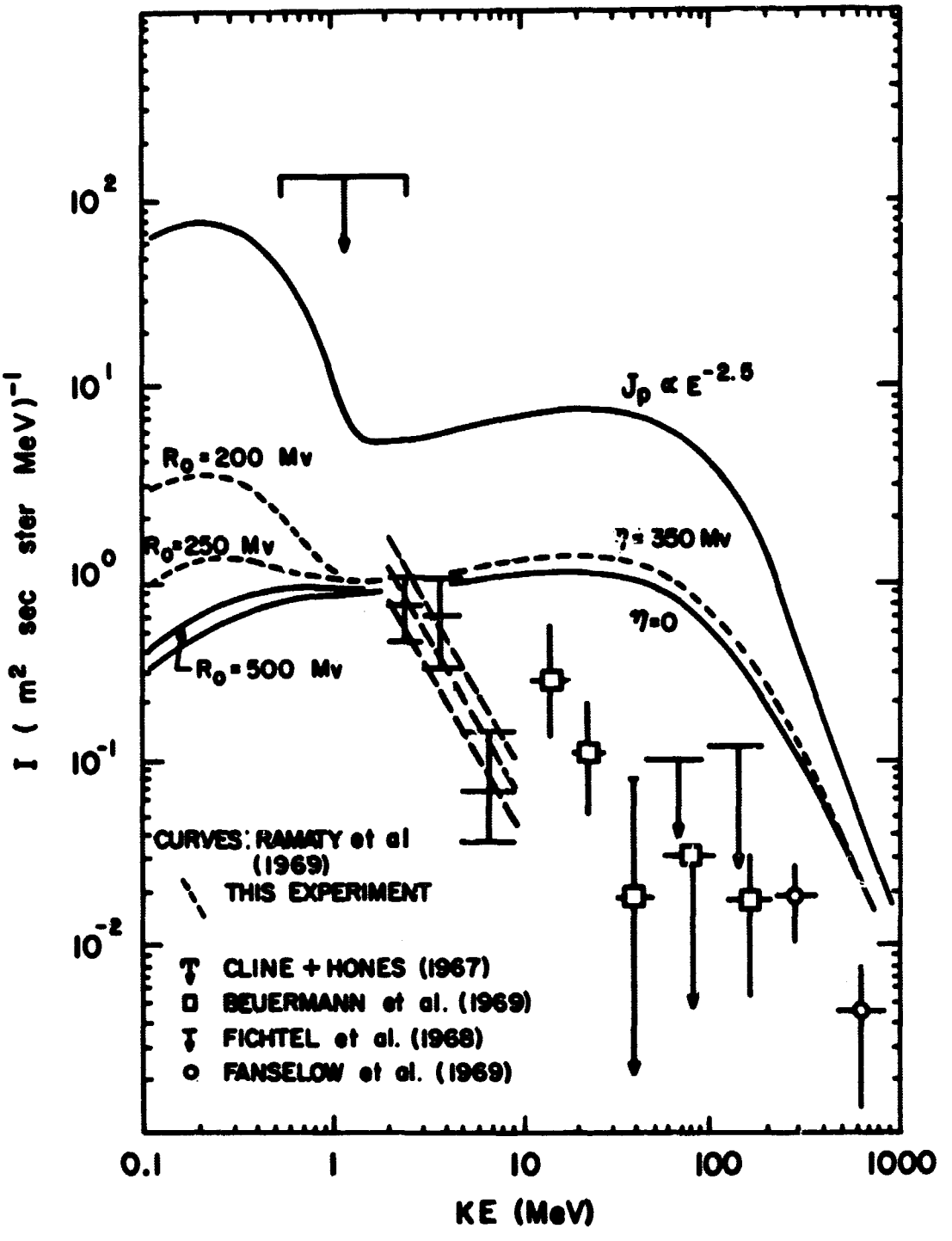

Figure 3. Positron intensity observations vs. calculated spectra

TIME VARIATIONS OF THE 4 TO 12-MEV INTERPLANETARY ELECTRON INTENSITY BETWEEN 1963 AND 1968

G. M. Simnett*, T. L. Cline and F. B. McDonald

NASA/Goddard Space Flight Center
Greenbelt, Maryland 20771 U.S.A.

ABSTRACT

The interplanetary electron intensity between 4 and 12 MeV has been monitored with the IMP-1, -3, and -4 spacecraft from November 1963 to April 1964, June 1965 to April 1967 and May 1967 to April 1969, respectively. There are a variety of types of time variations in the intensity; these include flare-associated and recurrent solar electron events, and other short-term effects, such as small quiet-time increases and Forbush decreases, superimposed on the longer-term modulation. The quiet-time intensity increases are strongly correlated with solar rotation, but are generally not coincident with increases of the low-energy proton intensity; in fact, there is frequently an anticorrelation between the two. This pattern indicates the possibility of a solar origin for the quiet-time increases. However, since the background electron intensity does undergo large Forbush decreases, not coincident with solar-flare electron events, the existence of a real solar modulation of the galactic intensity is also indicated. The overall change in the quiet-time background intensity between December 1965 at solar minimum and August 1968 is less than a factor of two, but is not interpreted as vanishingly small.

*NAS-NRC Postdoctoral Research Fellow

The study of the electronic component of the cosmic radiation has aroused considerable interest in recent years. Despite the vigorous experimental activity in this field, the origins of the electrons are not yet clearly established, although it is becoming nearly certain that the observed spectrum is composed of several different components whose relative importances are functions of energy. In the several-MeV energy region, solar production can dominate the interplanetary population following flare activity. In the absence of an electron component of obvious solar origin, the interplanetary electrons are usually assumed to be of interstellar origin; these cosmic-ray electrons are theoretically expected to be both galactic "secondaries," i.e., beta-decay electrons from excited nuclei, knock-on electrons, and meson-decay electrons from the $\pi \rightarrow \mu \rightarrow e$ process, and "primary" electrons, i.e., those which are accelerated with the nucleonic component of cosmic rays. However, at present two factors frustrate further progress towards a more complete understanding of the low-energy electron component. First, it is known that the interstellar spectrum is distorted by solar modulation as the electrons propagate into the interplanetary region. Second, since the sun is a local source of energy which is known to frequently produce energetic electrons and protons, it is important to ascertain the magnitudes of the interplanetary solar electron components, not only during the obvious occasions but at all times. Thus, the contribution of a possible quiet-time solar production must be understood in order to study both the short-term and long-term modulations of the galactic component.

The temporal behavior of the low-energy electron flux is complex in that a variety of types of effects are observed. To date, it has been possible to group most of these into the following five categories:

1) Flare-associated solar electron events, which generally display much the same characteristics as do the accompanying solar proton events, including a diffusive particle propagation and association with x-ray flares and microwave radio emission.

2) Recurrent electron events, which sometimes appear on the next solar rotation after a flare-associated event and contain electrons and protons displaying essentially the same time history. These particles are apparently stored in the same active region as that producing the original flare.

3) Quiet-time increases, which represent a new feature, can last for periods from a few days to two weeks, and can display a 27-day recurrence. The intensity may increase as much as a factor of five above the minimum quiet-time level at 1 A.U.; the energy spectra are not as steep as those observed for flare-associated increases ($\approx E^{-3}$) but can approach the value measured for the galactic component ($\approx E^{-2}$). These events are strikingly anticorrelated with low-energy proton events; it is most probably that they are of solar origin.

4) Forbush decreases, which are generally similar to those observed with high-latitude neutron monitors, except that the recovery phase for electrons is more rapid.

5) The long term or 11-year modulation of low-energy electrons. In this paper we are primarily concerned with the quiet-time intensity increases and with the long-term modulation of the galactic low-energy electrons.

Observations of the interplanetary intensity in the few-MeV energy region have been made with detectors on board the eccentric earth-orbiting satellites IMP-1, IMP-3 and IMP-4. The time periods for which the electron intensity was monitored were November 27, 1963 to May 5, 1964; June 4, 1965 to May 4, 1967; and May 24, 1967 to December 31, 1968, respectively. The first detection of the quiet-time electron energy component at these energies was made with IMP-1 (1) and solar electrons in this energy range were first unambiguously resolved with IMP-3 (2). More recently, a thorough and detailed analysis of the quiet-time spectrum was made from IMP-4 data (3); we are not concerned here with the energy spectrum but with the daily time variations of the total electron intensity between 4 and 12 MeV. From May 1967 to December 1968 the time histories of 0.3 to 0.9-MeV electrons and 3.3 to 5-MeV protons are also used for comparison.

The detector used for these measurements and its response to electrons and the background intensity have been discussed in detail in the literature (4, 3). Essentially identical instruments, employing the energy loss vs. energy technique, were flown on the three satellites having apogees of approximately 193,000 km, 250,000 km and 216,000 km. Data from IMP-1 and IMP-3 were excluded from our analysis below an altitude of 125,000 km, and data from IMP-4 were excluded below an altitude of 100,000 km. The data used for analysis are therefore not

contaminated by electrons from the earth's radiation belts. Use of the well-defined end point for stopping protons and the minimum-ionizing line for electrons allows for intercomparison of the three sets of data. Detailed comparison schemes, too lengthy to be described here, were employed to determine independently the absolute electron intensities for selected quiet times for each of the three satellites. Absolute normalizations were then made for all time periods. A plot of the resulting daily electron counting rate in the energy region 4 to 12-MeV over the periods covered by IMP-1, -3 and -4 is shown in Figure 1; a typical error for a "quiet" day with full data accumulation is indicated.

It is evident from the figure that there are many occasions when the intensity of electrons increases by an order of magnitude or greater above the general background level. The majority of these are associated directly with solar flares on the visible disk of the sun; the few exceptions are correlated with intense proton activity and are assumed to be "backside" events. Thus, there is justification for associating all the large increases with solar production of electrons. There are other less obvious instances when a smaller but significant increase does occur in coincidence with a solar flare; in such cases the expanded intensity vs. time plot leaves no doubt that flare particles are being directly observed. An example of this was the flare of July 5, 1967, when the intensity increase of electrons was observed for only a few hours so that the effect on the daily average was small. There are many other events when the intensity of electrons increases significantly above the background level for periods ranging from a few days to around two weeks. The identification of these events is subjective but the basic

criterion used was to select times when the intensity was approximately a factor of two above the running mean for either the preceding or succeeding weekly period (excluding impulsive, solar flare events). A summary of all such events is given in Table I.

The intensity increases which are not directly related to flare events can, as mentioned in the introduction, be grouped into two classes: recurrent events which sometimes appear on the next solar rotation after a flare increase, and quiet-time increases. In general, the first type contains an energetic nucleon component while the latter type is anticorrelated with low-energy proton events. The time histories of the two types tend to be similar, but are completely different from that of the typical flare-associated increase. In general, a flare event shows a very rapid rise to maximum (under 2 hours) and a power law decay; the quiet-time and recurrent electron events are more symmetrical and can last for periods as long as about 14 days. Series of quiet-time increases were observed from IMP-1 in early 1964, IMP-3 in August to October 1965 and IMP-4 in the latter half of 1967 (Table 1). Some increases in these series did reappear on a 27-day basis.

A typical superposition of the electron data on a 27-day base is shown in Figure 2 for the period August 17 to October 9, 1965; also shown are the passages of the most active calcium plage regions across the visible solar disk, a superposition of the Deep River neutron monitor results for this time period and the times of recurrent proton increases (5). We note that there is no correlation

between the recurrent electron increases and the neutron monitor intensity and that the proton increases occur at a local minimum in the electron intensity. The shaded portion of the electron intensity indicates the maximum possible contamination from a small solar flare on October 4. The events in 1966, given in Table I, are probably recurrent solar events; they all appear in coincidence with the passage across the visible solar disk of an active region which had produced a large solar flare on the previous rotation.

The 3.3 to 5-MeV proton intensity and the 0.3 to 0.9-MeV electron intensity from IMP-4 are shown in Figure 3 for comparison with the electron data. It is clear that the amount of quiet time is a very small portion of the total time, such that a cosmic-ray proton measurement made at a random moment would almost certainly be contaminated by solar protons. If we study the 4 to 12 MeV electron increases from IMP-4 in 1967 and compare them with the proton record, there is a striking anticorrelation. The electron events in September and October 1967 occur at times of very low proton intensity. They are also accompanied by very small and short-lived increases in the 0.3 to 0.9 MeV electron intensity; clearly, this effect influences an electron spectrum averaged for the total duration of an increase in such a way to make it harder. The electron events in November and December are also followed, rather than accompanied, by recurrent proton increases. We present this result as an observational fact; a solar origin of such electron increases may be inferred but it cannot be proved.

Data from IMP-3 and -4, taken at the times of large Forbush decreases which were not coincident with energetic solar electron events, are shown in Figure 4. A superposition of six events from each satellite is shown, together with corresponding superpositions of the Deep River neutron monitor results; the data were aligned at the commencement of the neutron monitor decreases. Eight quiet periods were selected at random and superpositions of the electron and neutron monitor data are also shown for comparison. A cross-correlation analysis was performed on these data and the resulting coefficients are shown in the figure. There is no doubt that the electron intensity is suppressed at the time of large Forbush decreases: it is also apparent that the electrons recover faster than the neutron monitor. The clearest examples are the IMP-3; the neutron monitor Forbush decreases during the lifetime of IMP-4 were smaller, averaging $\approx 2\%$ instead of $\approx 3\%$ for IMP-3, and the correlation is poorer. Almost zero correlation, however, is found at the quiet periods. The data used for this analysis were taken during time periods which did not include solar particle events; since the rapid decay of flare events does not appear to support the hypothesis that such particles might be stored for long periods in the interplanetary region, we contend that the positive correlation of the electrons with the neutron monitor intensity during Forbush decreases indicates a galactic origin for the background electron intensity.

Finally, we consider the change in what we believe is the galactic intensity from solar minimum, in 1965, until 1968. Averages were made of the data for

the time periods June 4 to July 31, 1965; October 10, 1965 to April 30, 1966; December 26, 1967 to March 4, 1968 and May 1 to September 24, 1968. The results are shown in Table II, in which the above intervals are designated as periods 1 - 4. An autocorrelation analysis performed on the data for period 3 showed a signal at ≈13 days and ≈27 days; since this time interval followed the intense flare activity at the end of 1967, it is reasonable to assume the presence of solar particle contamination. A similar analysis for period 2 gave no signal at 27 days. We have taken period 4 (excluding the indicated solar-active times) as representative of the modulated galactic electron intensity in 1968; if we consider periods 1 and 4, the level decreases a factor of ~1.8 from solar minimum to mid-1968. However, the high intensity observed during period 3 in early 1968, for which the possibility of solar contamination cannot be ruled out, casts some doubt on the existence of a long-term effect.

REFERENCES

1. T. L. Cline, G. H. Ludwig and F. B. McDonald, Phys. Rev. Letters, 13, 786, 1964.

2. T. L. Cline and F. B. McDonald, Solar Physics, 5, 507, 1968.

3. G. M. Simnett and F. B. McDonald, Ap. J. (to be published).

4. D. A. Bryant, G. H. Ludwig and F. B. McDonald, IRE Transactions on Nuclear Science, NS-9, 367, 1962.

5. J. J. O'Gallagher and J. A. Simpson, Phys. Rev. Letters, 16, 1212, 1966.

6. C. Y. Fan, G. Gloeckler and J. A. Simpson, Proc. of London Conf., 1, 109, 1965.

Table I

Date of Maximum	Comments
Feb. 12, '64 Mar. 11, '64 Apr. 7, '64 May 3, '64	Series of short-lived increases (2-4 Days) separated by 27 days. Not coincident with recurrent proton increases observed by Fan et al. (6).
Aug. 28, '65 Sep. 6-9, '65 Sep. 17-26, '65 Oct. 4, '65	Periodic set of increases separated by 27 days, coincident with active plage regions and not coincident with proton events observed by O'Gallagher & Simpson (5), Maximum intensity 5 x background.
Aug. 1, '66	Recurrent event in plage region MP 8413, which was the return of MP 8362 (region for July 7 event).
Oct. 4-7, '66	Recurrent event in plage region MP 8527, which was the return of MP 8484 (region for Sep. 14, event).
Oct. 19-25, '66	The increase is coincident with MP 8551, which was the third rotation of MP 8461 (region for Aug. 28 and Sep. 2 events).
Aug. 7, '67 Aug. 31-Sep. 3 '67	Increases separated by 27 days, probably associated with plage region MP 8905 and its reappearance as MP 8942. The latter increase is at a time of extremely low proton activity.
Oct. 13, '67	Not related to any solar phenomena other than that it is 27 days before the next increase in November, '67. The intensity is high for 13 days, during which time the 0.3-0.9 MeV electron intensity is high for 2 days and the proton intensity is very low.
Nov. 8-11, '67 Dec. 6-7, '67	Increases separated by 27 days, occurring at a time of high solar activity and followed by recurrent proton increases.
Dec. 28, '68	Accompanied by low-energy electrons and protons.

Table II

	Time Period	Electron Intensity (Arbitrary units)
1	June 4 - July 31, 1965	364 ± 25
2	October 10, 1965 - April 30, 1965	251 ± 14
3	December 26, 1967 - March 4, 1968 (Excluding February 8)	386 ± 25
4	May 1 - September 24, 1968 (Excluding June 6 to 11, July 5 to 15)	200 ± 18

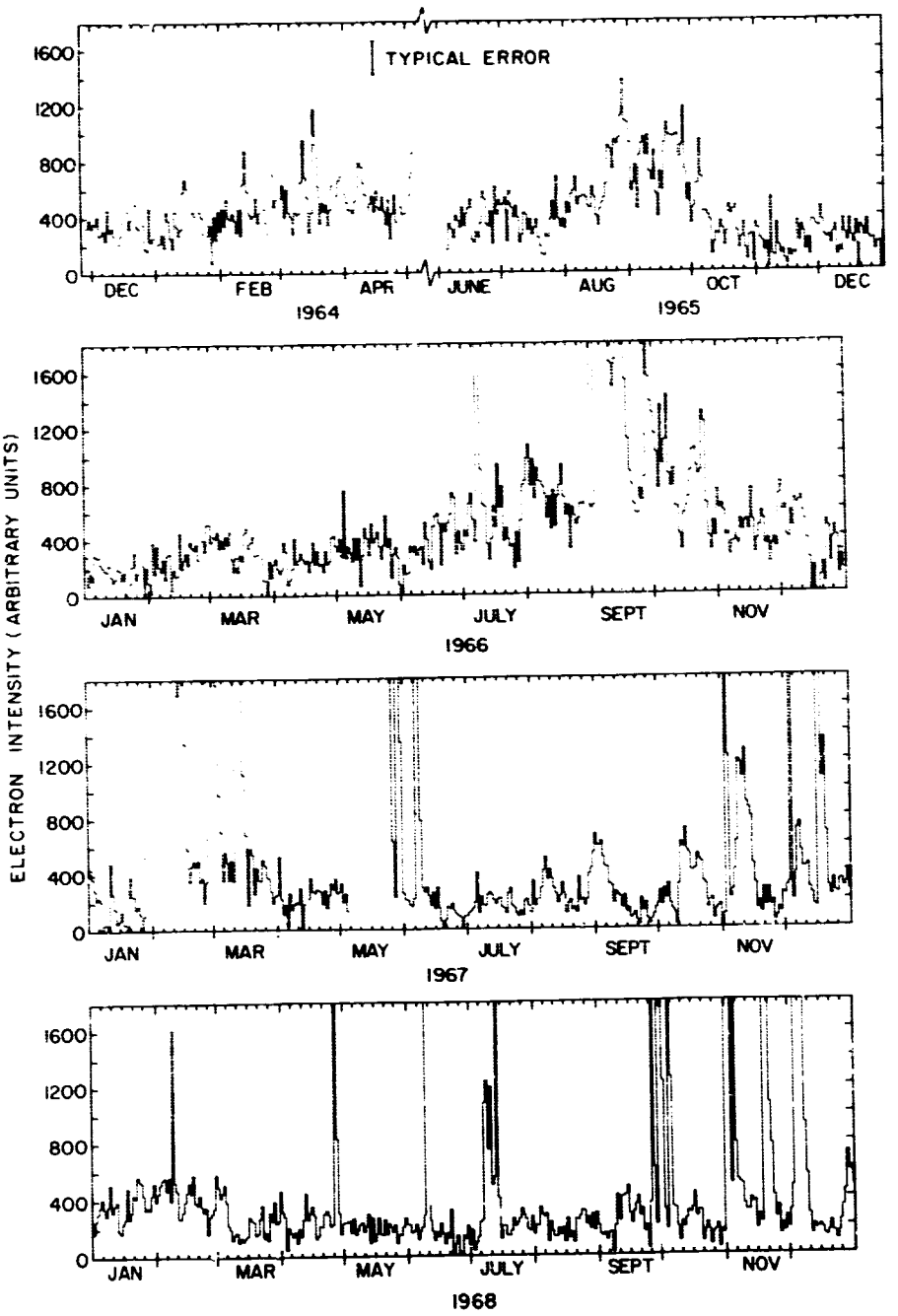

Figure 1. The 4 to 12-MeV interplanetary electron intensity observed between November 1963 and December 1968.

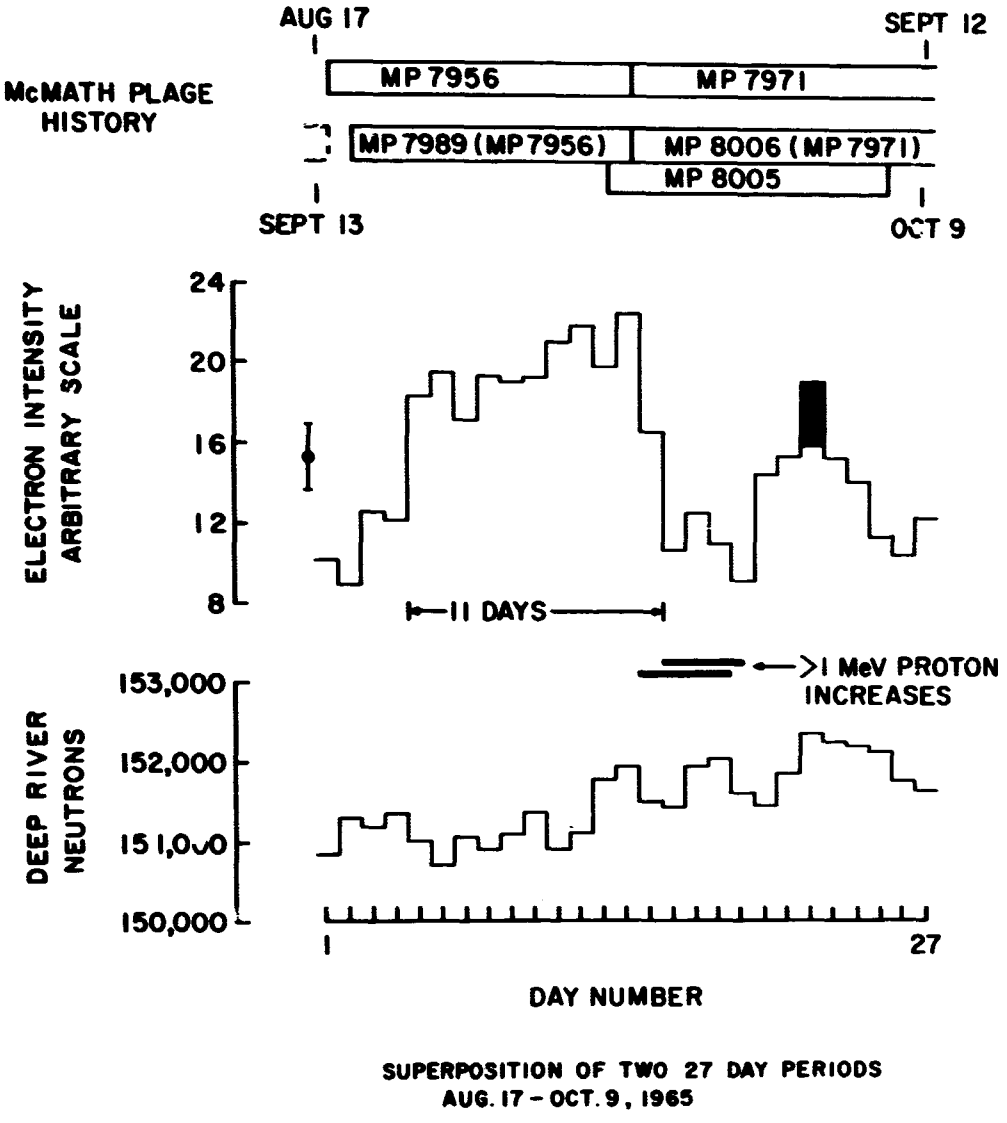

Figure 2. Correlation between the recurrent electron intensity, the Deep River neutron monitor results and the passage of large calcium plage regions across the visible solar disk.

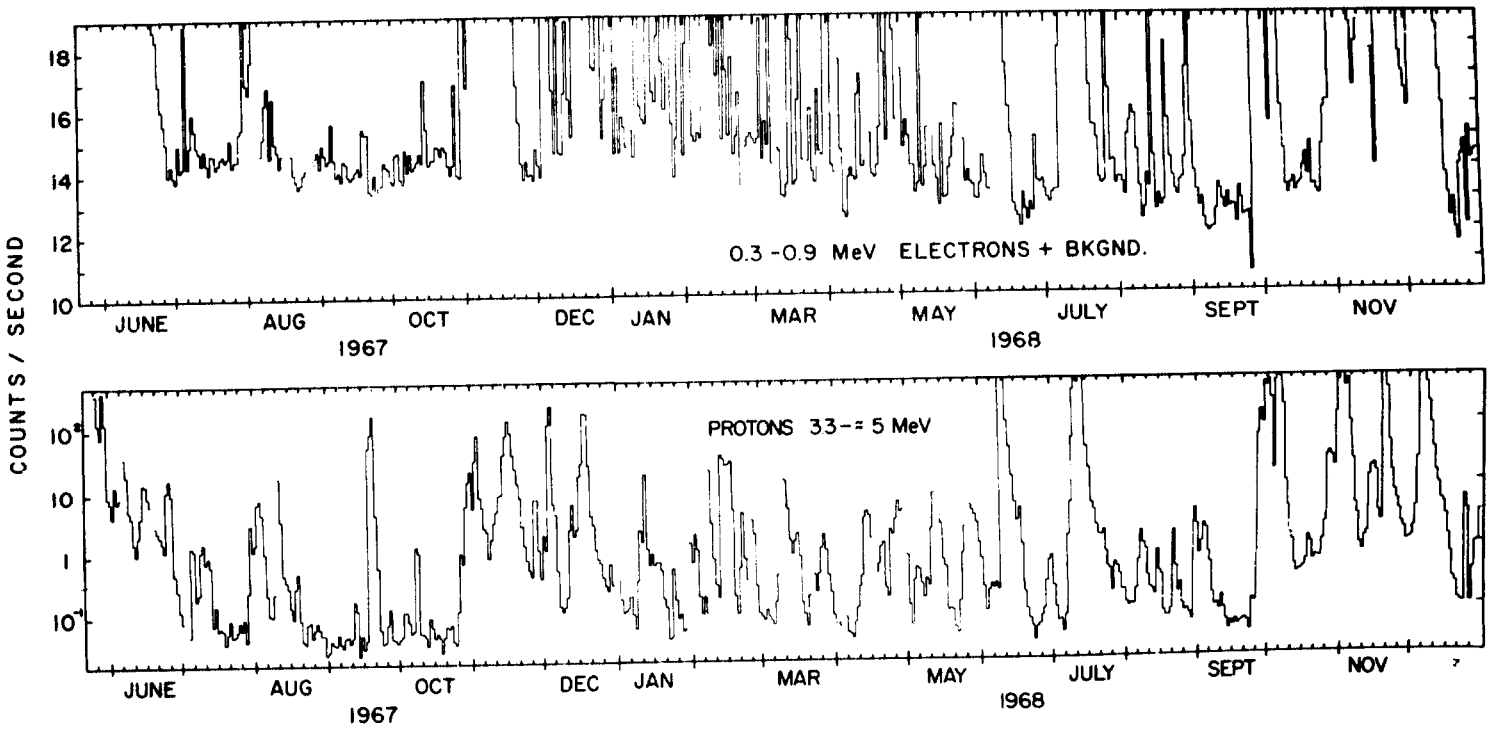

Figure 3. The intensity vs. time histories of the 3.3 to 5-MeV protons and 0.3 to 0.9-MeV electrons (plus background) for the period monitored by IMP-4; the gradual decrease of the baseline is attributed to a change in background.

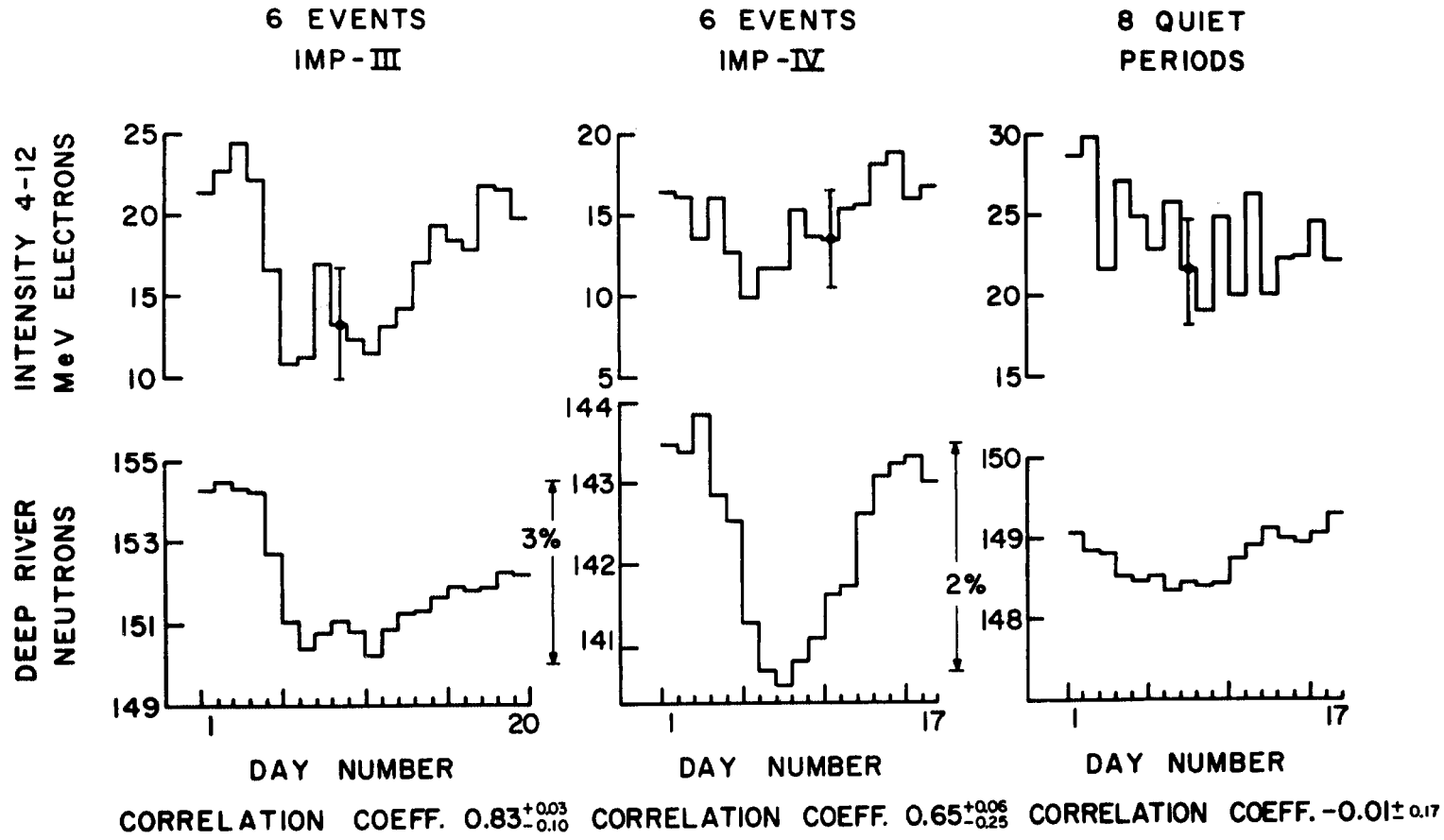

Figure 4. The correlation of the electron intensity with the Deep River neutron monitor results during large Forbush decreases; the lack of correlation at randomly selected quiet times is also shown.

LOW-ENERGY COSMIC RAY POSITRONS AND 0.51 MeV GAMMA RAYS FROM THE GALAXY

R. Ramaty and F. W. Stecker
NASA/Goddard Space Flight Center
Greenbelt, Maryland

and

D. Misra
University of Maryland
College Park, Maryland

Abstract

Large fluxes of low-energy cosmic rays in interstellar space may produce, via unstable CNO beta-emitters, large fluxes of low-energy positrons and/a detectable intensity of 0.51 MeV gamma rays. Even though on a galactic scale these cosmic-ray intensities are probably untenable since they conflict with the dynamics of the interstellar medium, they may exist on a smaller scale of the order of the stopping distances of both low-energy cosmic rays and positrons. We compare the results of a detailed calculation with direct positron measurements at the earth and we discuss the observability of the annihilation radiation above the isotropic x-ray background.

Low-Energy Cosmic Ray Positrons and 0.51 MeV Gamma Rays from the Galaxy

Measurements of the charge composition of cosmic-ray electrons in the energy range of a few MeV to several GeV (1), (2), (3) have indicated the existence of a detectable flux of cosmic-ray positrons which can best be interpreted as being of galactic origin. At lower energies, a measurement of Cline and Hones (4) has placed an upper limit on the positron flux at about 1 MeV, with a strong possibility that a significant fraction of this flux is of cosmic origin. It has been shown (5) that the measured positron flux above about 100 MeV is consistent with that expected from the decay of positive pions produced in strong interactions between galactic cosmic-rays and the interstellar gas.

Cosmic-ray positrons are produced not only from pion decay, but also from the beta-decay of unstable CNO nuclei produced primarily in relatively low-energy nuclear interactions. Since these interactions are nuclear transmutation, rather than pion-producing interactions, they involve relatively low threshold energies (of the order of 10 MeV rather than 300 MeV). Moreover, the beta-ray positrons are produced with a maximum energy of the order of 1 MeV, whereas the spectrum of pion-decay positrons peaks at about 35 MeV and decreases rapidly toward lower energies. Thus, if there exists a large flux of low-energy galactic cosmic-rays, these particles may provide the most copious source of low-energy cosmic-ray positrons. This source

then may contribute significantly to an observable flux near the earth at and below 1 MeV. Furthermore, because of their low energy, it is much more likely for beta-ray positrons to stop and annihilate in the galaxy to produce 0.51 MeV gamma-rays than the positrons from the pion decay process.

Preliminary results on positron production from CNO beta-emitters were reported by Ramaty and Misra (6) and this problem was considered in more detail by Misra (7). Estimates of positron production from the CNO process were also made by Stecker (8), in connection with galactic 0.51 MeV gamma-radiation, and by Verma (9), in an attempt to account for cosmic-ray electron measurements at low energies (10). The formal treatment of the problem of galactic positron production in connection with galactic positron annihilation and the resultant gamma-radiation was presented by Stecker (8).

In the present paper we shall summarize the unpublished calculations of Misra (7) and relate them to the problem of 0.51 MeV gamma-ray production. Because of the limited available space, we shall present a more detailed report in a separate publication. We shall discuss, however, the energetics of the problem and relate the results of our calculations to direct positron measurements at the earth and to the question of the observability of the annihilation radiation from the galaxy.

The principal positron-producing radio-nuclei, their formation reactions and threshold energies are given in Table 1, along with the

decay modes and maximum positron energies. The cross sections, the interaction and decay kinematics, and the positron losses in interstellar space are discussed in detail in the forthcoming paper, mentioned above.

The interstellar primary cosmic-ray intensities can be obtained from the solar minimum spectra by multiplying by a modulation function of the form

$$\mu = \begin{cases} \exp(\eta/R_o\beta) & \text{for } R < R_o \\ \exp(\eta/R\beta) & \text{for } R > R_o \end{cases} \qquad (1)$$

where R and β are rigidity and velocity respectively, R_o is a characteristic transition rigidity that depends on the distribution of interplanetary magnetic field irregularities, η = 350 MV (11), and we have treated R_o as a free parameter. As an extreme assumption, we have also used a cosmic-ray spectrum of the form $E_i^{-2.5}$ (power in kinetic energy per nucleon), with low-energy cutoffs, E_c, at 5, 15 and 100 MeV/nucleon.

The resultant fluxes in interstellar space, combined with the calculations of Ramaty and Lingenfelter (5) for positron production via the π-μ-e process, are shown in Figure 1, for a mean path length $x = 4 g/cm^2$, together with the available positron measurements below 1 GeV.

As can be seen, positrons with energies greater than about 2 MeV come principally from pion decay. At lower energies the relative contribution of the beta-emitters depends critically either on the

value of R_o (for η = 350 MV) or on the assumed low-energy cutoff (for a power law spectrum).

The energy densities of cosmic rays for the various cosmic-ray spectra are given in Table 2. As can be seen from Figure 1 and Table 2, unless the energy density in low-energy cosmic rays is of the order of a few tens of ev/cm^3, most of the positron flux at $\sim$ 1 MeV would come from pion decay rather than CNO beta-decay and would be small compared to the upper limit of Cline and Hones (4). If spread uniformly over the galactic disk, such energy densities lead to serious difficulties regarding the stability of the galaxy (12). On the other hand, since the ranges of both low-energy protons and positrons are short ($\sim$ 0.1 g/cm^2), the $\sim$ 1 MeV positron measurements sample only a small region of space which may not necessarily be representative of the galaxy as a whole.

For example, consider a 10 MeV proton; its range in hydrogen is 0.05g/cm^2 which, for an ambient density of n atoms per cm^3, leads to a lifetime $t \approx 2 \times 10^5/n$ years. The net streaming distance corresponding to t is $a \approx (4/3\lambda\beta Ct)^{1/2}$, where λ is the mean free path for diffusion. If λ = 1 pc, $a \approx 100/n^{1/2}$ pc. Since the rate of supernova explosions in the galaxy (volume $\approx 2 \times 10^{66}$ cm^3) is about 10^{-2} per year, in a spherical volume of radius $100/n^{1/2}$ pc a supernova would be expected to occur once every $2 \times 10^6 n^{3/2}$ years. For $n \gtrsim$ 1 atom/cm^3, this time interval is much larger than the lifetime against ionization given above. Therefore, if these protons are

produced in supernova explosions and not by more frequent events such as novae or flare stars, their intensities would exhibit sharp maxima close to the time of the explosion and decay to much lower values later on. According to Gold (13) a supernova explosion may liberate as much as 10^{52} ergs. Assuming that 50% of this is in low-energy cosmic-rays, the mean energy density for about $2 \times 10^5/n$ years over a sphere of radius $100/n^{1/2}$ pc would be $\sim 30\ n^{3/2}$ ev/cm^3. This is sufficient to produce a detectable flux of beta-ray positrons. On a galactic scale, however, the same sources of low energy cosmic rays occurring at a frequency of 10^{-2} per year would only produce an average energy density of $3/n$ ev/cm^3. For $n = 1$ this is somewhat large but not inconsistent with the overall energetics of the galaxy.

Since the large fluxes of low-energy cosmic rays are restricted to small volumes and short times, they do not conflict with observations that integrate over large distances, such as the temperature of HI clouds, based on 21 cm observations, and the density of free electrons, based on the observed spectrum of non-thermal radio emission. (The connection of these quantities with low-energy cosmic rays was discussed by Balasubrahmanyan et al. (14)). The $\sim$ 1 MeV positron measurements, however, by sampling only a small region of space corresponding to their range of 0.2g/cm^2, ($t \approx 10^5/n$ years, a $\approx 200/n^{1/2}$ pc) may provide evidence for these locally enhanced fluxes of low-energy cosmic-rays.

As can be seen from Figure 1, given a reasonable solar modulation, the positron measurements above a few MeV are all consistent with the calculated spectra from the π-μ-e process. Since the range of protons above pion production threshold is larger than $4 g/cm^2$, these spectra represent mean values over time periods comparable to the positron leakage lifetime from the galaxy. The spatial and temporal inhomogeneities discussed above which would allow large but localized low-energy cosmic-ray fluxes, do not apply to this energy domain. The positron spectrum, above a few MeV, obtained from a demodulated cosmic-ray distribution with η = 350 MV, would therefore be a good representation of the interstellar positron intensity.

We now consider the 0.51 MeV gamma-ray production from positron annihilation. The total number of positrons annihilating at or near rest per second per gram of interstellar gas, for $x = 4 g/cm^2$ and for the various cosmic-ray spectra discussed above, are given in Table 3. As an extreme case, we have computed the annihilation rates that would result from an interstellar positron flux which is of the same order as the upper limit given by Cline and Hones (4). Using a total positron intensity of 2×10^{-2} particles of 1 MeV per cm^2sec.sr we have computed a maximum annihilation rate corresponding to a positron lifetime against ionization of $10^5/n$ years, and a mean rate corresponding to an average time between supernova explosions of $5 \times 10^6 n^{3/2}$ years in

a spherical volume of radius $70/n^{1/2}$ pc. These rates are also given in Table 3.

It has been shown (8) that the positrons annihilate primarily from an S state of positronium with 75% of these annihilations producing a three-photon continuum rather than a two-photon line at 0.51 MeV. Therefore, on the average, one 0.51 MeV photon is produced for every two positrons which annihilate. Thus, the intensity of 0.51 MeV gamma-rays observed along the line of sight as a function of galactic coordinates is given by

$$I_{0.51}(l^{II},b^{II}) = Q_{T,rest}\ M(l^{II},b^{II})/8\pi \qquad (2)$$

where $M(l^{II},b^{II})$ in g/cm^2 is the amount of interstellar gas in the direction of observation. The resultant gamma-ray intensities for various directions of observation are given in Table 4. The values of $M(l^{II},b^{II})$ obtained from 21 cm observations are taken from Ginzburg and Syrovatskii (15). The values of $M(l^{II},b^{II})$ designated by "missing mass hypothesis" are based on the discussion of Stecker (16) as needed to explain the recent observations of 100 MeV gamma-rays from the galaxy (17) as due to bremsstrahlung and π°-production.

As discussed in the previous paper (8), $I_{0.51}(l^{II},b^{II})$ must be greater than 3×10^{-4} cm^{-2} sr^{-1} sec^{-1} in order to be observable above the X-ray background continuum by a detector with an energy resolution of 5 keV which is the theoretical width of the 0.51 MeV line. This intensity is therefore a reasonable lower limit on the 0.51 MeV

line intensity which must be present in order for the annihilation line to be detectable. By comparing this lower limit with the calculated intensities given in Table 4, we see that the annihilation radiation could only be detected toward the galactic center, and, with the "missing mass hypothesis", probably also as a disc average. The calculated gamma-ray fluxes, however, were obtained by assuming that the primary cosmic-ray intensities are spread uniformly along the line of sight over which the annihilation radiation is formed. Such an assumption, for the demodulated cosmic ray spectrum with η = 350 MV and R_o = 200 MV and for the power law distribution, requires a mean cosmic-ray energy density of $\sim$ 50 eV/cm^3 in order to produce a detectable annihilation line. This energy density is at least an order of magnitude higher than that allowed by the general dynamics of the interstellar medium (12). The energy requirements for the power-law spectrum with E_c = 100 MeV/nucl are smaller and therefore not necessarily inconsistent with the energy arguments mentioned above. A primary cosmic-ray spectrum of this form, however, conflicts with the H^2 and He^3 calculations (11) and possibly with the positron measurements in the 10 to 10^3 MeV region (see Figure 1), and therefore is probably not a good representation of the overall galactic cosmic-ray distribution.

We conclude that the 0.51 MeV annihilation gamma-ray intensity, produced by positrons from both pion and CNO beta emitters for a homogeneous disc model will be smaller than the observed X-ray background (18) and hence be unobservable with the presently available instrumentation.

As can be seen from Table 4, however, if the positron measurement at 1 MeV of Cline and Hones (4) is regarded as real flux rather than an upper limit and is spread uniformly along the line of sight, the annihilation line would be observable, both toward the galactic center and as a disc average. However, if these 1 MeV positrons are produced in supernova explosions and exhibit spatial and temporal inhomogeneities corresponding to their short ranges, the resultant gamma-ray flux would again be below the X-ray background and unobservable.

Since the galactic center is known to be an intense source of high-energy gamma-rays (17) and since the energy arguments that we have used do not necessarily hold for that region, the galactic center may be a detectable source of 0.51 MeV gamma rays. It may thus be more profitable to look for this radiation with a high-spatial-resolution detector than to look for a diffuse galactic flux. This argument is valid even if a diffuse flux is detectable, since as can be seen from Table 4, such a flux would still be more intense toward the galactic center.

Acknowledgment:

The authors wish to acknowledge and thank Mr. Joseph Bredekamp for programming some of the numerical calculations essential to this paper.

REFERENCES

1. T. L. Cline and G. Porreca, EOS, Trans. Amer. Geophys. Union, 308, 1969.
2. K. P. Beuermann, C. J. Rice, E. C. Stone, and R. E. Vogt, Phys. Rev. Letters 22, 412, 1969.
3. J. L. Fanselow, R. C. Hartman, R. H. Hildebrand, and P. Meyer, EFI Preprint 69-22, 1969.
4. T. L. Cline and E. W. Hones, Canadian J. Phys. 46, S527, 1968.
5. R. Ramaty and R. E. Lingenfelter, Phys. Rev. Letters 20, 120, 1968.
6. R. Ramaty and D. Misra, EOS, Trans. Amer. Geophys. Union, 50, 308, 1969.
7. D. Misra, Thesis, University of Maryland, 1969.
8. F. W. Stecker, Astrophys. and Space Sci. 3, 479, 1969.
9. S. D. Verma, Ap. J. 156, L79, 1969.
10. G. M. Simnett and F. B. McDonald, Ap. J., in press, 1969.
11. R. Ramaty and R. E. Lingenfelter, Ap. J. 587, 1969.
12. E. N. Parker, Ap. J. 145, 811, 1966.
13. T. Gold, Nature, 221, 25, 1969.
14. V. K. Balasubrahmanyan, E. Boldt, R.A.R. Palmeira, and G. Sandri, Canadian J. Phys. 46, S633, 1968.
15. V. L. Ginzburg and S. I. Syrovatskii, The Origin of Cosmic Rays, Macmillan Comp., N. Y., 1964.
16. F. W. Stecker, Nature, 222, 865, 1969.
17. G. W. Clark, G. P. Garmire, and W. L. Kraushaar, Ap. J. Letters 153, L203, 1968.
18. A. E. Metzger, E. C. Anderson, M. A. Van Dilla, and J. R. Arnold, Nature, 204, 766, 1964.

19. C. E. Fichtel, T. L. Cline, and D. A. Kniffen, Bull. Amer. Phys. Soc., 13, 1710, 1968.

Table 1

Beta Emitter and Decay Mode	Maximum Positron Energy (MeV)	Production (Mode)	Threshold Energy (MeV)
$C^{11} \rightarrow$	0.97	C^{12} (p, pn) C^{11}	20.2
$B^{11} + \beta^+ + \nu$		N^{14} (p, 2p2n) C^{11}	13.1
		O^{16} (p, 3p3n) C^{11}	28.6
$N^{13} \rightarrow$	1.19	N^{14} (p, pn) N^{13}	11.3
$C^{13} + \beta^+ + \nu$		O^{16} (p, 2p2n) N^{13}	5.54
$O^{14} \rightarrow$	1.86	N^{14} (p, n) O^{14}	6.4
$N^{14} + \beta^+ + \nu$			
$O^{15} \rightarrow$	1.73	O^{16} (p, pn) O^{15}	16.54
$N^{15} + \beta^+ + \nu$			

Table 2

Cosmic Ray Energy Density (eV/cm^3)

Solar Minimum	η = 350 MV $\left(E \geq 5 \frac{MeV}{Nucl}\right)$		Power Law		
	R_o = 500 MV	R_o = 200 MV	$E_c = 100 \frac{MeV}{Nucl}$	$E_c = 15 \frac{MeV}{Nucl}$	$E_c = 5 \frac{MeV}{Nucl}$
0.5	0.6	57	3.1	17	50

Table 3

Positron Annihilation Rates ($g^{-1}\ sec^{-1}$)

Solar Minimum	η = 350 MV		Power Law		$j_+ = 2 \times 10^{-2}\ cm^{-2}\ sec^{-1}\ sr^{-1}$	
	R_o = 500 MV	R_o = 200 MV	$E_c = 100\ \frac{MeV}{Nucl}$	$E_c = 5\ \frac{MeV}{Nucl}$	Mean	Maximum
1.1×10^{-3}	1.8×10^{-3}	4.3×10^{-2}	3.3×10^{-2}	1.3×10^{-1}	$\frac{2.2 \times 10^{-2}}{n^{5/2}}$	0.5

Table 4

	Solar Minimum	η = 350 MV		Power Law		$j_+ = 2 \times 10^{-2}$ cm^{-2}sec^{-1}sr^{-1}	
		R_o = 500 MV	R_o = 200 MV	$E_c = 100 \frac{\text{MeV}}{\text{Nucl}}$	$E_c = 5 \frac{\text{MeV}}{\text{Nucl}}$	Mean	Maximum
Average (including Halo) (21 cm) $\frac{1}{4\pi}\int d\ell^{II} \sin b^{II}\, db^{II} \times M(\ell^{II}, b^{II}) \simeq 1.6 \times 10^{-3}$	7.0×10^{-8}	1.1×10^{-7}	2.8×10^{-6}	2.1×10^{-6}	8.3×10^{-6}	$\frac{1.4 \times 10^{-6}}{n^{5/2}}$	3.2×10^{-5}
Anticenter (21 cm) $M(\pi, 0) \simeq 1.2 \times 10^{-2}$	5.6×10^{-7}	8.6×10^{-7}	2.1×10^{-5}	1.6×10^{-5}	6.2×10^{-5}	$\frac{1.0 \times 10^{-5}}{n^{5/2}}$	2.4×10^{-4}
Galactic Center (21 cm) $M(0, 0) \simeq 6 \times 10^{-2}$	2.7×10^{-6}	4.3×10^{-6}	1.0×10^{-4}	7.9×10^{-5}	3.1×10^{-4}	$\frac{5.3 \times 10^{-5}}{n^{5/2}}$	1.2×10^{-3}
Disc Average (missing mass hypothesis) $\frac{1}{2\pi}\int d\ell^{II} M(\ell^{II}, 0) \simeq 6 \times 10^{-2}$	2.7×10^{-6}	4.3×10^{-6}	1.0×10^{-4}	7.9×10^{-5}	3.1×10^{-4}	$\frac{5.3 \times 10^{-5}}{n^{5/2}}$	1.2×10^{-3}
Galactic Center (missing mass hypothesis) $M(0, 0) \simeq 0.2$	8.8×10^{-6}	1.4×10^{-5}	3.4×10^{-4}	2.6×10^{-4}	1.0×10^{-3}	$\frac{1.7 \times 10^{-4}}{n^{5/2}}$	4.0×10^{-3}

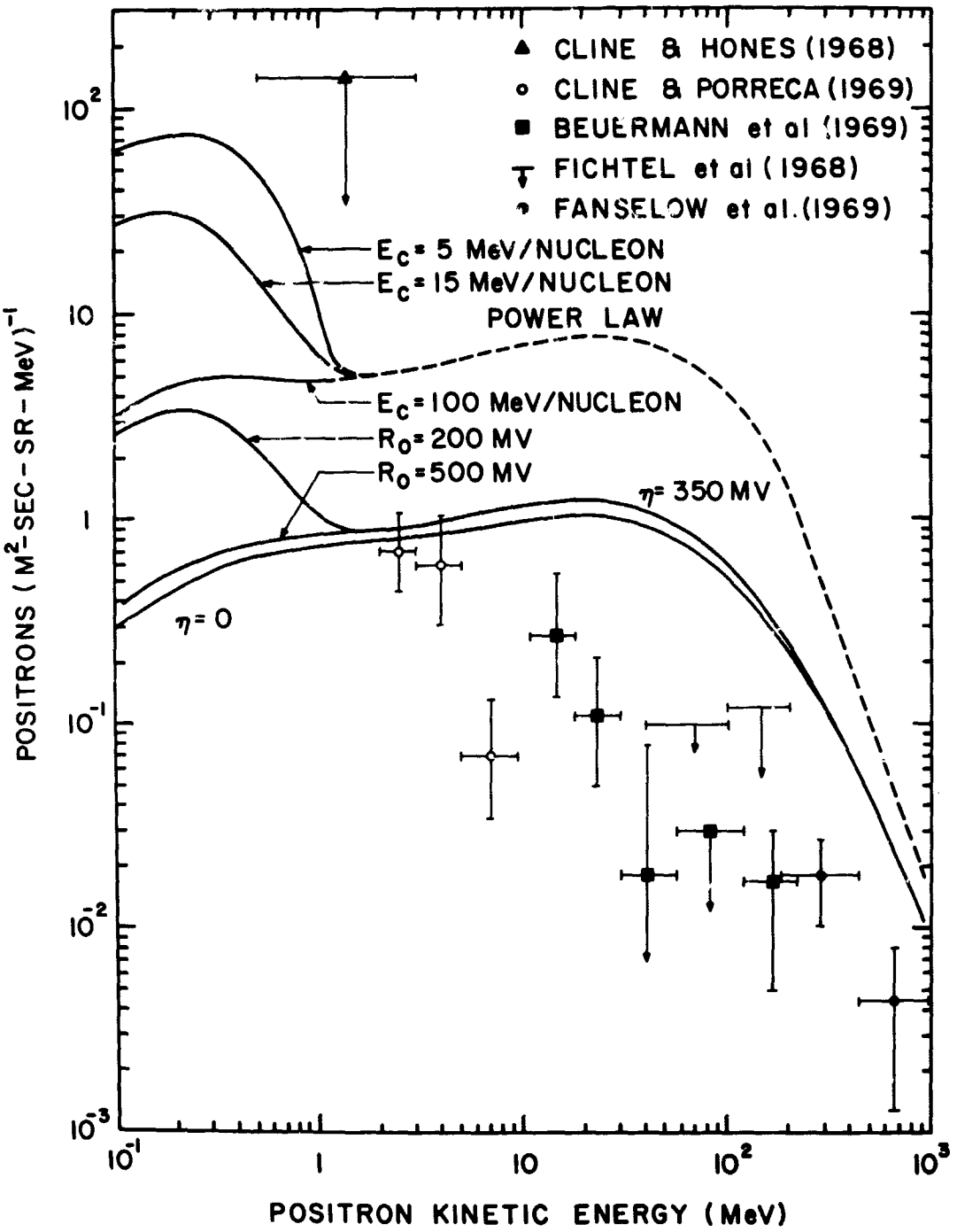

Figure 1. Positron intensities in interstellar space together with the available positron measurements below 1 BeV. (Cline and Porreca (1), Beuermann et al. (2), Fanselow et al. (3), Fichtel et al. (19)).

INTERPLANETARY POSITRONS NEAR 1 MeV FROM OTHER THAN THE $\pi \rightarrow \mu \rightarrow e$ PROCESS

T. L. Cline
NASA/Goddard Space Flight Center
Greenbelt, Maryland 20771 U.S.A.

and

E. W. Hones, Jr.
Los Alamos Scientific Laboratories
Los Alamos, New Mexico 87544 U.S.A.

ABSTRACT

Evidence is presented for a spectral component of interplanetary positrons separate from that produced by the decay of interstellar mesons from cosmic-ray interactions. Results from observations made with the OGO-3 satellite indicate the detection of $\gtrsim$ 0.5 MeV positrons with a differential intensity near 100 $m^{-2}sec^{-1}ster^{-1}MeV^{-1}$, two decades higher than the maximum expected from cosmic-ray meson production. Data, accumulated for nearly 2 years, have been examined for the existence of temporal or spatial variations; accelerator exposures of the detector have also been made in order to determine if the particles observed in space might be local secondaries. To date, there is no indication of any solar or geophysical production mechanism, or effect local to the detector, which would account for the observed positron rate. The observed cosmic-ray positron intensity, taken to be of cosmic-ray origin, is compared with the calculated values for interstellar beta emission by cosmic-ray excited nuclei; qualitative agreement exists only if a high, possibly local, low-energy

cosmic-ray intensity is used. A heliocentric acceleration or some quite different source may instead be required to provide the observed intensity.

The investigation of interplanetary positrons and electrons of energies up to a few MeV is one of the more recently developed cosmic-ray particle studies. This component, which forms the lowest-energy cosmic radiation, is characterized by particles which have the same velocities as most cosmic-ray protons while having rigidities orders of magnitude lower. Thus, such electrons are certainly subject to solar modulation effects unlike those influencing other cosmic rays. Further, their origins can be assumed to be different not only from those of nuclei but also from those of higher-energy, 0.1 to 10 BeV, electrons. That is, in addition to the pion-decay and directly accelerated cosmic-ray electrons included in this energy interval, particles of a few MeV may certainly be produced by other characteristic sources. There may be galactic primary electrons at these low energies. Possible components of galactic secondaries certainly include knock-on electrons and beta-decay positrons and electrons, including neutron-decay electrons, and perhaps include cascade positrons and electrons and compton and inverse-compton electrons. Finally, there is the remote possibility of the mixing of plasma and antiplasma well outside the solar system, allowing positrons to propagate to detection. Complicating the problems of the origins and modulations of the low-energy electrons and positrons is the question of galactic propagation, storage and escape, as a function of energy. Within the interplanetary medium there may also be low-energy electrons and positrons

from a solar electric-field acceleration or deceleration, and quiet-time solar electron production, quite apart from the well-known solar flare and recurrent beam particles. Thus, the challenging question of the interplanetary electrons and positrons of up to a few-MeV energy is quite separate from that concerning higher-energy particles, and its resolution promises to provide a considerable amount of information not otherwise attainable.

In this paper we discuss an experiment flown in interplanetary space to search for low-energy positrons. A description of the detector, some preliminary data and a brief discussion of the results were previously published (1). In this paper we outline efforts, made possible with over 1.5 years of data, to determine the origin of the unexpectedly high, apparent intensity of >0.5-MeV positrons encountered. Studies of the intensity vs. time, location and aspect were carried out and detector background evaluations were made in order to conduct a control experiment to fix the genuine interplanetary flux. To date, there is no indication that the positrons are not really interplanetary in nature.

The detector, which has been orbiting on the OGO-3 satellite since June 1966, can be briefly reviewed as follows. As illustrated in Figure 1a, particles can enter the central scintillator 'C' only from within the collimated aperture without registering in one of the anticoincidence scintillators 'P'. If a positron comes to a stop in the central scintillator, there is a certain probability that its annihilation quanta will enter the gamma-ray spectrometers 'A' and 'B', and be absorbed so as to cause a coincidence of 0.51-MeV energy-loss pulses in the

$ABC \cdot \bar{P}$ logic mode. All pulse-height pairs are transmitted twice, for complete redundancy of data. Figure 1b shows a sample plot of the intensity vs. A vs. B pulse heights taken with that logic mode in interplanetary space, clearly indicating the coincident 1/2-MeV by 1/2-MeV peak near the center of the grid. This value corresponds to several hundred positrons $m^{-2}sec^{-1}ster^{-1}$ into the detector aperture. For the exploratory study contemplated, the apparatus was not designed to have detailed spectral resolution but to specialize on selecting and identifying positrons out of presumably higher intensities of cosmic radiations and cosmic-ray secondary effects local to the detector. Thus, only two energy bins are used; the three-fold coincidence mode $ABC\bar{P}$, corresponds to 0.5 to about 2.5-MeV kinetic energy, while the two-fold $AB\bar{P}$ mode is sensitive to positrons down to nearly zero kinetic energy. Altogether four independent modes of data collection are used to evaluate the detector operation: both spectrometers are gated whenever (i), a 3-fold, or (ii), a 2-fold, coincidence occurs, as indicated above, and also whenever (iii), either single spectrometer is in coincidence with the central crystal or (iv), either single spectrometer registers a single event. Thus, random and coherent coincidence effects can be determined.

A variety of circumstances may be considered to evaluate possible background sources of events which imitate genuine interplanetary positrons; they are much the same as those production schemes previously outlined for possible cosmic-ray positron origins. In the absence of trivial electronic effects such as random coincidences, those background possibilities which may concern us are pion

production, positive beta emission from excited nuclei and cascade showers, which may produce positrons in the detector, and local annihilation radiation in coherent coincidence which may masquerade as positron events.

1). Pion production and subsequent positron creation in the detector cannot account for the observed intensity (even though some of the higher-energy positrons lose energy by bremsstrahlung so as to stop or annihilate in flight), since the observed positron intensity is such a large fraction of the total high-energy cosmic-ray intensity. 2). Beta emission in the detector, minimized by the use of beryllium instead of aluminum for the housing, also appears to be inadequate. Various materials in the detector, such as carbon in the scintillators, can be excited so as to beta decay, but all calculations indicate that this effect is much too small. Since nuclear excitation is accomplished by low-energy protons in the 10 to 100-MeV region, as opposed to 1 to the 10-BeV region as for pion production, this effect should be enhanced by the presence of solar protons if it is responsible for the detected flux; a study of the decay phases of events in 1966 and 1967 showed no apparent positron intensity increase. Further, the detector was exposed to a 42-MeV proton beam from the NRL cyclotron and an upper limit of $\approx 10^{-4}$ was established for detector positron enhancement at that proton energy value; the flux of low-energy protons at solar quiet-times is definitely insufficient to account for the observed position rate in terms of positive beta production. 3). Soft cascade showers, created throughout all material exposed to cosmic radiation, can be eliminated. Background of this sort was minimized by flying the

instrument on the far edge of the solar paddle, several meters from the satellite body and pointed away from all material. The flux of secondaries at the detector corresponds to only a few grams cm^{-2} equivalent of atmospheric background but it is incident only on the side of the instrument. A detailed estimate was made of their contribution to the observed positron rate, taking into account the geometry of the detector; it was also found to be inadequate, considering the narrow slice of the possible spectrum involved, 4). Coherent gamma-ray coincidences which may appear to be single positrons, can occur in cascade shower events, both because a single photon can produce a compton electron in one spectrometer and scatter into the other, and because multiple-photon shower fronts within such small distances are common. If coherent coincidences were causing most of the events, however, the $ABC\bar{P}$ pulse grid would be a similar pattern to the $AB\bar{P}$ grid reduced only in absolute intensity. Instead, within the 3-fold pulse grid, the 1/2 MeV x 1/2 MeV peak is well enhanced over the background relative to its strength in the 2-fold pulse grid; selectively stringent coincident requirements could not produce this effect unless positrons were being preferentially selected. Further, the ratio of the intensity of apparent positrons with single gamma-ray detection in the $AC\bar{P}$ mode to that for dual gamma-ray detection in the $ABC\bar{P}$ mode is compatible with stopping positrons. We conclude that the evidence for the positive identification of interplanetary positrons is too strong to assume that it is caused by some background effect yet to be found.

Studies of temporal and spatial variations in the intensity have been made to determine if all observed are consistent with cosmic-ray origin. 1). In

particular, the circumstance of the failure of the on-board stabilization of the OGO-3 satellite less than two months after launch made possible taking data with the detector spinning and with knowledge of the celestial coordinates corresponding to each particle event, accurate to within an angle smaller than the aperture of the detector. The satellite orientation data were made available to us on a mass-production basis nearly two years after the spinning mode commenced; these data were used to determine the solar-ecliptic coordinates of each event satisfying all requirements for positron identification, i.e., 425 to 575-keV energy loss in A and in B, using the $ABC\bar{P}$ mode. In a study in the summer of 1966 with the appropriate orientation, the analysis showed no evident preference for the ecliptic plane or for its north pole direction, to within 30 percent. At present, these studies are being improved in accuracy and extended to investigate possible interplanetary field-direction correlations. 2). Positron data were also studied vs. orbital position relative to the Earth. Each orbit was broken into 16 sections and orbits were grouped for periods of time for differing sun-earth-apogee angles, allowing studies of the intensity of positrons vs. distance from the Earth to be made for the leading and trailing regions of the transition region. Results to date indicate no statistically meaningful intensity variation with distance from the Earth. Similar studies, made with the IMP > 3-MeV electron data have shown that interplanetary electrons also have constant intensities from beyond the shock front down to the edge of the trapped radiation (unpublished). 3). A time history of the quiet-time electron intensity is as yet

incomplete because of technical problems with the raw data; however, selected quiet-time monthly averages show no significant variation. All three results are consistent with the behavior of the few-MeV interplanetary electrons, but they do not prove that the positrons are properties of the interplanetary medium. Of course, if the positrons are isotropic and roughly constant in time for two years, as they might well be if they are cosmic-ray in origin, then the existence of a control experiment (analogous to anisotropy in astronomical observations) is without possibility.

A solar origin for the particles seems unlikely: secondaries to cosmic-ray interactions at the sun would be less intense at 1 AU than those seen from near the top of the atmosphere. Further, there is no solar-ecliptic anisotropy, which might be evident to some degree if they were all streaming outwards. We are thus led to the contention that they are cosmic-ray positrons. As Ramaty et al. discuss in the accompanying paper (2), an intensity of this sort can be created by beta decay only if the low-energy proton intensity is rather high. Comparison with OGO-5 data on positrons in the region above 2 MeV (3) suggests that beta emission is a compatible explanation; a sharp cutoff in the intensity is seen between ≈ 0.5 MeV, where the positron to electron ratio is so high, and the >2-MeV region where it is very low, as illustrated in Figure 2. Certainly all the explanations invoking other secondary processes are ruled out by this property of the spectrum.

We wish to thank C. Thomas and H. Costlow for their great assistance with the detector calibration and preparation, G. Porreca for the electronic design and implementation, and W. Andersen, C. Cattell, and Mrs. J. Holloway for assistance with the data processing.

REFERENCES

1. T. L. Cline and E. W. Hones, Jr., Can. J. Phys., 46, S527-529, 1968.

2. R. Ramaty, F. W. Stecker and D. Misra, Budapest Conference, (1969).

3. T. L. Cline and G. Porreca, Budapest Conference, (1969).

4. G. M. Simnett and F. B. McDonald, to be published in Astrophys. J. (Goddard preprint X-611-68-450).

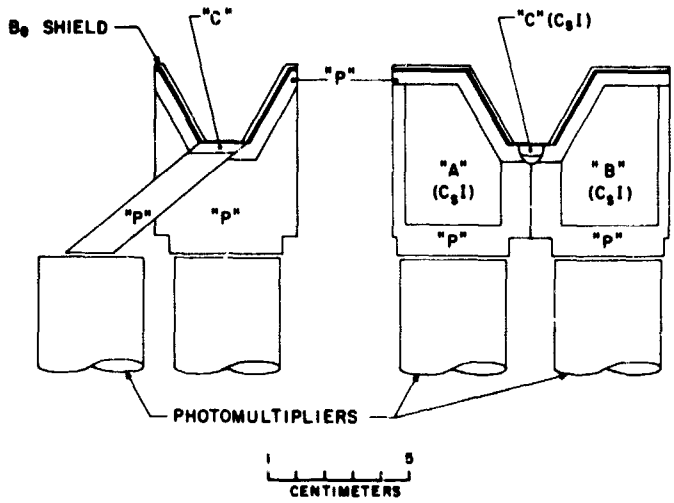

0	1	4	6	5	2	0	4	3	1	2	0	1	1	0
0	2	3	7	9	4	10	4	7	0	1	1	1	2	1
0	0	4	3	7	2	2	3	1	1	0	1	3	1	0
0	1	10	7	13	5	9	7	4	2	3	0	1	0	2
0	4	17	12	9	5	14	19	7	2	4	1	1	1	0
0	3	21	26	19	11	30	28	11	4	1	4	1	1	4
0	4	26	33	28	24	32	50	22	9	2	4	1	1	2
0	6	28	26	26	17	34	33	19	9	7	2	5	4	0
0	3	30	30	20	19	18	23	16	11	7	3	2	8	3
0	14	39	33	28	19	17	15	14	8	6	2	6	4	3
?	21	55	54	35	23	20	25	17	10	9	6	4	10	4
0	34	120	58	53	34	34	38	33	15	9	10	7	5	7
2	96	353	145	83	37	32	43	21	18	9	8	2	9	11
3	1323	1312	126	41	30	23	24	19	10	4	4	5	2	5
45	2229	1	0	1	0	0	0	0	0	0	0	0	0	0

A ↑

→ B

Figure 1. Schematic of the detector and a sample data grid

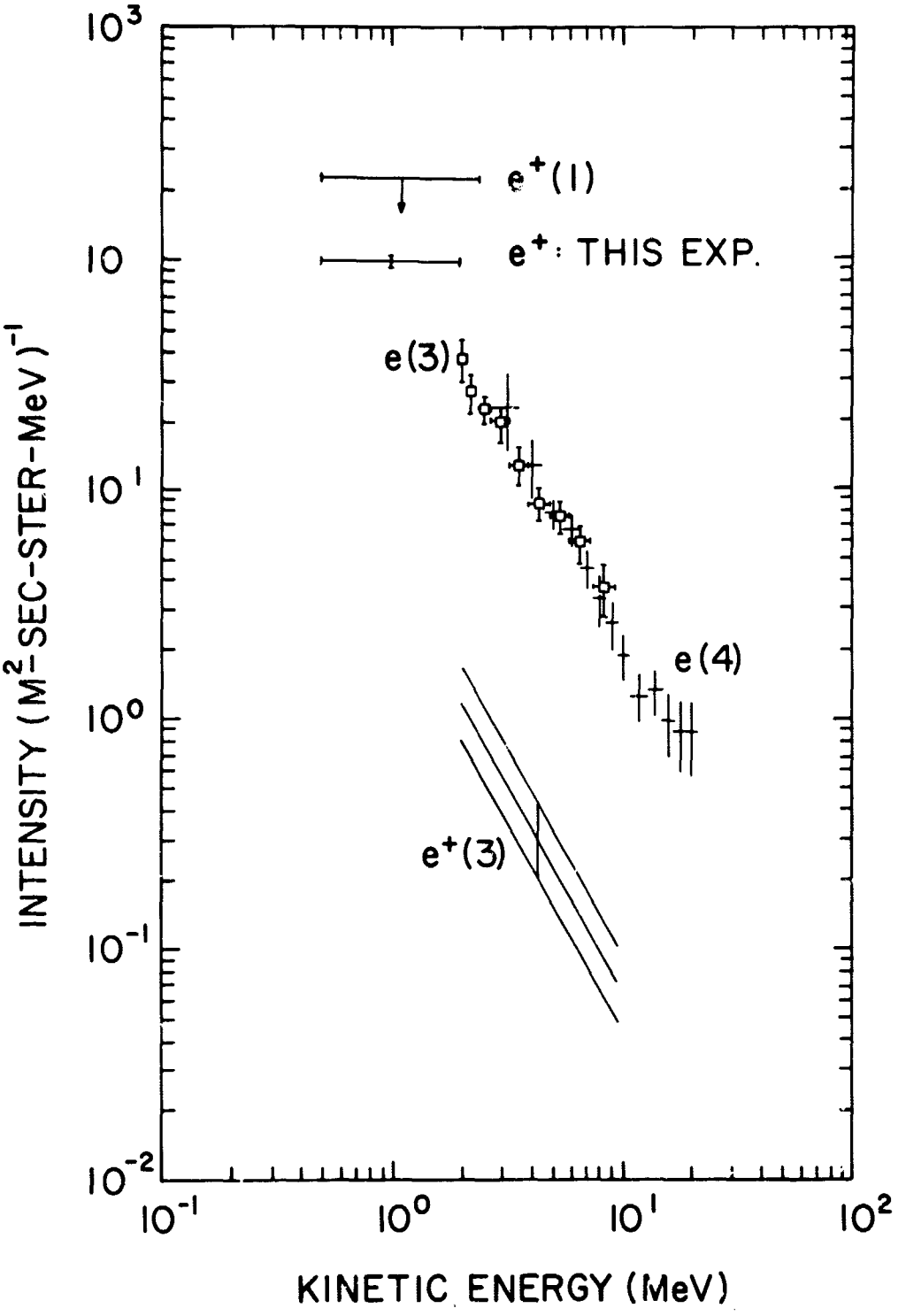

Figure 2. Spectra of interplanetary positrons and electrons below a few MeV, including data from Simnett and McDonald (4) and Cline and Porreca (3)

OG-31

COSMIC-RAY POSITRONS AND NEGATRONS OF ENERGIES 10 TO 250 MeV AT 85° GEOMAGNETIC LATITUDE

D. A. Kniffen, T. L. Cline and C. E. Fichtel

NASA/Goddard Space Flight Center
Greenbelt, Maryland

ABSTRACT

Measurements of the differential intensities of cosmic-ray positrons and negatrons were carried out in 1967 and 1968 with balloon flights from Resolute, Canada, near the north geomagnetic pole. The detector used consisted of a magnetic spectrometer incorporating counters and digitized spark chambers; it is capable of identifying incoming electrons and of separating positrons from negatrons from 20 to 250 MeV/c. The 25 August 1967 flight at 2.25 g cm^{-2} atmospheric depth, yielded the following upper limits, expressed in particles m^{-2} sec^{-1} $ster^{-1}$ MeV^{-1}:

	e^+:	e^-:	$e^+ + e^-$
35 to 110 MeV:	<0.08	<0.03	<0.09
110 to 220 MeV:	<0.07	<0.05	<0.11

The 31 August 1968 flight was made with the detector modified by the addition of a gas Cerenkov counter and with a larger geometric factor. Its results also failed to yield measurable intensities of positrons and of negatrons partially because of an instrument malfunction which made the net area-solid angle-collecting time factor similar to the previous year. These findings are compared with the other available results from cosmic-ray positron and negatron experiments in the

energy region appropriate to interstellar meson production. It is shown that there is considerable depression of the expected positron intensity presumably by solar modulation effects throughout the entire energy range examined.

INTRODUCTION

The electronic component of the cosmic radiation is becoming the subject of one of the most interesting primary cosmic-ray studies. Through theoretical considerations, the measured differential intensities of positrons and negatrons can be directly linked to a number of important astrophysical quantities. Experimentally, the spectra both of positrons and of negatrons appear to exhibit a considerable amount of structure, so that we can expect detailed measurements to be very productive. In the intermediate 10 MeV to 10 BeV region, it is possible to calculate the expected intensity of cosmic-ray positrons originating from the decay of pions formed in interaction of cosmic rays with interstellar material (1). Since this process is expected to be the only significant source of positrons in that energy interval, and since it depends on the cosmic-ray proton spectrum only in the high-energy region where it is both well-known and relatively free of solar modulation, the positron intensity above 10 MeV outside the solar system is believed to be accurately inferred. Thus, comparison of the interplanetary positron energy spectrum with the calculated intensity will yield an estimate of the absolute energy dependence of the solar modulation at 1 AU from the sun for particles in the rigidity and velocity region covered, i.e., electrons above 10 MeV. In addition, assuming that the intensities of negative and positive

electrons are modulated by the same amount at these energies, the interplanetary negatron intensity from sources other than the decay of pions produced in collisions of cosmic-rays with interstellar matter can be calculated.

In the experiment described here, we have undertaken to measure separately the spectra of positrons and negatrons in the intermediate energy region appropriate to secondary meson production and to primary electron acceleration. A number of measurements made in recent years (2), (3), (4), (5), (6), (8) have already indicated that the positron to electron ratio in the energy range from .5 to 10 GeV is incompatible with the hypothesis of meson production as the only source of electrons; that is, those observations have found a considerable excess of negatrons, as compared with the expected e^-/e ratio from interstellar meson production of $\lesssim 0.5$. This initial result pointed to the need for intensive and detailed measurement of the charge ratio as a function of energy to quantitatively describe the contribution to electron production by each possible source. To date, however, the spectrometers required for the measurement in the energy region above 10 or 20 MeV have been too massive for launch on typical scientific satellites, while balloon measurements, usually conducted from the locality of Ft. Churchill, Canada, have suffered from the problems of return albedo, as well as from atmospheric contributions.

The goal of our experiment was to make detailed measurements of the positron and negatron spectra in the critical energy region from 20 to 250 MeV, in which the differential positron intensity should have its peak. To accomplish

this objective a new instrument, employing a digitized spark chamber with a direct link to the ground by telemetry, was flown from Resolute, NWT, Canada, a location immediately adjacent to the north magnetic pole where the albedo problem should not exist. In this report we wish to outline our results from the first two balloon flights.

APPARATUS

The instrument used in the Resolute balloon flights is shown in cross section form in Figure 1 in its 1968 configuration. Common to both the 1967 and 1968 detectors is the use of a permanent magnet for deflecting the incident particles and the arrays of digitized spark chambers for obtaining the trajectory of each particle. A scintillation detector and Cerenkov counter telescope is used to select incoming particles appropriately and trigger the instrument. The spark chambers are digital in nature using wires with magnetic-core readout; all data are thus capable of being directly telemetered. The particle trajectory information provided by this device is sufficiently accurate not only to identify the overall angular deflection in the magnetic field, but also to allow an accurate calculation of the integral of the field times path-length product for each trajectory, taking into account the details of the magnetic field structure. Several features of the instrument were changed between the two flights. The earlier detector, flown in 1967, used a lucite Cerenkov counter to select downward moving high energy particles (e.g. protons above 320 MeV) and required a coincidence between the Cerenkov counter and the two scintillation counters indicated. This

arrangement selected all particles within the desired collimation cone, but did allow some small-angle scattering in the central scintillator. The second detector minimized the material in the particle path by employing a scintillator in the anticoincidence mode, with a hole slightly smaller than the magnet gap. Electrons then pass through the system with as little Coulomb scattering as possible. The requirement for triggering purposes was a pulse from the gas Cerenkov counter at the top, and one from the solid Cerenkov counter at the bottom, with the central scintillator in anticoincidence. The incorporation of the gas Cerenkov counter greatly reduced the number of relativistic protons and heavier cosmic rays which were accepted by the telescope logic. Although these particles possess rigidities too high to be confused with electrons, their inclusion decreases the telemetry time available for electron analysis. The magnets differed in the two detector systems; the second one yielded a larger geometric factor and allowed measurements to be made to lower energies. The properties of the two detector systems are summarized in Table I.

The wire-grid spark chambers have a number of important advantages. Not only does the wire-grid system allow for digitization and hence straightforward telemetry of the data, but it eliminates the necessity for continuous plate or foil electrodes; thus, the amount of material in the active volume is reduced to a minimum. In this way electron scattering is reduced within the region in which the deflection is being measured, making possible the cleanest possible measurement of each particle's rigidity. In addition, since the chambers

Table I

Properties of the Detector Systems

	Flight 1 August 1967	Flight 2 31 August 1968
Geometric Factor	2.7 cm^2 sr	6.6 cm^2 sr
Proton Threshold	320 MeV	13.8 BeV
Electron Threshold	4 MeV	7.5 MeV
$\int B dl$	31.5 Gauss-cm	14.5 Gauss-cm
Coincidence Mode	$A \cdot B_2 \cdot C_2$	$C_1 \cdot A_2 \cdot \overline{B}_2 \cdot C_2$

Notes: C_1 = gas Cerenkov Counter
B_2: Converted from coincidence counter (1967) to anticoincidence counter (1968). See text.

use orthogonal wire grids, the .15 millimeter resolution* the instrument provides is obtained in both vertical planes, not only in the plane defined by the magnet pole pieces. This feature allows for a better determination of the effective solid angle and makes possible elimination of spurious scattering of particles by use of redundant trajectory analysis.

Both balloon flights were carried out from Resolute, N.W.T., Canada, and balloons remained within telemetry range for the duration of both flights. The balloons floated at 2.25 and 2.37 g/cm^2 with durations of about 20 and 10 hours in 1967 and 1968, respectively.

*There are three adjacent spark chambers at each level, each one of which has a resolution of .3 mm leading to the indicated resolution for the three taken together.

The processing of the particle trajectory data started with raw events of the type pictured in Figure 2 and continued with a series of computer programs which, first, reanalyzed the events with more exact criteria as to their acceptability and, second, determined the rigidity for the optimum fit of the trajectory and arrival direction for each accepted particle. This fitting procedure consisted of a series of iterations on the integration of the equations of motion of the particle through the magnetic field to obtain rigidity values accurate to within several percent. Each analyzed event was then classified as to charge, energy and arrival time. The total numbers of negatron and positron events were, however, so small in each case that the data have been grouped for presentation in very wide energy bins in spite of the good energy resolution.

The events were then grouped into time intervals during balloon ascent and correlated with residual atmospheric pressure to provide information on the atmospheric depth dependence of the observed intensities. From the growth curve thus obtained the data was fitted to an assumed depth dependence of the form

$$j(E, d)\, dE = C_1\, P(E, d)\, dE + C_2\, S(E, d)\, dE$$

where j is the differential intensity of the component being considered and C_1 P and C_2 S are the primary and secondary contributions to this intensity. C_2 S is assumed to be linear with pressure for depths, d, small compared to a radiation length of air. In this manner C_1 P is obtained for the appropriate depth at which the balloon floated during the exposure. Extrapolated to the top of the atmosphere, C_1 P represents the measured primary intensity.

The results of the 1967 flight indicated no statistically significant primary intensity. The numerical results are quoted in the abstract and shown together with the results of other observers in Figure 3. A partial loss of pressure in the spark chamber in 1968 resulted in a considerable loss of data, and effectively reduced the sensitivity of the 1967 value in spite of the improvements discussed previously. Again no statistically significant primary intensity was detected, and limits were obtained. The upper limits for this flight are given in Table II. For clarity only the 1967 results are plotted in Figure 3.

CONCLUSION

From the results reported here and by others, it is apparent that accurate determinations of the intensity of primary negatrons and positrons in the 20-200 MeV range are greatly hampered by the influence of secondary electrons produced in the atmosphere above the detector. The resulting uncertainties in the measurements prevent a detailed analysis of the structure of the spectra of the two species in the 10-200 MeV energy range, but the data are sufficient to allow a few important conclusions.

Table II

1968 Upper Limits (1σ)

	e^+:	e^-:	$e^+ + e^-$
35 to 110 MeV	<0.11	<0.16	<0.25
110 to 220 MeV	<0.06	<0.09	<0.14

First, it appears that the 20-100 MeV data fall below a smooth curve connecting the data below 10 MeV with those above 200 MeV. It has been suggested (10) that the data below 20 MeV can be explained by proton-electron and electron-electron knock-ons produced in interstellar collisions. This conclusion depends upon the assumption that there is very little solar modulation in this energy range. Measurements over the time span from 1964 to 1968 indicate no time dependent modulation effects, but the possibility cannot be excluded that there is a major, if not dominant contribution from the primary source spectrum with the accompanying solar modulation.

The strong depression of the >200 MeV spectrum between 1966 (12) and 1968 (9) with an accompanying neutron monitor decrease, gives evidence for a strong modulation effect. However, the exact form of the modulation function cannot be determined without a knowledge of the interstellar spectrum.

As discussed earlier, a measurement of the positron spectrum in the 20-200 MeV energy region, offers the missing link to an understanding of the form of the modulation, since the interstellar positron is known. The upper limits to the positron intensities reported here do not provide sufficient quantitative data to speculate on the exact nature of the modulation, though it is clear from a comparison of the measurements with the calculations of Ramaty and Lingenfelter (1) that there is modulation present and the data are sufficient to provide limits on the form it can take. Though the limits do not conflict with the modulation function deduced by Beuermann, et al. (8), the data have a

sufficiently large statistical uncertainty that many other functional forms cannot be excluded by existing data. It appears that balloon borne detectors cannot provide the detailed data needed, due principally to the contamination of the measured intensities by atmospheric conditions. A satellite experiment capable of measuring the composition and energy spectra in the 20-200 MeV energy range is needed.

ACKNOWLEDGMENT

We wish to express our appreciation to Messrs. S. M. Derdeyn, C. H. Ehrmann, A. F. Mascaro, R. W. Ross, and R. L. Smith, Jr. for electronic and mechanical support. For their support in arranging the flights from Resolute we are indebted to Mr. H. Demboski and Cmdr. D. Sumner of the Office of Naval Research, and for their capable launch services we are grateful to the balloon launch crew of Raven Industries. Finally we thank the Joint Canadian-U. S. Arctic Weather Station at Resolute for their hospitality in making available the facilities required to conduct the flights.

REFERENCES

1. R. Ramaty and R. E. Lingenfelter, Phys. Rev. Letters, 20, 120 (1968).
2. J. A. DeShong, R. H. Hildebrand and P. Meyer, Phys. Rev. Letters, 12, 3 (1964).
3. B. Agrinier, G. Boella, G. DegliAntoni, C. Dilworth, Y. Koechlin, B. Parlier, L. Scarsi and G. Sironi, Phys. Rev. Letters, 13, 377 (1964).
4. R. C. Hartman, R. H. Hildebrand and P. Meyer, J. Geophys. Res., 70, 2713 (1967).
5. R. C. Hartman, Ap. J., 150, 371 (1967).
6. J. L. Fanselow, R. C. Hartman, R. H. Hildebrand and P. Meyer, Bulletin of the American Physical Society, 13, 1460 (1968).
7. C. Y. Fan, J. J. L'Heureux and P. Meyer, Midwest Cosmic Ray Conference at Baton Rouge, March 1969.
8. K. P. Beuermann, C. J. Rice, E. C. Stone and R. E. Vogt, Phys. Rev. Letters, 22, 412 (1969).
9. J. Rockstroh and W. R. Webber, Preprint (1969).
10. G. M. Simnett and F. B. McDonald, Preprint (1968).
11. T. L. Cline and G. Porreca, Transactions, American Geophysical Union, 50, 308, (1969).
12. W. R. Webber, J. Geophys. Res., 73, 4905, (1968).

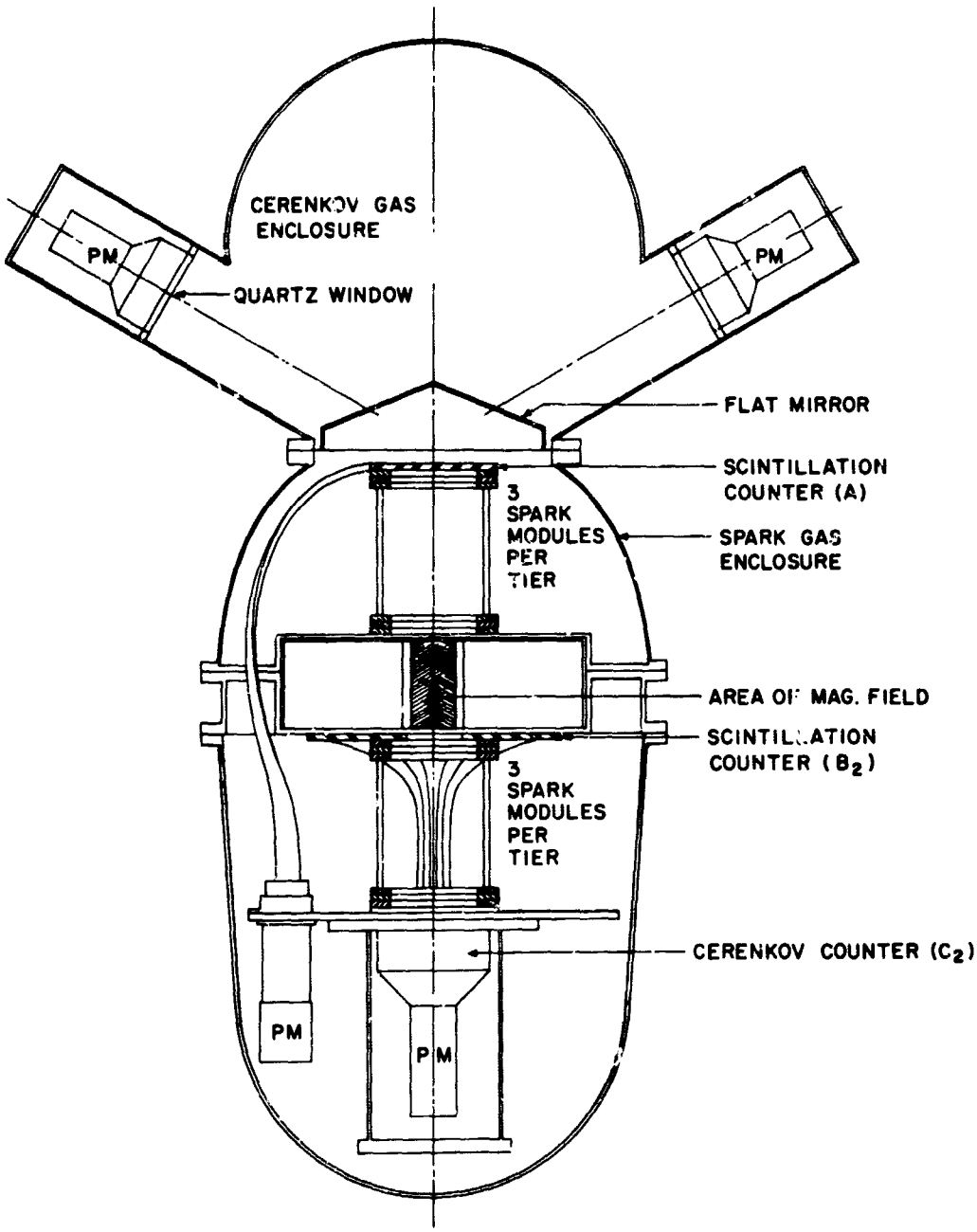

Figure 1. A schematic view of the negatron-positron spark chamber spectrometer. The 1968 detector is represented here, with the gas Cerenkov counter the most significant addition to the 1967 detector.

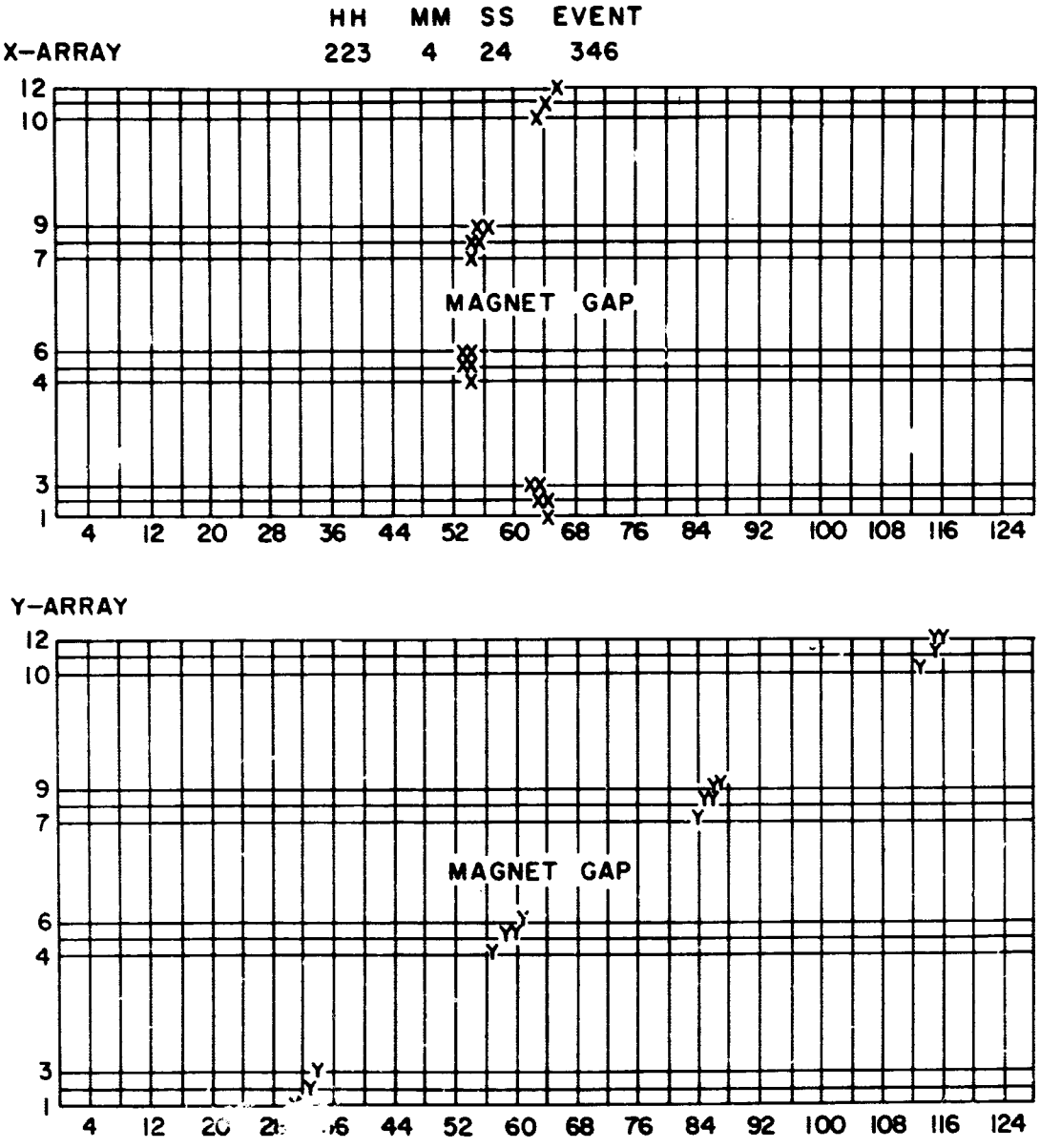

Figure 2. A typical computer reproduction of a spark event with an X-Z and Y-Z coordinate display. The X-Z plane is the deflection plane with the sense of deflection observed here applying to negatrons.

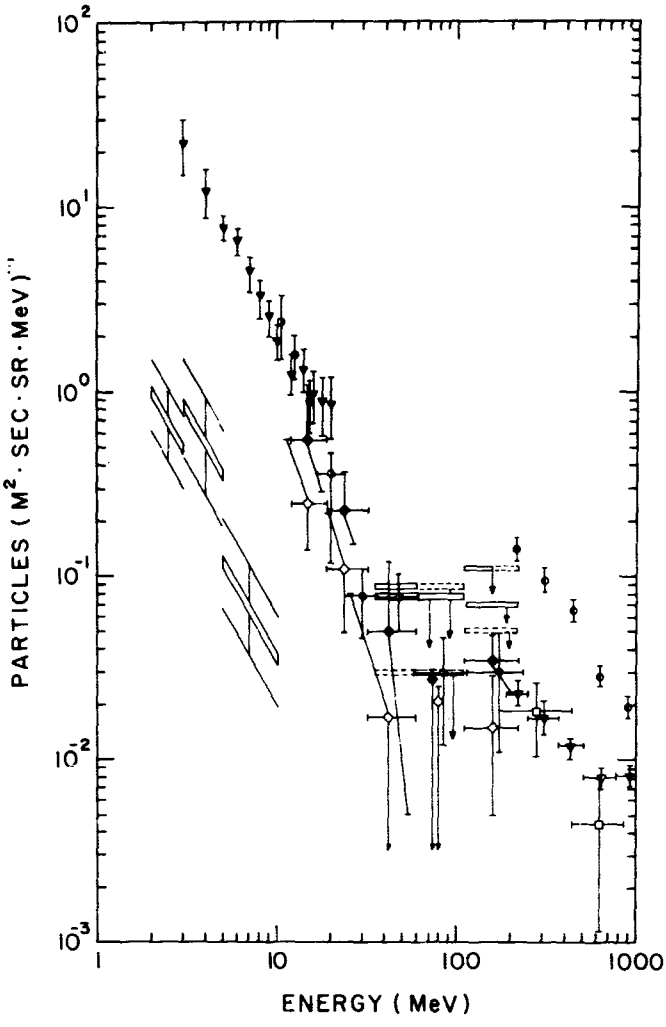

Figure 3. A selection of recent experimental results on the intensity and charge composition of primary cosmic ray electrons between 2 and 300 MeV.

Open Points: Positrons

Black or Dashed Points: Negatrons

Combination: Electrons (Positrons and negatrons)

: Reference (7) 1968 measurements

: Reference (6) 1966 measurements

: Reference (8) 1968 measurements

: Reference (9) 1968 measurements

: Reference (10) 1967 measurements

: Reference (11) 1966 measurements

: This work 1967 measurements

: Reference (12) 1966 measurements

SPECTRA AND CHARGE COMPOSITION OF THE LOW ENERGY GALACTIC COSMIC RADIATION FROM Z = 2 to 14

B. J. Teegarden, F. B. McDonald, and V. K. Balasubrahmanyan

NASA/Goddard Space Flight Center
Greenbelt, Maryland 20771 U.S.A.

ABSTRACT

Results from the Goddard Cosmic Ray Experiment on OGO-V for the study of charge and energy spectra are presented.

The detector system, designed to study the energy range from 5 - 800 MeV/nucleon and charge range from 1 to 14 consists of three different detectors. The low-energy detector consists of a semiconductor dE/dx vs. E telescope. The medium-energy detector has three CsI detectors which act as a dE/dx vs. E telescope for stopping particles and as a triple dE/dx telescope for penetrating particles. The high-energy detector consists of two CsI scintillators for redundant dE/dx measurements and a sapphire window Cerenkov counter.

The energy spectra and relative abundance data are presented and compared with other relevant measurements. Some new features are seen in C/O, C/He and O/He ratios which seem to favor the hypothesis of a two component model for the origin of cosmic rays. A nearer source which supplies most of the cosmic ray particles up to 100 MeV/nucleon seems to have an abundance differing in detail with respect to the high energy cosmic rays particularly in the relative abundances of carbon and oxygen. It appears that all the features seen in the

experimental results are not easily explained by considering a single source and different propagation models for path length distributions.

INTRODUCTION

The study of the chemical composition of galactic cosmic rays at low energies has recently provided new and interesting information pertinent to the origin and propagation of cosmic rays in our galaxy. A great deal of nuclear abundance data at higher energies ($\gtrsim$ 200 MeV/nucleon) has been accumulated for more than a decade, and has among other things been used to estimate the lifetime of cosmic rays in our galaxy and to test various models for the origin of the cosmic radiation. The behavior of the chemical composition at low energies is expected, however, to be different from that at higher energies due to the influence of energy loss from ionization during passage through the interstellar gas. This effect adds another element of experimental information important for the testing of models of the origin and propagation of cosmic rays.

The Goddard experiment on OGO-V was designed to measure the chemical composition and energy spectrum of the cosmic radiation over a broad energy range (5-800 MeV/Nucleon) including the interesting low energy region discussed above. The spacecraft was launched on March 4, 1968, and we will present data accumulated between March and October 1968.

DESCRIPTION OF THE EXPERIMENT

A schematic representation of the OGO-V experiment is shown in Figure 1. The experiment consists of a coordinated set of three charged particle telescopes

referred to, respectively, as the low energy detector (LED), medium energy detector (MED), and high energy detector (HED). The LED is a solid state dE/dx vs. E telescope. The dE/dx element G (see Figure 1) is a thin (150 micron) silicon surface barrier device, and the H element consists of two identical 1 mm thick surface barrier devices. The J element, a plastic scintillator, acts as a guard. Only events of the type $GH\bar{J}$ are analyzed. The low energy telescope covers approximately the 8-40 MeV/nucleon interval for carbon and oxygen nuclei.

The medium energy detector is composed entirely of scintillators which form a dE/dx vs. E telescope for particles which stop within the detector and a triple dE/dx telescope for particles which penetrate the detector. The D and E elements are, respectively, thin and thick CsI scintillators providing the dE/dx and E measurements. The F element is a combination plastic and CsI scintillator which serves both as a guard and as a dE/dx element. A phoswitch is used to distinguish between the fast output from the plastic and the slow output from the CsI.

The high energy detector is a double dE/dx and cerenkov telescope covering the energy range from 200 and 800 MeV/nucleon. The A and B elements are identical thin CsI crystals providing redundant dE/dx measurements. The cerenkov measurement is obtained using a sapphire window phototube.

These three experiments are complementary in the sense that they each cover essentially the same range in charge but over separate energy intervals.

The detectors have been designed such that there is a region of overlapping response between one detector and the next; thus permitting cross-calibration between the detectors.

EXPERIMENTAL RESULTS

We show in Figure 2 the charge distribution for the medium energy detector. Statistics in the LED were much too poor to permit a similar distribution to be drawn for that detector. The characteristic signatures of carbon and oxygen stand out clearly. It is clear that for $Z > 10$ we are not able to resolve the odd Z elements. One of the difficulties contributing this situation is the presence of rather large temperature variations on the OGO-V spacecraft. These variations induce gain shifts in each of the detectors of the order of 10% during the time period covered in this analysis. We have, of course, corrected for these shifts, but we cannot be certain that all temperature effects have been removed.

In Figure 3 we show a slightly expanded version of the same charge distribution in the fluorine region with the bin positions optimized for the fluorine line. The small "bump" at the expected position of fluorine is very tantalizing. Unfortunately, since there are only three counts in our fluorine "peak" we are not justified, purely on the basis of statistics, in saying that our detector has resolved fluorine. If we assume that there is no background in the fluorine region we obtain a fluorine to oxygen ratio of .015 + .08 in the 60-180 MeV/nucleon interval. This number is in agreement with the recent University of Chicago results (Simpson, 1968) and with the results of Lezniak and Webber (1969) at higher

energies. If one assumes that the counts in the fluroine region are background then an upper limit on the F/O ratio of .031 (95% confidence) is obtained.

In Figure 4 we have plotted the energy spectra for alpha particles and for heavier nuclei ($Z \geq 6$). The lines drawn for the various nuclei are intended only as an aid in reading the graph and are not necessarily suggestive of the true spectral shape. All spectra are accumulated over a 7 month period centered in June 1968. Active periods have been removed using rather stringent criteria. The He^4 spectrum exhibits remarkable regularity above 40 MeV/nucleon. The presence of noise in the low energy alpha particle region in both the LED and MED has prevented the plotting of a more continuous alpha spectrum.

Certainly, the most significant feature in all these data is the behavior of the carbon and oxygen spectra at low energies. The spectra of these elements are relatively steep between 50 and 200 MeV/nucleon. However, below 50 MeV/nucleon one observes a much flatter spectrum. Our measurements at ~25 MeV/nucleon indicate that carbon and oxygen are much more abundant at low energies than would be expected from a simple extrapolation of the spectrum above 50 MeV/nucleon. Due to the small geometry of the LED (.6 cm^2-ster) only a small number of carbon (5) and oxygen (9) nuclei were accumulated. This unfortunately precludes the possibility of obtaining more than one point on the spectrum below 50 MeV/nucleon. It is possible, however, to make a qualitative statement about the shape of the spectrum over the interval covered by the LED (~8 - 40 MeV/nucleon). The distribution of the LED events in energy space is more heavily

weighted towards high rather than low energies, or alternatively, it can be said that no turn-up is observed in either carbon or oxygen spectra for energies as low as 10 MeV/nucleon.

The spectra of elements heavier than oxygen up to Z = 16 are plotted in Figure 4. Extremely low count rates in the low energy detector prevent the extension of these spectra to very low energies. The spectra in the region of 150 MeV/nucleon appear to become steeper with increasing Z. This behavior is expected as a consequence of the increased rate of energy loss due to ionization of the higher Z nuclei as they traverse the intersellar medium.

In Figure 5 we present separately the carbon to helium and oxygen to helium ratios as a function of kinetic energy/nucleon. The reason for the individual study of these elements (rather than, e.g., the medium elements as a group) will become apparent later. The carbon to helium ratio is seen to exhibit a more pronounced dependence on kinetic energy/nucleon than does the oxygen to helium ratio. The variation in the C/He ratio above 50 MeV/nucleon suggests a fairly steep source spectrum, e.g. power law in rigidity or kinetic energy/nucleon. The existence of a steep source spectrum, however, implies within the framework of a one-component model that the C/He ratio should continue to decrease as one approaches lower energies. This behavior is, however, not seen in our data. The C/He ratio at ~25 MeV/nucleon is roughly the same as the ratio at 65 MeV/nucleon. A similar behavior is seen for the O/He ratio, although the variation above 50 MeV/nucleon is not as pronounced. This behavior is not explainable in

terms of the passage of all cosmic rays through an average amount of material of the order of a few gm/cm^2. Even the assumption of path length distributions heavily weighted towards short distances (e.g. exponential distribution) will probably not resolve this difficulty. The simplest hypothesis that will explain this behavior is the presence of a second nearby source of low energy cosmic rays, as has been recently suggested by Comstock (1966, 1969) and others. The problem of the overabundance of low energy carbon and oxygen is then solved since at low energies the average path length traversed is small and the effects of ionization loss are not important.

We turn now to examine the ratio of carbon to oxygen as a function of kinetic energy/nucleon. This is shown in Figure 6. Also included is the balloon data of Von Rosenvinge, et al. taken in 1966 and 1967. The agreement of our highest energy points with Von Rosenvinge's data is quite good. There does, however, appear to be a small systematic difference as one approaches lower energies, with our points lying approximately 20% above those of Von Rosenvinge, et al. The most striking feature of our data is the rather sudden decrease in this C/O ratio below 150 MeV/nucleon. The C/O ratio that we measure at 25 MeV/nucleon is approximately a factor of two lower than that measured above 150 MeV/nucleon. Again, the two-component hypothesis provides an attractive explanation for the behavior of our data. We postulate, first, that there exists a separate nearby source for the low energy cosmic rays, and second that this source has elemental abundances (at least for carbon and oxygen) that are more like the solar or

universal abundances than the abundances high energy cosmic rays. The characteristic C/O ratios measured in solar cosmic rays are of the order of .6 (Biswas and Fichtel, 1965) and the universal abundance ratio is .27 Cameron, 1958). The C/O ratio that we measure at 22 MeV/nucleon is $.65 \pm .35$ which is certainly more consistent with the abundance of solar rather than galactic cosmic rays. Our model would then require that a transition occur in the vicinity of 100 MeV/nucleon between the dominance of distance sources having more carbon than oxygen and the dominance of one or more nearby sources having more oxygen than carbon.

The question arises whether or not our nearby source of low energy cosmic rays could, in fact, be the sun. There are several arguments against this. First, we have used stringent requirements in rejecting time periods when the sun was active. Any data in which an enhancement in the helium intensity above 10 MeV/nucleon occurred was eliminated. Second, the C/O ratio begins to decrease at ~130 MeV. This fact seems hard to reconcile with the characteristically soft solar spectra. Third, we pointed out earlier that we saw no evidence for a turn-up in either the low energy carbon or oxygen spectra. It is difficult to conceive how a significant solar contribution could be present at low energies without the existence of a turn-up reflecting the characteristic steep solar spectrum.

REFERENCES

1. Biswas, S., and C. E. Fichtel, Space Science Review, IV, 709-36, 1965.

2. Cameron, A. G. W., Ap. J., 129, 676, 1965.

3. Comstock, G. M., C. Y. Fan, and J. A. Simpson, Ap. J., 146, 51, 1966.

4. Comstock, G. M., Ap. J., 155, 619, 1969.

5. Lezniak, J. and W. R. Webber, Ap. J. Letters, 156, L73, 1969.

6. Von Rosenvinge, T. T., W. R. Webber, and J. F. Ormes, University of Adelaide Preprint No. ADP56, 1968.

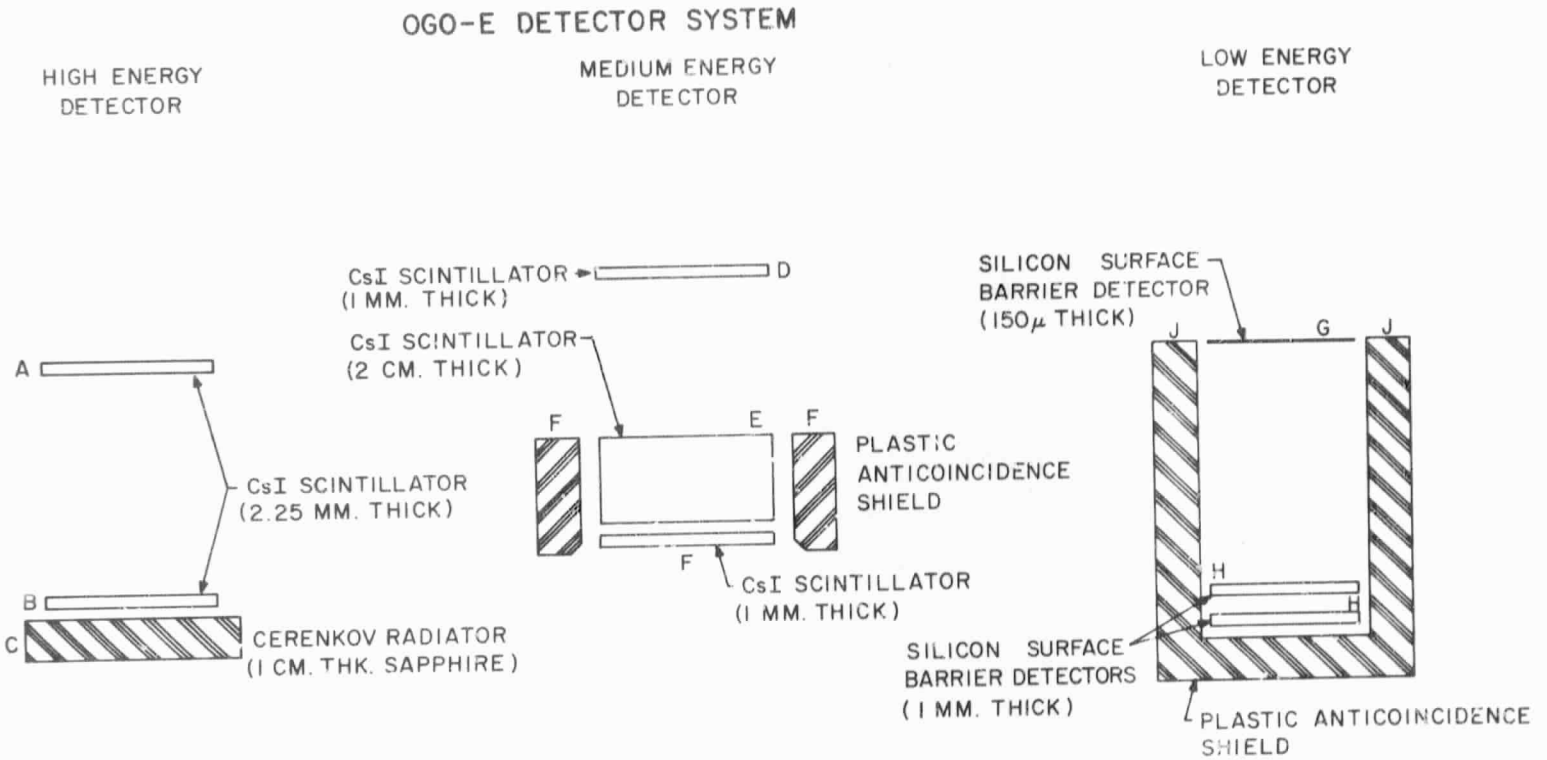

Figure 1. A schematic representation of the OGO V cosmic ray detector system. Only the solid state detectors and scintillators are shown.

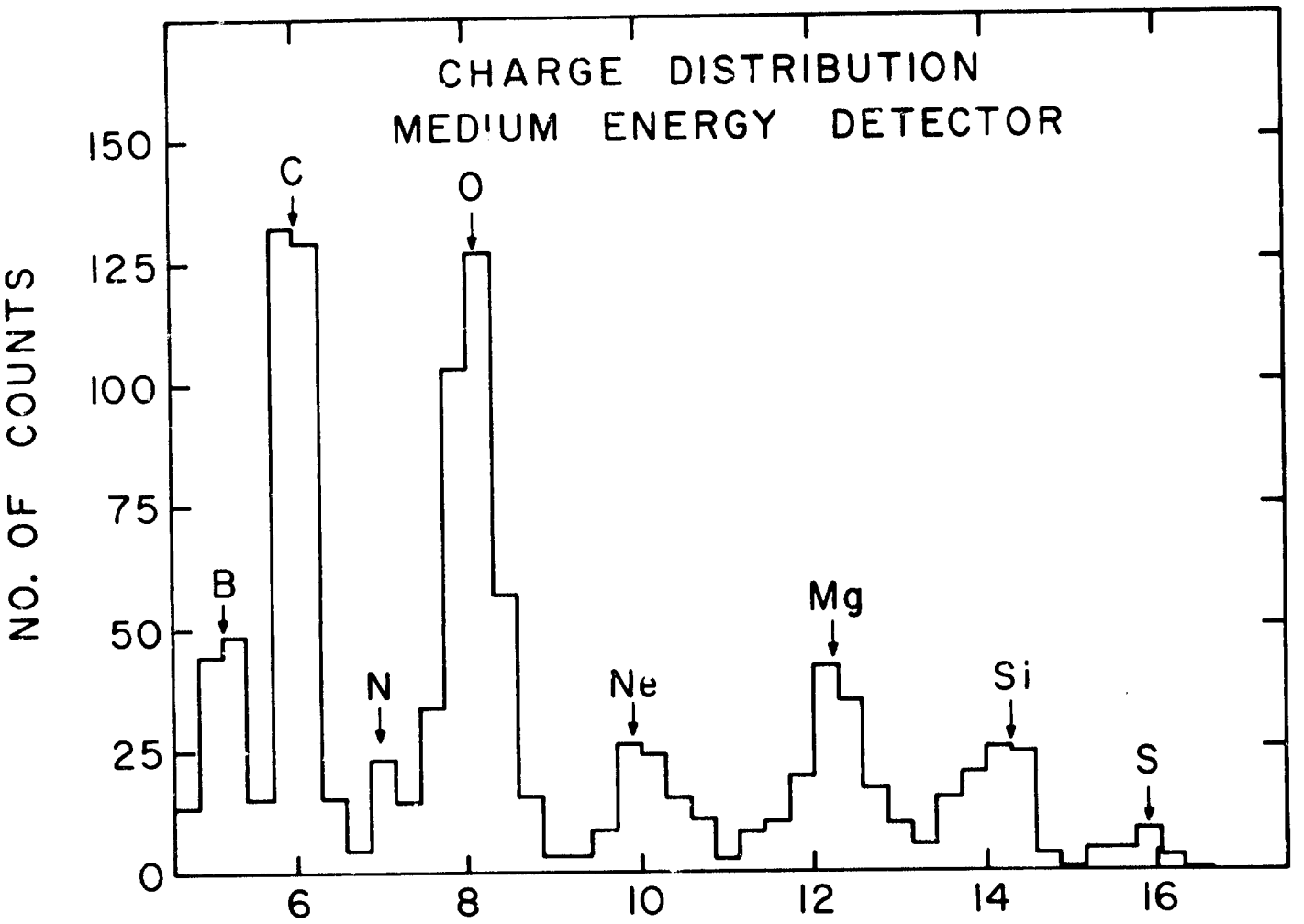

Figure 2. The charge distributi derived from the medium energy detector. Energy intervals vary from 53 – 148 MeV/nucleon for carbon to 163 – 268 MeV/nucleon for sulfur.

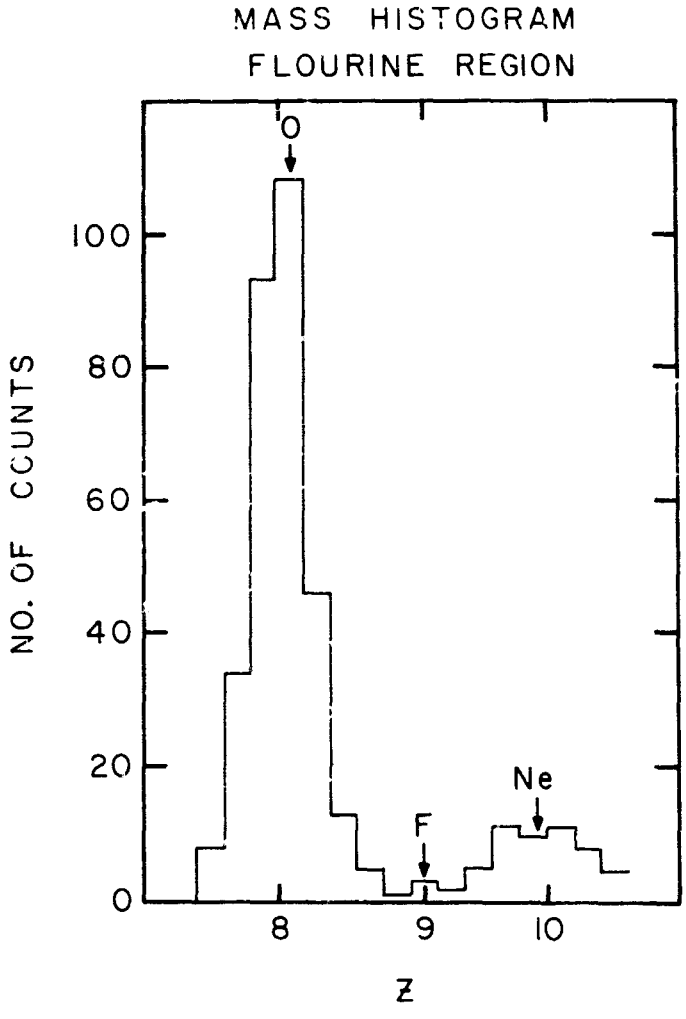

Figure 3. Expanded charge distribution in the fluorine region. Bin positions are optimized with respect to the fluorine line.

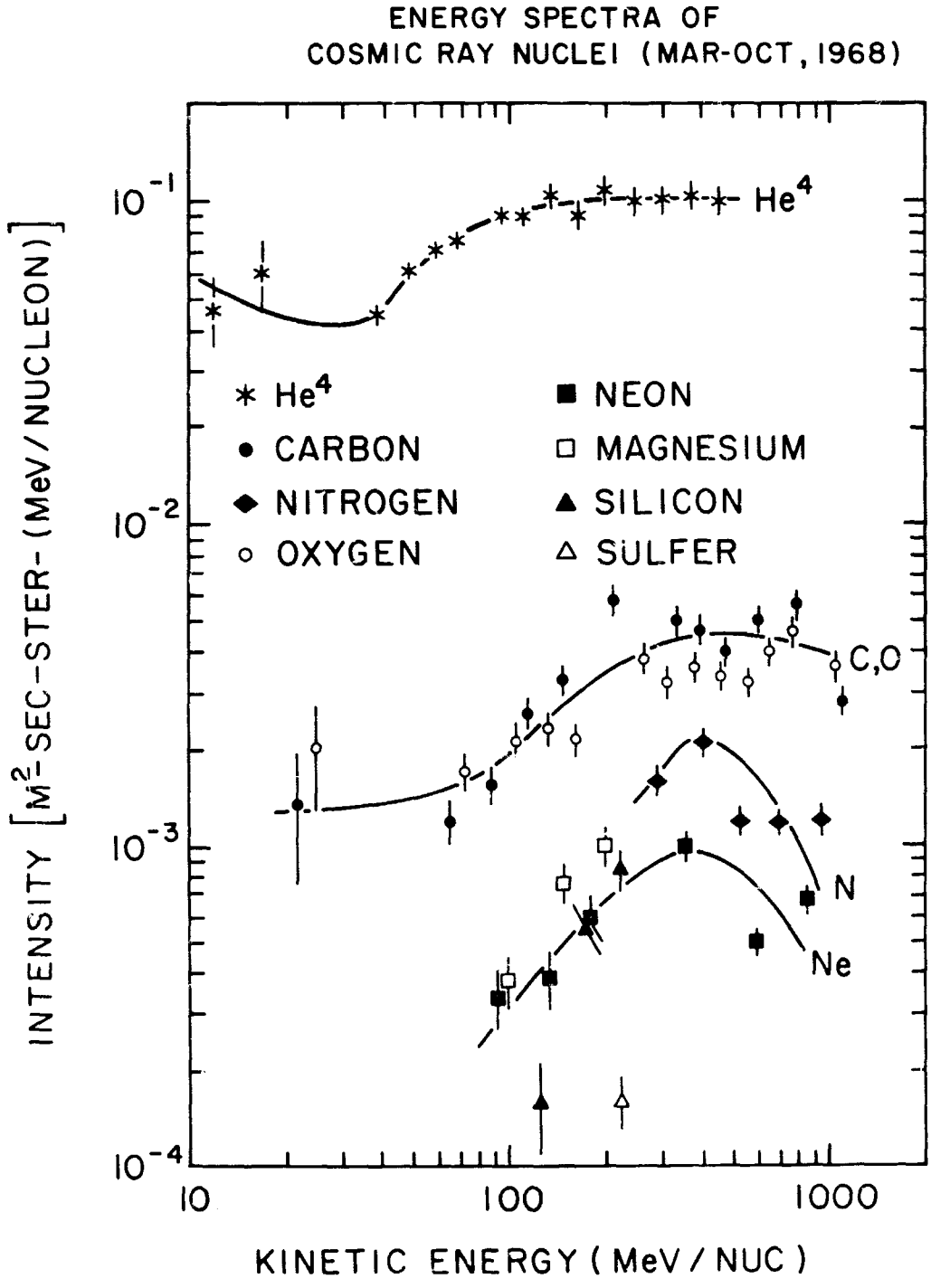

Figure 4. Spectra of various components of the cosmic radiation as a function of kinetic energy/nucleon. Periods when the sun was active have been removed.

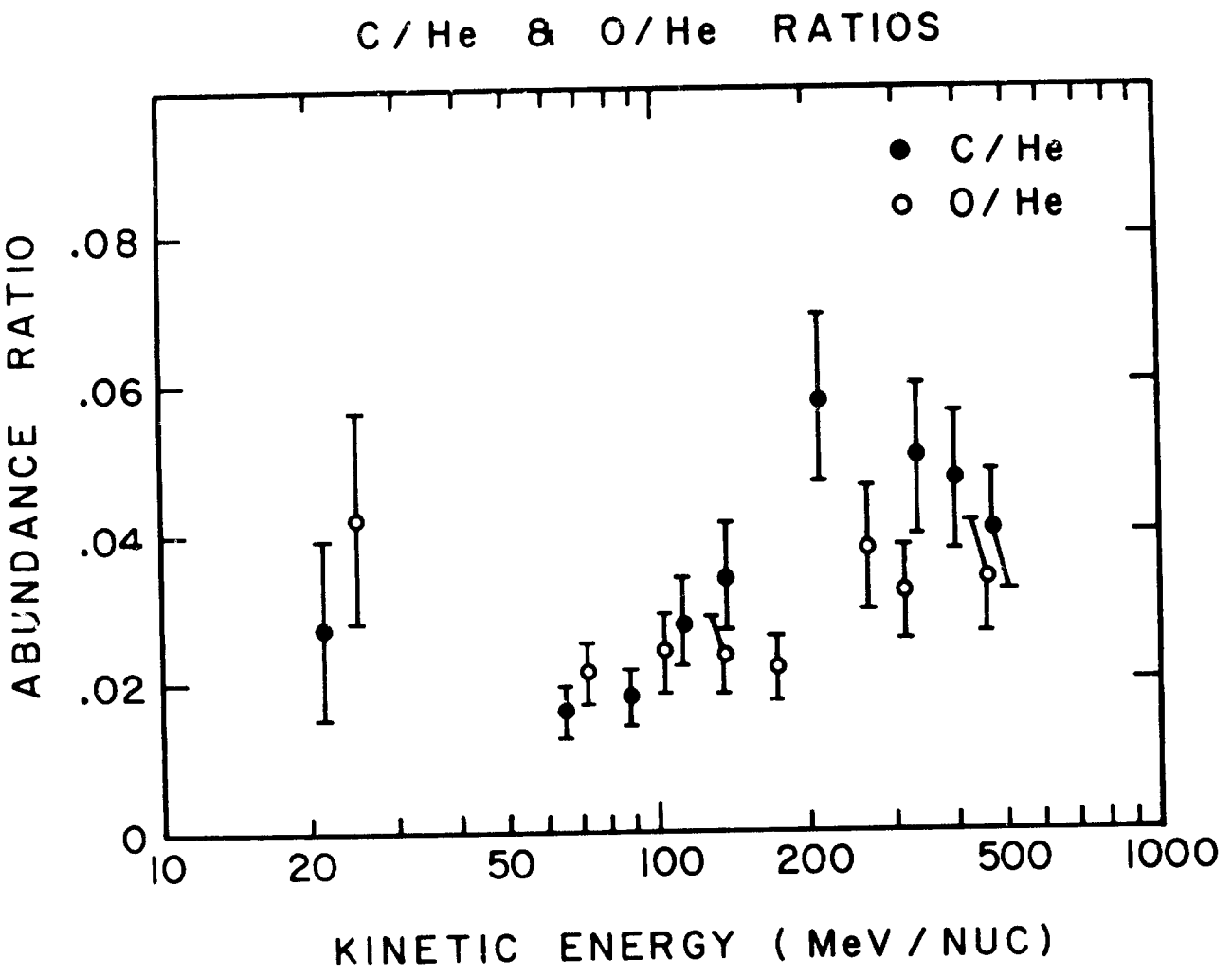

Figure 5. Carbon to helium and oxygen to helium ratios as a function of kinetic energy/nucleon.

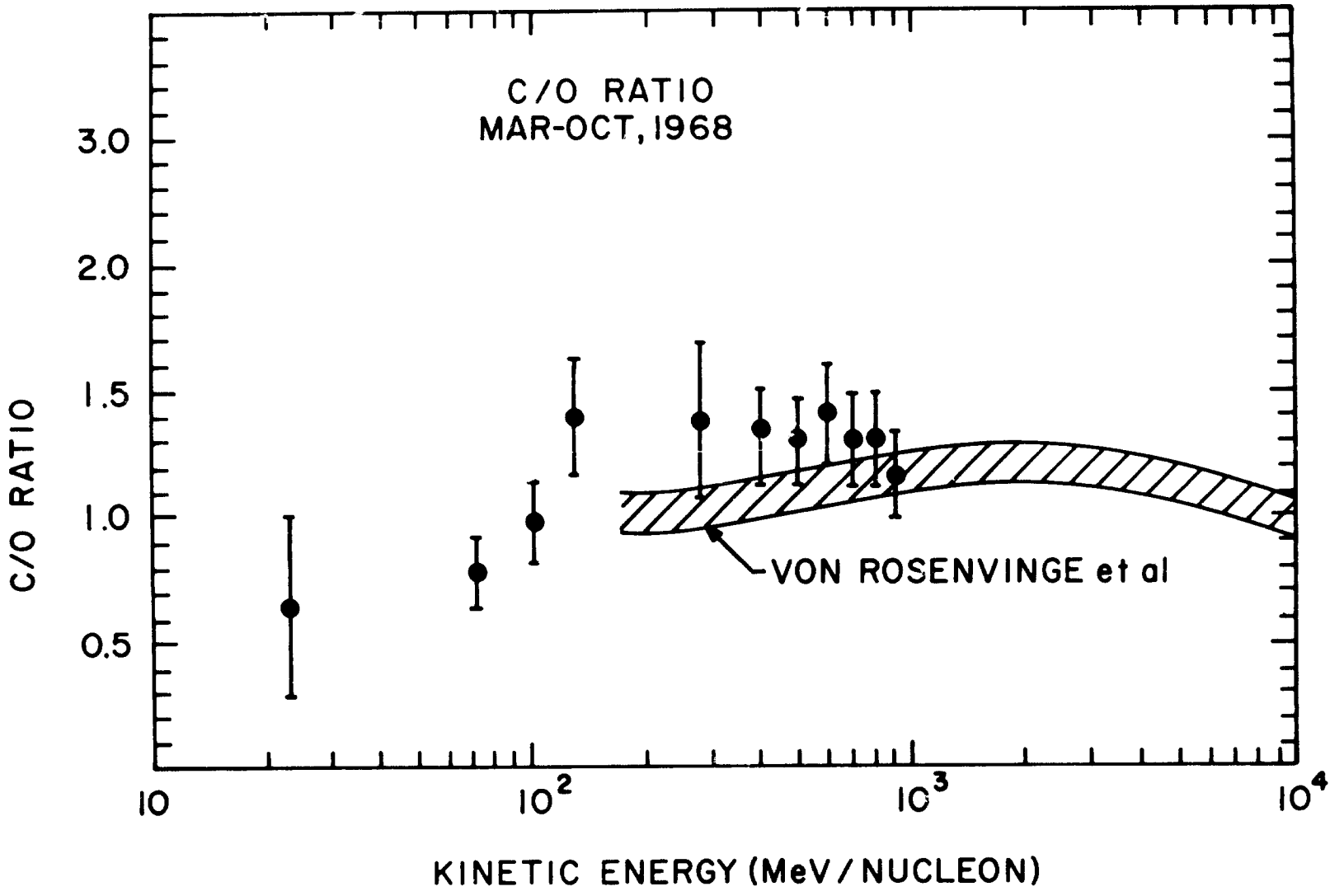

Figure 6. Carbon to oxygen ratio as a function of kinetic energy/nucleon. Also shown are the data of Von Rosenvinge et al. (1968).

COMPOSITION OF RELATIVISTIC COSMIC RAYS DETECTED ON GEMINI XI

F. W. O'Dell, M. M. Shapiro, R. Silberberg, B. Stiller and C. H. Tsao
Laboratory for Cosmic Ray Physics
Naval Research Laboratory, Washington, D. C.

N. Durgaprasad, C. E. Fichtel, D. E. Guss and D. V. Reames
NASA-Goddard Space Flight Center, Greenbelt, Maryland

SUMMARY

We present final results on the first satellite experiment on abundances of cosmic-ray nuclei having a mean energy of several GeV per nucleon. A nuclear emulsion detector, exposed on Gemini XI in a near-equatorial orbit ranging between geographic latitudes ±29°, collected 619 high-quality tracks above the earth's atmosphere. Time resolution (within about 5 minutes) was provided by movement of a lower emulsion stack relative to an upper one. The detector was covered by only 0.07 g/cm^2 of aluminum, and was favorably oriented for 18 hours. The results on abundances, requiring no correction for secondary production in the atmosphere, are characterized by: (a) a pronounced odd-even effect, with low abundances for elements of atomic number 7, 9, 11 and 13, compared to those of neighboring elements with even Z; (b) approximately equal fluxes of neon, magnesium and silicon, each being about one-fourth that of oxygen; and (c) an abundance gap in the region $15 \leq Z \leq 19$. The composition is similar to that observed at $\approx$100 MeV/nucleon on satellites; however, the abundances of the "Heavy" nuclei ($Z \geq 10$) relative to oxygen are higher in this experiment by approximately one standard deviation, or $\approx$20%, than those at low energies.

I. INTRODUCTION

The composition of the heavy nuclei in the galactic cosmic radiation can shed light on the nature of cosmic-ray sources, on interactions of cosmic rays with the tenuous interstellar gas, and on the amount of material traversed before escaping the galaxy. In previous work at high energies (≥1 GeV/nucleon), even in good high-altitude balloon flights, one had to correct through about 0.1 or 0.2 of a mean free path of atmosphere to deduce the primary composition. These corrections involve uncertainties due to insufficient knowledge of fragmentation cross sections. Hence, an experiment above the atmosphere can help resolve certain ambiguities. The Gemini XI emulsion experiment is the first flight above the atmosphere with a sufficient time-area factor for track collection to explore some of the relative abundances of elements at energies ≥1 GeV/nucleon, and to verify previous assumptions regarding partial fragmentation cross sections in air. The orientation of the spacecraft, and the location of the high-altitude orbits were optimized to reduce detrimental effects of the slow Van Allen belt protons on the search for heavy primary nuclei. Even under these circumstances, detection of the lightly ionizing lithium was prohibitively difficult, and the efficiency for beryllium was low.

II. EXPERIMENTAL DETAILS RELATED TO SPACE FLIGHT

The experimental package was contained in a metal box 3.0 inches by 8.5 inches laterally, and 6.0 inches deep. A 250-micron thick aluminum window

interposed a minimum of material between the collection face of the stack and the incident radiation consistent with a light-tight pressure seal.

The time history of arrival of the nuclei was obtained by moving a lower stack relative to an upper stack at the rate of 25μ per minute. It was thus possible to separate the "useful" tracks due to particles from the sky—formed during the oriented portion of the flight—from those registered at other times. A time history of cutoff rigidities was also provided thereby. Figure 1 is a schematic view of the flight package, showing the top stack and the main stack, which had a potential travel length of 2.0 inches. Movement of the lower stack of emulsions was initiated 102 minutes after launch.

To keep the emulsions within tolerable temperature limits, a coolant was circulated through the walls of the well in which the detector was placed. In addition, the upper surface of the metal box was covered with a thin thermal reflective coating. During launch, a covering hatch protected the package from atmospheric heating. Additional details of the apparatus have been published elsewhere.[1]

The spacecraft was oriented so that the emulsion layers were nearly vertical for as much of the time as would be commensurate with other operational requirements during the period of data collection. To minimize the background effect of Van Allen particles accumulated in the region of the South Atlantic anomaly, the attitude of the spacecraft was maintained such that the collection face of the detector was approximately normal to the magnetic field lines in the

region. In this way the mirroring particles produced tracks mainly at right angles to those of the primary nuclei sought by the scanners. About 24 hours after launch, pilot Richard Gordon opened the hatch for his "space walk," and extracted the package from its well. Command pilot Charles Conrad then stowed the package safely inside the Gemini command module.

III. DATA REDUCTION

The upper stack of nuclear emulsions was 1/2-inch deep and consisted of Ilford K.5 emulsions, 600 microns thick. K.5 emulsions were selected so that even minimum-ionizing tracks left by particles coming from interactions could be seen. Below this shallow stack was a 2.25-inch deep stack that could move with respect to the former. This stack consisted of emulsions (600μ) of different sensitivities arranged in a repeating sequence of emulsion types: K.2, K.5, K.2, G.O, K.2. The variety of sensitivities helped identify the nuclei. The emulsions were chemically processed at NRL and then divided between the GSFC and NRL groups for scanning and data reduction.

The K.2 and K.5 pellicles in the lower stack were scanned along a line 5 mm below the upper edge of the stack for tracks satisfying the criteria: (1) projected track length per plate $\geq$2 mm, (2) projected angle with the normal to the collection edge $\leq$60°, (3) ionization $\geq$9 times minimum. (With the latter criterion, most of the low-energy protons could be excluded from the initial scan.) Coordinates at 3 or more points along each track that passed through the scan plate were recorded using three-coordinate digitized microscopes.

The upper stack was scanned at 4 mm above its lower edge. Segments of tracks that passed through both upper and lower stacks were matched by means of a computer program. The displacement of a track in the lower stack from the position it would have had if the stack had not moved is a measure of the time of arrival of the particle that made the track. Figure 2 gives a frequency distribution of track displacements, and hence of elapsed time. The small peak at the left shows tracks that arrived prior to actuation of stack motion. The more pronounced peak at the right represents the tracks arriving after cessation of stack motion. From the shape of this peak we deduced that the uncertainty in arrival time of particles was ±5 minutes.

Tracks accumulated between the two peaks in Figure 2 were followed for their entire length in the emulsion; those which interacted above the scan line in the lower plate were rejected.

In a partial rescan, the overall scanning efficiency was found to be a function of Z. It varied from 0.77 ± 0.2 for beryllium to 0.98 for heavy nuclei.

Estimates of charge were based on delta-ray measurements in K.5 emulsion, and grain density (or blob-hole density) measurements in the less sensitive K.2 and G.O. emulsions. Two or more independent charge determinations were made for most of the tracks. The results obtained by the various techniques have been shown by O'Dell et al.[1] The observed charge distribution in Figure 3 displays adequate resolution up to magnesium. Figure 3 includes only the "good"-time tracks described below.

Since the spacecraft was not always oriented so that the emulsion stack was facing upward, it was necessary to determine the arrival direction of each particle in the earth's coordinate system. Tracks were accepted for analysis only if their arrival directions were within 73° of the local vertical. The uncertainty in the arrival time introduced a spread into the estimated arrival directions. Tracks with a probability of less than 0.7 of having arrived within 73° of the vertical were rejected. (Actually, about 80% of the accepted tracks had probabilities >0.999 of being within 73°.)

In order to look for possible variations in charge composition with energy we determined the geomagnetic cutoff rigidity corresponding to the arrival time (hence also to the geographic position) and arrival direction of each particle.

IV. RESULTS

The observed cosmic-ray composition between beryllium and nickel is shown in Figure 4. The plotted values have been corrected for scanning efficiency and for fragmentation loss in the emulsion above the scan line. The maximum fragmentation correction amounts to 11% for the ratio of nuclei with $20 \leq Z \leq 28$ to oxygen. (Since nearly all interactions above the scan line were observed, only the total interaction mean free paths had to be used rather than uncertain fragmentation parameters.) The results are characterized by: (a) a pronounced odd-even effect, with low abundances for elements of atomic number 7, 9, 11 and 13, compared to those of the neighboring elements with even Z; (b) approximately equal amounts of neon, magnesium and silicon, each being

about one-fourth that of oxygen; and (c) an abundance gap in the region $15 \leq Z \leq 19$. The abundances obtained, normalized to oxygen as unity, are given in Table 1.

The results shown are similar to those obtained in balloon experiments at relativistic energies, and to satellite measurements[2] at a much lower energy ($E \lesssim 200$ MeV/nucleon). Any variation in composition with energy is not large. However, the relative abundances of elements heavier than oxygen are somewhat higher in the present experiment. Thus, the abundances of the group of heavy nuclei ($Z \geq 10$) relative to oxygen is higher by approximately one standard deviation ($\approx$20%). If the observed differences are real, the lower abundances obtained in the satellite experiments at low energies might be accounted for by the presence of greater ionization losses at these energies. In the high-energy data at balloon altitudes, the difference may stem in part from uncertainties in fragmentation parameters used in correction for passage through air.

By assigning a cutoff rigidity to each particle from its arrival time and direction, we could crudely explore the charge composition versus energy in the relativistic domain sampled in this flight. The statistical weight of the results is limited, but the B/M, H/M and VH/M ratios are consistent with constancy of the composition between rigidities of 4 and 30 GV.

REFERENCES

1. F. W. O'Dell, M. M. Shapiro, R. Silberberg, B. Stiller and C. H. Tsao, NRL; N. Durgaprasad, C. E. Fichtel, D. E. Guss and D. V. Reames, NASA-GSFC, Can. J. Phys. 46, S569 (1968).

2. G. M. Comstock, C. Y. Fan and J. A. Simpson, Astrophys. J. 155, 609 (1969); and unpublished data of M. Garcia-Munoz and J. A. Simpson.

TABLE 1

Charge Composition

Z	4	5	6	7	8	9	10	11	12	13	14	15-19	≥20
$N_{observed}$	8	50	178	42	162	≤ 6	39	≤ 5	43	≤ 10	39	15	30
Scan Efficiency	0.77	0.91	0.94	0.94	0.95	0.97	0.98	0.98	0.98	0.98	0.98	0.98	0.98
Absorption Correction	1.169	1.179	1.189	1.200	1.208	1.218	1.226	1.235	1.243	1.251	1.259	1.284	1.346
N_{true}	12.1	64.8	225.2	53.6	206.0	≤ 7.5	48.8	≤ 6.3	54.5	≤ 12.8	50.1	19.7	41.2
N/N_{oxygen}	0.06 ±.03	0.31 ±.05	1.09 ±.08	0.26 ±.04	1.00* ±.08	$\leq .04$	0.24 ±.04	$\leq .03$	0.26 ±.04	$\leq .06$	0.24 ±.04	0.10 ±.03	0.20 ±.04

*The error in oxygen has not been incorporated into the errors for the ratios.

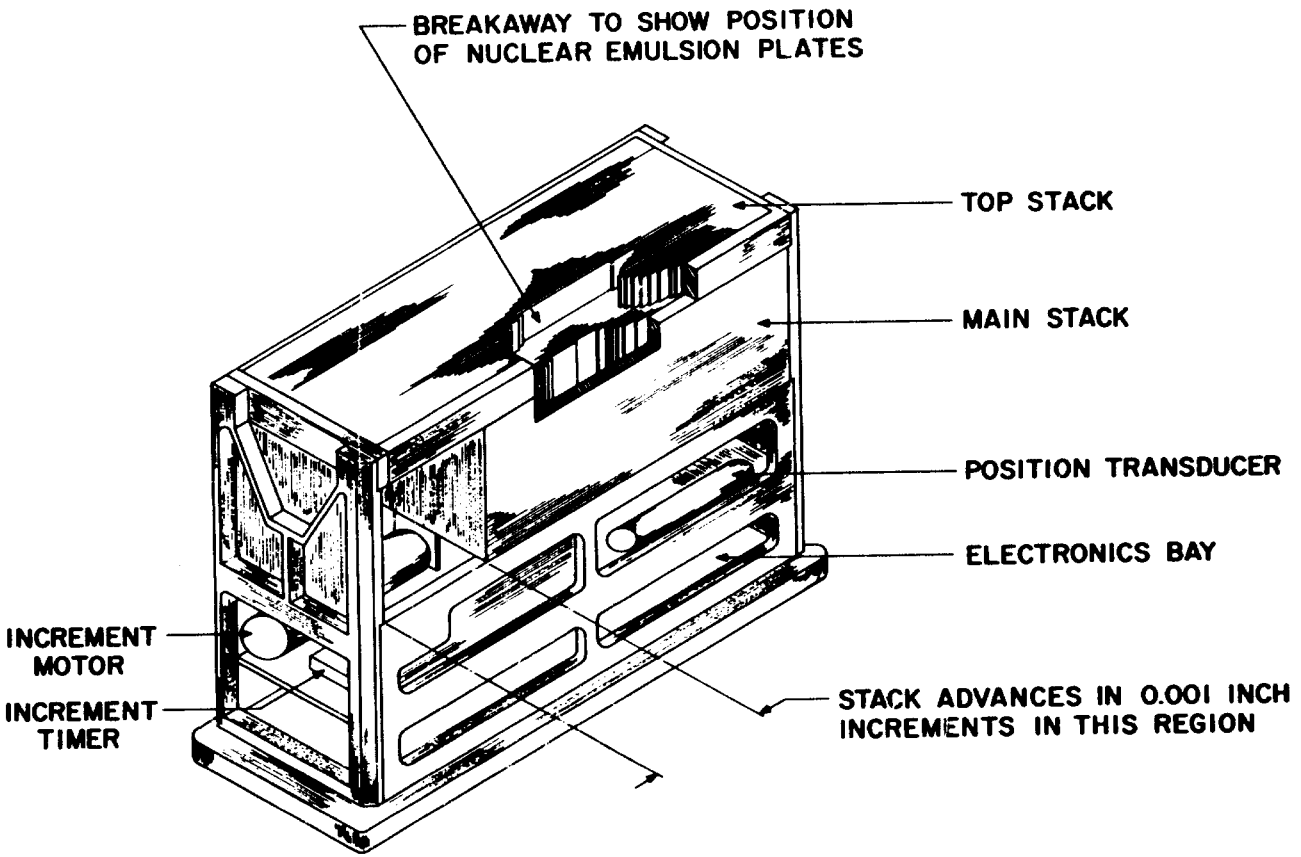

Figure 1. Experimental flight package.

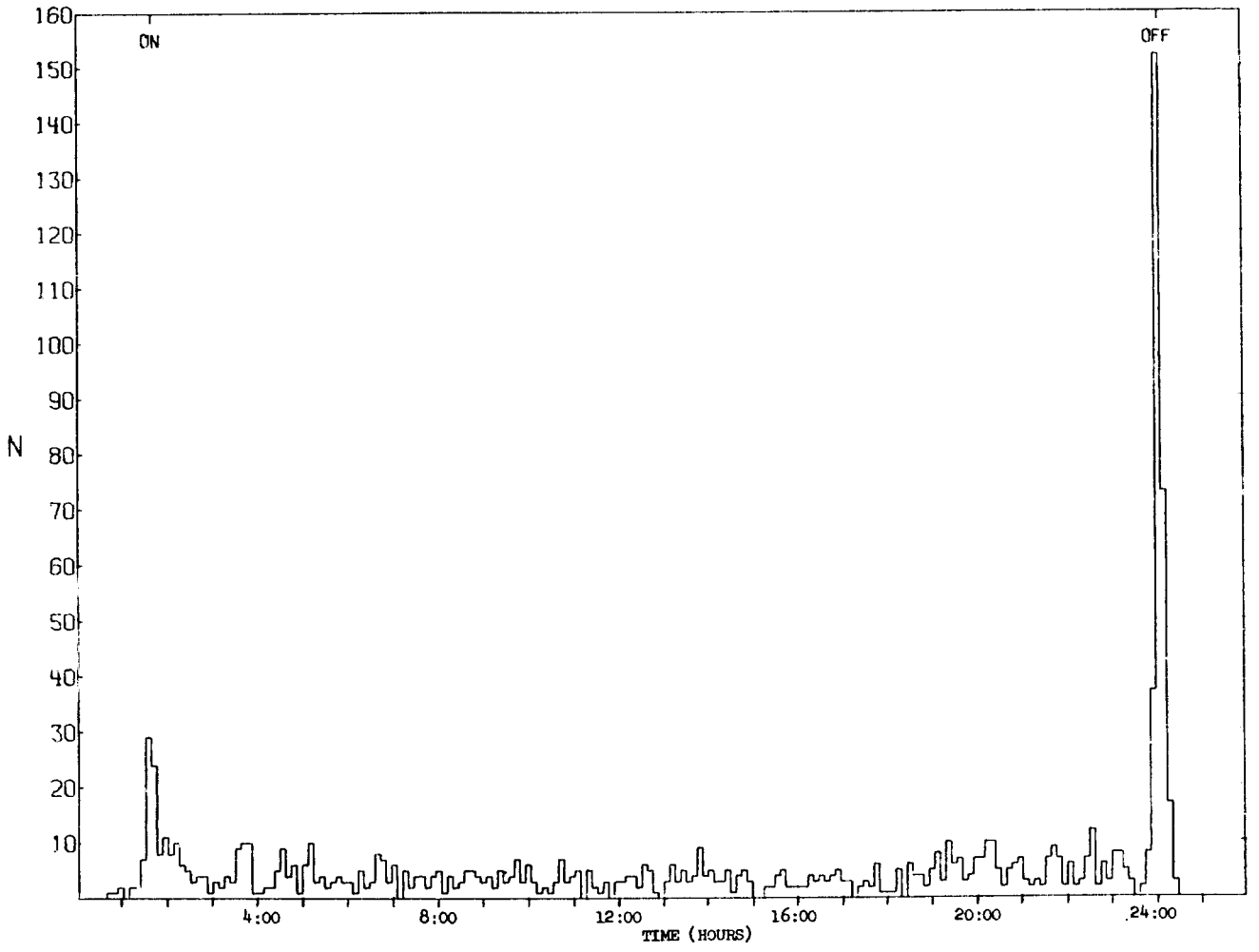

Figure 2. Distribution of arrival times of heavy primary nuclei.

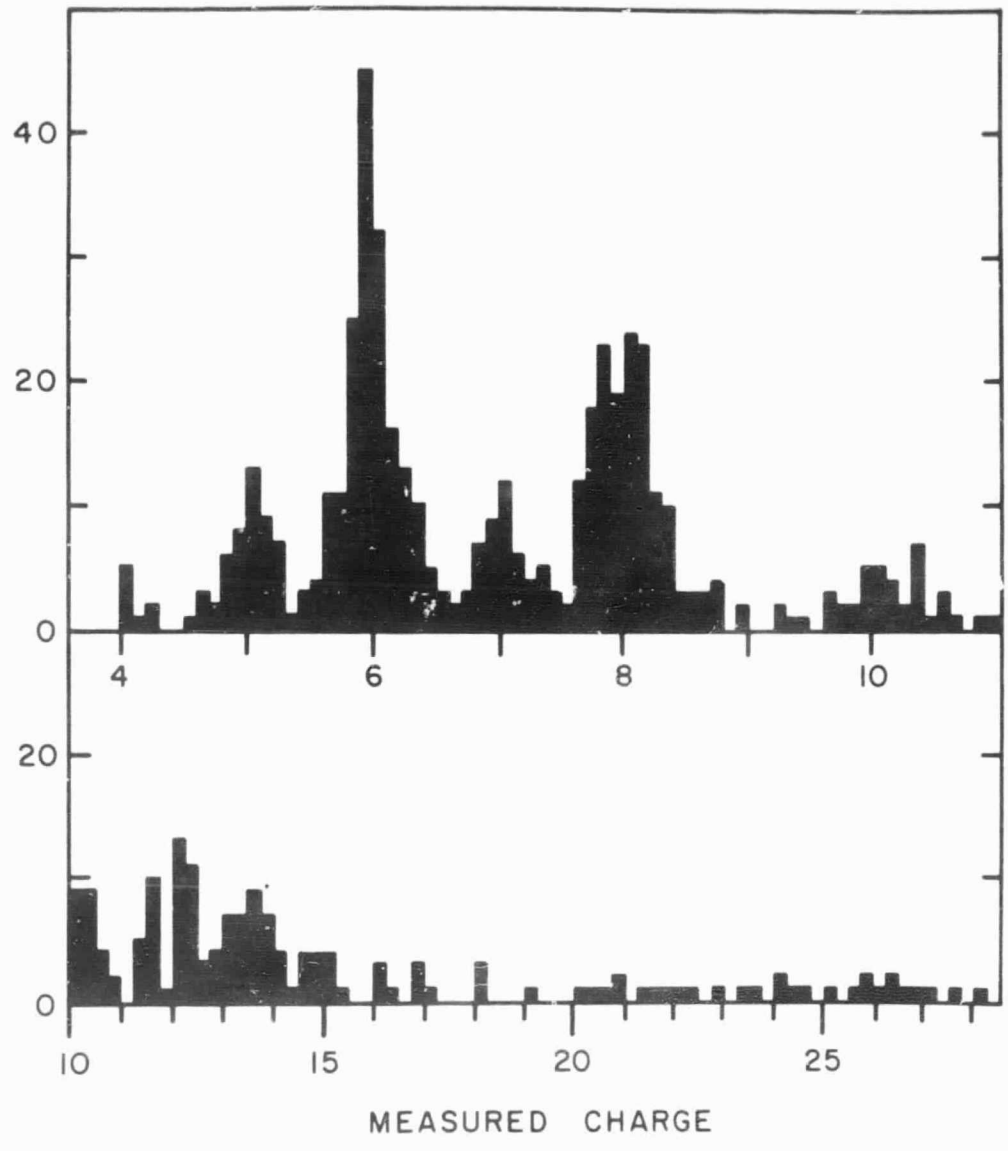

Figure 3. Charge estimation from combination of various ionization loss measurements.

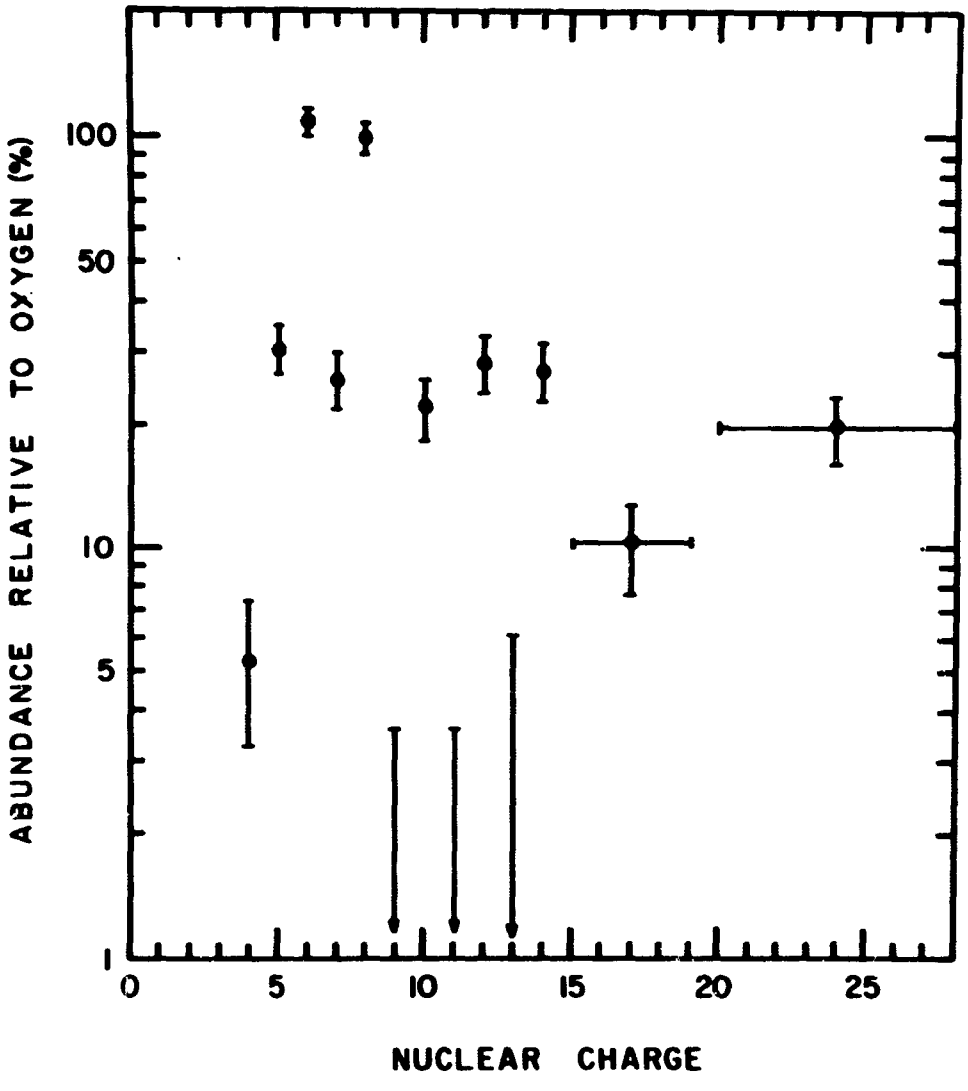

Figure 4. Relative charge composition of cosmic-ray nuclei. (Normalized relative to oxygen.) The abundances of Ne, Mg and Si shown include minor contributions from the neighboring odd-charge elements.

MO-33

DELAYED APPEARANCE OF RELATIVISTIC ELECTRONS 5 DAYS AFTER A SOLAR FLARE

G. M. Simnett,* T. L. Cline, S. S. Holt and F. B. McDonald

NASA/Goddard Space Flight Center
Greenbelt, Maryland 20771

ABSTRACT

An analysis of interplanetary 0.3 - 10 MeV electron and proton intensities between 6 July and 16 July 1968 indicates that the event had some unusual features. Comparison with solar radio, optical and X-ray data indicate that in this case a large electron increase on 13 July was produced at the latest on 8 July. Features of the solar flares from 6 - 16 July are discussed. The peak electron and 1 - 6 MeV proton intensities on 13 July show an inverse velocity dispersion: the peak electron intensity, for example, occurs 4 hours after the latest proton peak. We discuss the relative merits of several propagation models: storage or continuous acceleration of electrons at the sun.

*N.A.S.-N.R.C. Associate

We report evidence for the occurrence of an unusual type of energetic solar particle event between July 6 - 14, 1968. The unusual features of this event were a) an intensity increase, by two orders of magnitude, of interplanetary 0.3 - 10 MeV electrons on July 13 which reached a peak during the decay phase of the low-energy proton intensity and b) the absence of a suitable parent flare for the electrons during the period preceding the increase by at least 5 days. We compare solar proton, radio, optical and X-ray data obtained during the period in question to support these contentions. Finally we examine two possible models to explain these data.

The problem of separating the propagation characteristics of solar flare particles from their properties at production has become central in the understanding of either process. For example, studies of solar flare radio and x-ray emissions originally led to the hypothesis that electrons are directly responsible for most of these radiations at the sun,[1,2] whereas protons carry most of the energy observed near the Earth.[3] Interplanetary electron events have since been observed,[4] and have been found to be frequent occurrences.[5] Recent studies of solar events distinguish the following 3 basis propagation modes, each characterized by its particular geometry. (1) High-energy particles can follow flares by delays of minutes to hours with a propagation that appears to be mainly diffusive; in fact, some proton events obey a strictly velocity-ordered diffusion law.[6] Relativistic but low-rigidity solar electrons can also fit the same relationship.[7] In such events all velocity components follow the same

distribution in path length of travel, peaking at a few AU path length, and persisting for over 100 AU. Similar propagation from the unseen disk of the sun also seems likely to account for some events.[7,8] (2) Beams of lower-energy solar protons, often found to have a several-day delay time after flares, are interpreted as accompanying a shock front, delayed by its travel from the sun to the earth.[9] More recently, interplanetary electron events of this sort were also observed.[10] (3) Recurrent events are observed in which particles propagate out through co-rotating regions, revolving with the sun's 27-day period. These events were first seen occurring up to 3 to 4 weeks after visible flares in the same region,[11] but were then found to repeatedly occur with a regular pattern for over a year's duration in the absence of parent flares.[12,13]

We report here the observation of a spectacular example of what appears to be either an unusual combination of 2) and 3) or a newly observed particle propagation mode. A large intensity increase of relativistic electrons, detected on 13 July 1968 in interplanetary space with the IMP-4 satellite, was characterized by an approximately symmetrical rise and fall in intensity (unlike prompt, diffusion events) but was not accompanied or followed by an increase in any form in the interplanetary proton intensity at equal or greater energies (unlike delayed co-rotating events). Solar electron production is generally related to solar radio and X-ray emission from the production region. This electron event was not preceded by a solar flare with suitable X-ray and radio emission for several days.

We first review the chronology of relevant solar electron, proton, X-ray, radio and optical flare events. Figure 1 shows the occurrence of hard (>80 keV) solar X-ray bursts we have observed with the OGO-5 satellite, soft (2 - 12 Å) X-ray bursts, as reported by the University of Iowa from the Explorer 33 and 35 results, radio bursts observed at frequencies of 8800 and 1415 MHz (having peak intensities greater than 20×10^{-22} W m^{-2} Hz^{-1}) and optical flares from the McMath plage region MP 9503 during 6 to 16 July 1968. The flares which are not from MP 9503 are shown as dotted lines. The overall picture of particle emission during the passage of this plage region across the visible disc is indicated in Figure 2 with sample time histories from IMP-4 of the 300 to 900-keV electrons and the 11 to 100-MeV protons. First, slow increases in both electrons and protons are observed following the class 1N flare on the solar east limb at 0946 UT on 6 July. This flare was accompanied by intense microwave and hard X-ray bursts. Another X-ray and microwave flare of similar size occurred on 8 July at 1711 UT, but was not followed by an observable particle event. The electron intensity from 6 July slowly decayed away until late on 9 July when an additional increase occurred over a 12-hour period. This increase may have been associated with a class 2B flare at 1816 UT on 9 July, which was a lower intensity flare than the earlier two. The electron intensity slowly decayed away until a new increase occurred at ≈1410 UT on 12 July. A flare from a plage region which was ≈20°W. of MP 9503 commenced at 1341 UT; the possible relation of this flare to the particle event is discussed below. The electron intensity

continued to rise slowly until 1600 UT on 13 July when a 3-fold increase occurred within 8 minutes, followed by a maximum at approximately 2200 UT on 13 July. Thus, the electron intensity rose monotonically for 32 hours to a maximum at 150 electrons cm^{-2} sec^{-1} sr^{-1} between 0.3 and 0.9 MeV. The decay from maximum may be separated into two parts: a) an exponential decay until approximately 1000 UT on 14 July, and b) a power-law decay lasting at least until the end of 16 July. It is the electron intensity-time history which starts at 1410 UT on 12 July and peaks at 2200 UT on 13 July that we claim is a very unusual phenomenon.

The other unusual feature of this event is the temporal dispersion of the protons and electrons. Intensity-time histories of five different low-energy proton groups and two relativistic electron groups are shown in Figure 3. It is noted that the lowest-energy protons reach maximum intensity first and the electrons reach maximum intensity last, some four hours later. The velocity of these protons is only ≈ 0.05 c, compared with > 0.9 c for the electrons. There is an apparent velocity dispersion in the peak intensities of the different energy proton groups. On an expanded time scale the short term features occur simultaneously, within 5 minutes, at all observable energies. The behavior noticed in Figure 3 indicates that these features are stronger at low energies at earlier times, and vice versa.

CONCLUSIONS

A complete examination of the solar electromagnetic data for the time period 6 to 16 July eliminates flare acceleration and diffusive propagation of electrons as the source of this event. Energetic electron acceleration is accompanied by microwave radio emission and X-ray emission. We find five occasions during this time period when microwave emission was correlated with some X-ray emission and an optical flare, indicated with arrows in Figure 1. Dark arrows mark the intense X-ray flares previously mentioned; the shaded arrows show smaller flares which might have accelerated electrons; the plain arrow shows one which probably did not. The flare of 1341 UT on 12 July fits the time criterion, but it is a poor candidate in all other respects. The low ratio of high-frequency to low-frequency radio intensities is indicative of synchrotron emission from electrons stored in the corona (i.e. in low field regions), rather than electrons accelerated lower in the solar atmosphere; this contention is supported by the fact that there is no indication of hard X-ray emission, and an attempt to fit the time history of the electrons for diffusion, either at the sun or in interplanetary space, fails. To eliminate the possibility that the electrons were accelerated in an event on the back of the sun, we consider the magnetic field lines from a backside flare region. These lines will not connect the earth with a path length of several AU (if at all); thus, particles from a backside event would have to diffuse onto field lines connecting with the earth to be observed. We feel that the lack of any observed diffusive pattern for the particle emission

eliminates impulsive injection as a source of the particles observed late on the 13th, from either disk of the sun.

We consider now as a possible explanation for this event that the electrons were produced by some or all of the many flares in plage region MP 9503. The electrons, after each event, are partially trapped and partially released from the active region. The bulk of the released particles stream outwards from the sun along the field lines, whereas a part of them diffuse onto field lines connecting with the earth. As the region co-rotates, the majority of particles also co-rotates. At 1612 UT on July 13 there was a sudden commencement (S.C.) at earth. This occurred within 10 minutes after a sharp rise was observed in the 0.3 - 0.9 MeV electron intensity (Figure 4). The SC is interpreted as being caused by a shock front which is moving outwards from the sun. The bulk of the low energy protons observed before and after the SC are energetic storm particles. These are, however, superimposed on a co-rotating particle event. The combination of these two effects gives the appearance that the electrons are delayed. If the energetic storm particles include no electrons, it is possible to construct a proton component to accompany the electrons which is consistent with co-rotation.

There is a more speculative explanation which can also account for the observed data. The electrons, and probably the protons, were accelerated on July 6 or 8, or both. The flare on July 8 is the more likely candidate as particle emission was observed from the July 6 flare. The particles were stored in the

corona with small losses through leakage until July 12. The onsets of the particle increases on July 12 were triggered by the flare at 1341 UT, or by a disturbance associated with this flare, even though this flare was not in the plage region MP 9503. A plot of onset time versus $1/\beta$ for different velocity protons and electrons is shown in Figure 5. The straight line through the origin (at 1341 UT) and the electron point (which is the clearest defined) also fits the protons in a manner consistent with velocity dispersion in which all particles commenced their release at 1341 UT.

On release from the trapping region, the particles stream outwards from the sun along a tube of magnetic field lines connected to the point of release. Diffusion of particles from the source onto adjacent field lines also occurs; while IMP-4 is outside the main tube of field lines only these particles are observed. At 1600 UT on 13 July the spacecraft enters the tube of field lines, a sharp increase in the intensity of 0.3 - 0.9 MeV electrons is measured. The only particles undergoing a sharp increase at this time are the electrons which have small gyroradii. This behavior is entirely consistent with particle streaming along lines of force coming from the sun. The protons have gyroradii typically two orders of magnitude greater than the electrons (about 10^5 and 10^3 km, respectively, in a 3×10^{-5} gauss field). Since the solar frame rotation velocity at 1 AU is 400 km sec^{-1}, the observed rise time of less than 8 minutes for the electrons is long compared with the earth's travel time through a distance equal to the electrons' gyroradius. However, this is not the case for the protons, so

that a fast proton increase would not be expected. This picture is consistent with near-solar (rather than classical, interplanetary) diffusion. The time histories of the proton channels within the flux tube demand that the intensity variations be temporal, not spatial, in order to satisfy the following conditions: (a) If the region is co-rotating at the peak intensity, little difference is expected in the times of proton maxima. Also, the electrons should peak first.[14] (b) If the particles were released simultaneously, normal velocity dispersion should be observed. (c) The slow increase in the electron intensity continues for 6 hours after the spacecraft enters the flux tube. After maximum is reached, the electron intensity falls exponentially until the boundary of the flux tube is reached at ≈1000 UT on 14 July. After that time the intensity fits the power law $t^{-3/2}$. (d) The decay of the protons shows a change at ≈1000 UT on 14 July, more evidence that the spacecraft then moved out of the flux tube.

We can now examine the feasibility of this model by calculating the number of electrons required to account for our hard X-ray measurements and the observed radio emissions on 6 and 8 July in terms of the properties of the production region. It has been shown that >80 keV X-rays provide an unambiguous signature of non-thermal electrons.[15] Detailed calculations[16,17,18] involving the time histories, spectral shapes and magnitudes of both the microwave and X-ray bursts have been evolved on the basis of electron observations[7] in the earlier events of 7 July and 14 September 1966. Since the 6 and 8 July events compare directly with the event of 7 July 1966, we can conclude that the X-ray

emission on 8 July yields about 3×10^{34} electrons above 300 keV, if the hard X-ray decay is collision-dominated. This result is consistent with the 5×10^{33} electrons > 300 keV we estimate to be released into 1 steradian, since the efficiency of storage may not be great. The flux event of 6 July was somewhat larger than that of 8 July, but we believe it to be the less likely candidate since it was followed by a prompt, diffusive particle event.

REFERENCES

1. A. Boischot and J. F. Denisse, Compt. Rend. 245, 2194 (1957).
2. J. P. Wild, J. Phys. Soc. Japan 17, Suppl. A-II, 249 (1962).
3. K. A. Anderson, Phys Rev. Letters 1, 336 (1958).
4. J. A. Van Allen and S. M. Krimigis, J. Geophys. Res. 70, 5737 (1965).
5. K. A. Anderson and R. P. Lin, Phys. Rev. Letters 16, 1121 (1966).
6. D. A. Bryant, T. L. Cline, U. D. Desai and F. B. McDonald, Astrophys. J. 141, 478 (1965).
7. T. L. Cline and F. B. McDonald, Solar Physics 5, 507 (1968).
8. G. M. Simnett, Midwest Cosmic-Ray Conference, 1968 (unpublished).
9. D. A. Bryant, T. L. Cline, U. D. Desai and F. B. McDonald, J. Geophys. Res. 67, 4983 (1962).
10. R. P. Lin and K. A. Anderson, Solar Physics 1, 446 (1967).
11. D. A. Bryant, T. L. Cline, U. D. Desai and F. B. McDonald, Phys. Rev. Letters 11, 144 (1963).
12. C. Y. Fan, G. Gloeckler and J. A. Simpson, Goddard IMP Symposium, 1964 (unpublished).
13. D. A. Bryant, T. L. Cline, U. D. Desai and F. B. McDonald, Phys. Rev. Letters 14, 481 (1965).
14. K. A. Anderson, Solar Physics 6, 111 (1969).
15. T. L. Cline, S. S. Holt and E. W. Hones, Jr., J. Geophys. Res. 73, 434 (1968).
16. S. S. Holt and T. L. Cline, Astrophys. J. 154, 1027 (1968).

17. R. Ramaty and R. L. Lingenfelter, Solar Physics 5, 531 (1968).

18. S. S. Holt and R. Ramaty, Solar Physics 8, 119 (1969).

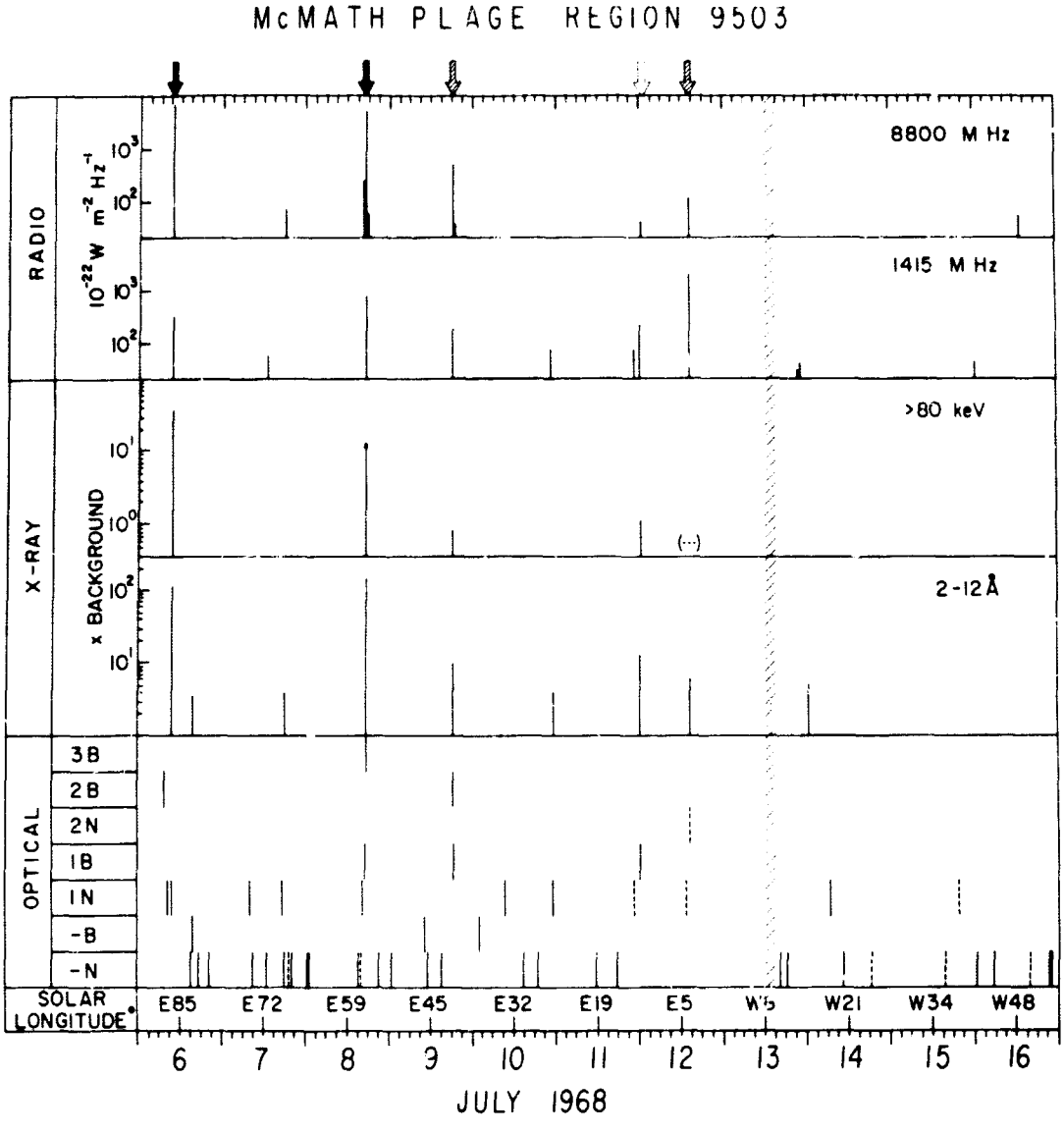

Figure 1. Solar flare X-ray, optical and radio data for 6 to 16 July 1968. The high-energy X-ray data are from OGO-5; low-energy X-ray and optical flare data are from ESSA bulletins. The radio data, provided by the Sagamore Hill, Mass. (42°N, 71°W) and Manila, P. I. (15°N, 121°E), observations represent complete temporal coverage for this period. The solar longitude of the center of McMath plage region 9503 at 1200 UT on each day is also indicated.

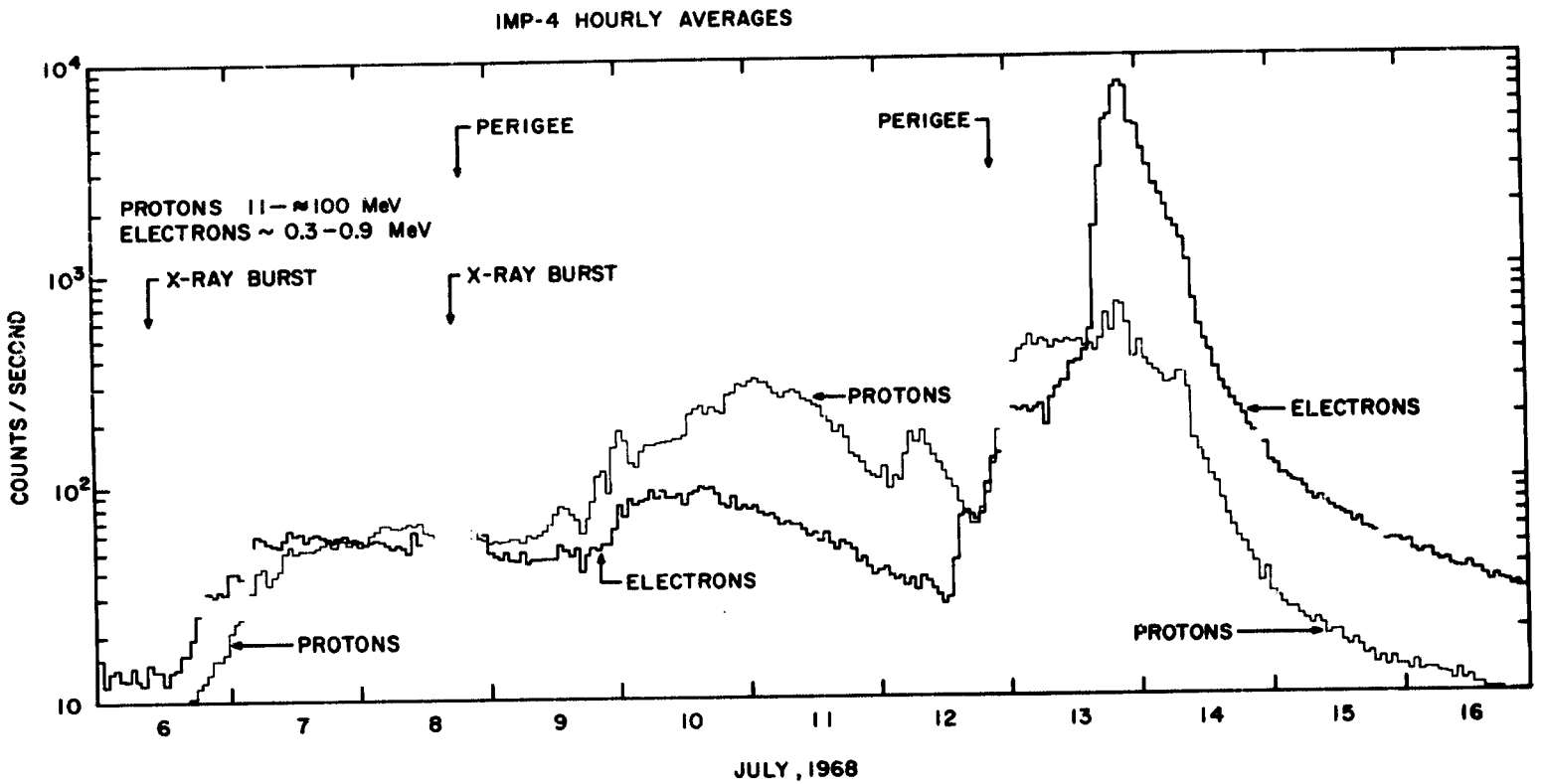

Figure 2. Time histories from IMP-4 of the intensities of interplanetary 0.3 to 0.9 MeV electrons and 11 to 100 MeV protons, omitting passes through the trapped radiation. Quiet-time background is included; that for the protons is about 9 counts per second.

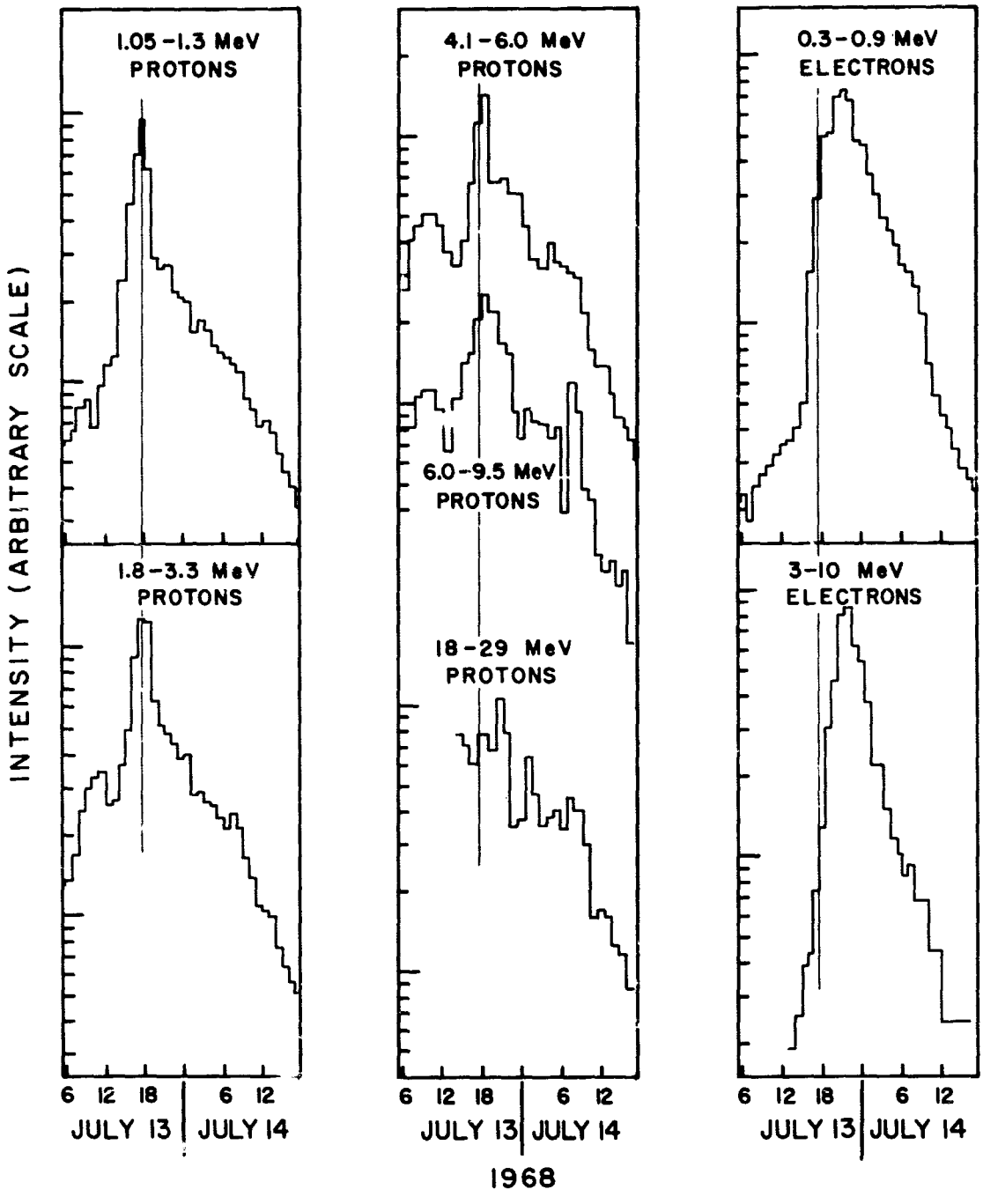

Figure 3. Time histories of a variety of electron and proton energy groups for the intensity increase in question.

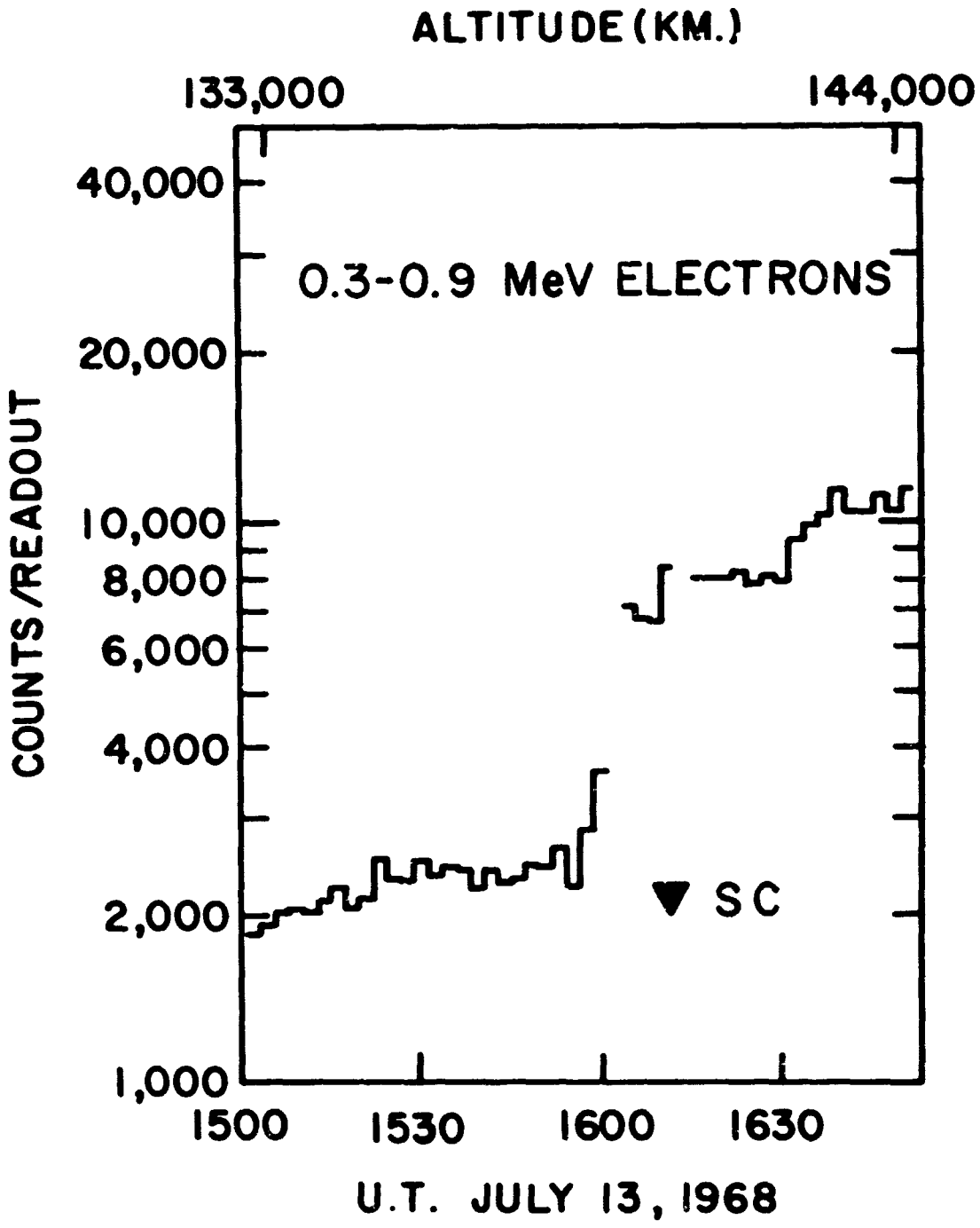

Figure 4. The abrupt increase in the 0.3 - 0.9 MeV electron intensity prior to the sudden commencement at 1612 UT on 13 July.

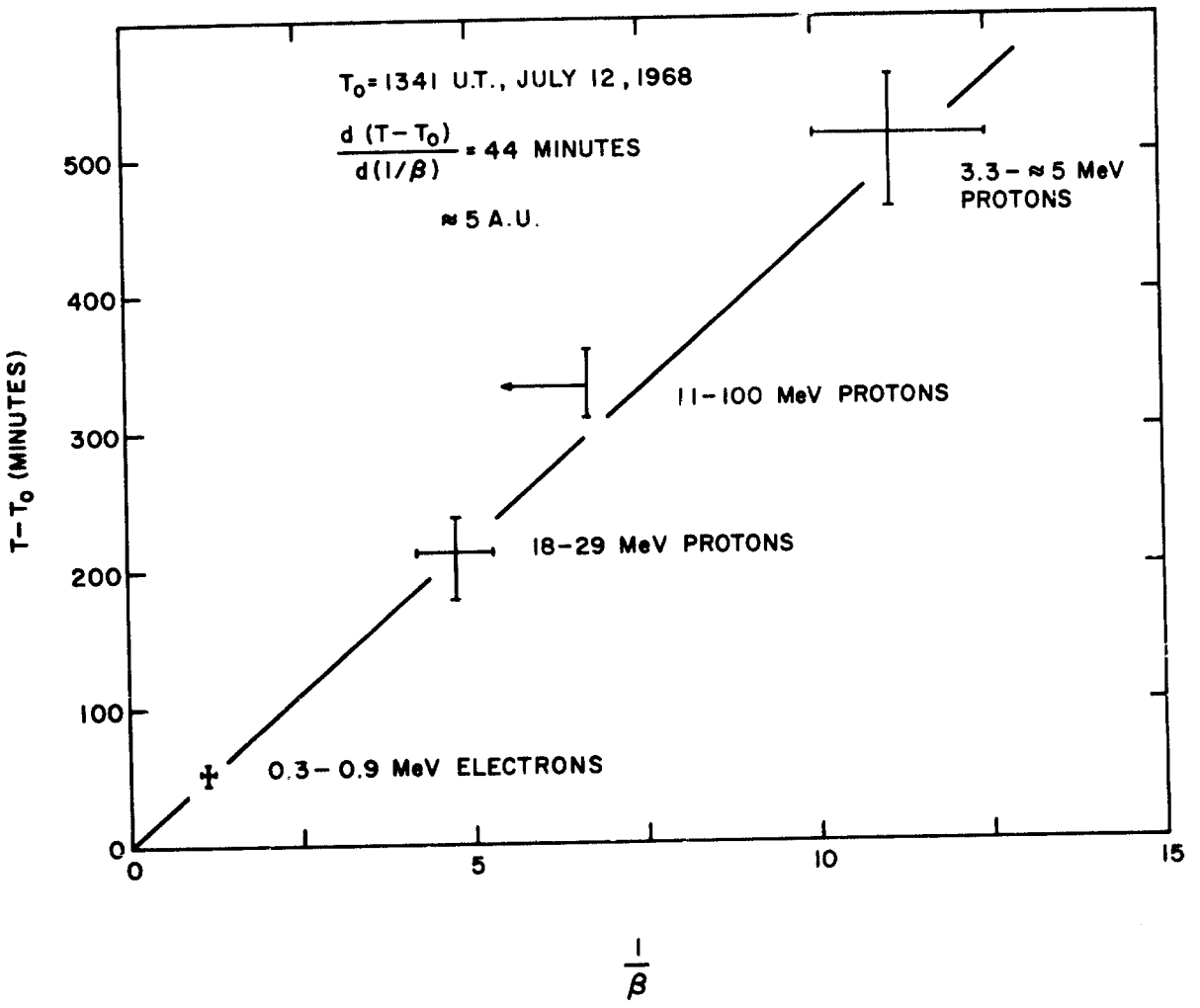

Figure 5. A plot of the onset times of the intensity increase on 12 July for various components versus the corresponding inverse velocity.

CO-ROTATING MODULATIONS OF COSMIC RAY INTENSITY DETECTED BY SPACECRAFTS SEPARATED IN SOLAR AZIMUTH

V. K. Balasubrahmanyan and E. C. Roelof*
NASA/Goddard Space Flight Center
Greenbelt, Maryland

R. P. Bukata and R. A. R. Palmeira
Southwest Center for Advanced Studies
Dallas, Texas

ABSTRACT

The daily cosmic ray intensity from the IMP-C (Explorer XVIII) geiger-counter monitor (Ep $\gtrsim$ 50 MeV) and Pioneer VI scintillation telescope (Ep $\gtrsim$ 7.5 MeV) have been statistically analyzed by the use of correlation functions. When the two spacecrafts are close to each other, the cross-correlation function agreed closely with the auto-correlation function of either detector, showing that both detectors were responding comparably and reliably to cosmic ray fluxes. When Pioneer VI and IMP-C were separated by ~50° (October-December 1966), the variations in the detector rates appear to be mainly due to galactic cosmic rays. Solar flare contributions $\gtrsim$7.5 MeV have been eliminated from the Pioneer VI data by regression analysis using low energy rates (7.5 MeV $\lesssim$ Ep $\lesssim$ 44 MeV). Comparison of IMP-C and neutron monitor rates shows no detectable variations in solar proton outflow of Ep $\gtrsim$ 50 MeV. The cross-correlation function between

*NAS/NASA Resident Postdoctoral Research Associate. Present address, Department of Physics, University of New Hampshire, Durham, N. H.

the detectors during this quiet period reaches a significant peak (0.67 ± 0.05) with a lag of ~3 days between data from IMP-C and Pioneer VI. Also, the cross-correlation function (displaced by -3 days) is qualitatively similar in form to the auto-correlation function from IMP-C. It is proposed that there are numerous long-lived regions of modulated cosmic ray flux following the general spiral configuration of the interplanetary magnetic field as the field structure co-rotates with the sun. This interpretation is consistent with the observations of recurrent Forbush decreases in early 1966 reported by McCracken, Rao, and Bukata (1966).

INTRODUCTION

It is well known that the interplanetary magnetic field controls the propagation of cosmic rays in the solar system. Low energy cosmic rays of solar or galactic origin remain linked to the magnetic tube of force along which they are propagating. Since the magnetic field is "frozen" in and convected by the solar wind, co-rotation of cosmic ray particles with the sun could result. For solar flare particles O'Gallagher and Simpson (1967), McCracken et al. (1967), and Lin et al. (1968) have presented evidence for co-rotation and studied the azimuthal dependence of their propagation. The studies of Bryant et al. (1965), and McCracken et al. (1966) on recurrent modulation phenomena have resulted in much information on co-rotating shock fronts where low energy particles may be continuously accelerated (Rao et al., 1967) and galactic particles are modulated in a manner similar to Forbush decreases. These regions have a long life time and have been followed through several solar rotations.

In the case of galactic cosmic rays, the diurnal anistropy and the 27 day recurrent Forbush decreases are prime examples of the co-rotation effect. Bukata et al. (1968), using their Pioneer VI and VII detectors, separated in solar azimuth by ~53°, have studied Forbush decreases associated with solar flares (blast waves) as well as recurrent co-rotating shock fronts. All the above phenomena deal with reasonably disturbed conditions in the interplanetary magnetic field. In this paper the results from the cosmic ray monitors on Explorer XVIII and Pioneer VI are compared during a quiet time. The co-rotation phenomena associated with quiet time conditions are studied to obtain information regarding the spatial and temporal structure of the interplanetary field and its interaction with galactic cosmic rays.

EXPERIMENTAL DETAILS

The IMP-C GM counter monitors the omnidirectional intensity of protons with energies above ~50 MeV. The threshold energy for detected electrons is ~4 MeV. The counting rate of the monitor is ~100/sec resulting in a daily statistical accuracy of ~.1%. The satellite was launched on May 9, 1965 into a highly eccentric geocentric orbit of apogee 41.5 R_E with a period of 5.8 days covering the entire period of interest in this paper, the monitor behaved very reliably. An inflight comparison with a similar detector aboard OGO-1 has shown that there were no detectable long term drifts in the behavior of the counter. A detailed description of the GM counter monitor may be found in Balasubrahmanyan et al. (1965).

The Pioneer VI data were obtained from the scintillation counter telescope experiment to study the azimuthal anisotropy of solar and galactic cosmic rays. The data considered in this paper consist of the cosmic ray intensity for particles with energy >7.5 MeV. The detector characteristics and other essential experimental information are described in detail by Bartley et al. (1967) and McCracken et al. (1967). Solar particle contribution to the data has been eliminated by a method involving a regression analysis of the integral intensity channel (>7.5 MeV) and the channel for particles with energy between 7.5 MeV and 45 MeV. This procedure is described in the work of McCracken et al. (1966) and Bukata et al. (1968). Pioneer VI was launched into solar orbit on December 16, 1965. During the early part of 1966 the satellite-sun-earth angle remained small, increasing gradually to $\sim 53°$ by the end of the year. Its radial distance from the sun varied between 1.22×10^8 km to 1.47×10^8 km. Fig. (1) shows the angular and radial coordinates of Pioneer VI during 1966. The trajectory of the satellite lies in the ecliptic plane.

RESULTS

The Pioneer VI solar azimuth during the first eighty-five days of 1966 was less than 5°. There was extensive data coverage for both the IMP-C and Pioneer VI spacecrafts during this period resulting in very little missing data.

Fig. (2) shows the regression plot of the daily average counting rates from IMP-C and Pioneer VI for the first 85 days of 1966. The correlation coefficient is .96 and the excellent agreement between the data from the two detectors shows

that both instruments are responding reliably and comparably to cosmic ray fluxes. Also plotted in the figure are monthly averages from the two satellites for the entire period. These monthly averages line up very well along the linear regression plot of the daily rates, showing that there has been no appreciable systematic long term drift of the detectors. This observation provides a measure of confidence for the analysis performed for the later period (after day 240) when data coverage in Pioneer VI data becomes spotty.

From day 240 onwards the azimuthal angle Φ remains approximately 52°. September was disturbed by a number of solar events. The period after day 276 up to the end of the year was relatively quiet and was considered in this study.

The daily average counting rates of the Deep River neutron monitor, IMP-C, and Pioneer VI (when available and corrected for solar out flow) for this period are shown in Fig. (3). There are three noticable decreases commencing on October 23, November 16, and December 12. The latter two are separated by 27 days (suggesting a recurrent event) but the first two are 24 days apart while their minima are only 21 days apart. The Forbush decrease of December 12 has been studied in detail (Bukata, et al., 1968) and comparison of data from Pioneer VI and Pioneer VII (the latter then near the earth) established that it was not a co-rotating structure.

It should be emphasized that the three detectors used to obtain the data plotted in Fig. (3) have thresholds of ~10 MeV, 100 MeV and 1000 MeV. Thus

we may establish that low energy galactic cosmic rays over two decades of energy display similar co-rotating phenomena. Although such features are apparent in Fig. (3) we have applied the more rigorous technique of cross-correlation to the analysis of the data.

The cross-correlation function of the Deep River neutron monitor daily averages N(t) and the IMP-C averages I(t) is presented in Fig. (4) along with the even auto-correlation functions of N(t) (plotted for positive lag), and I(t) (plotted for negative lag). The similar behavior of the two detectors is established not only by the high cross-correlation at zero-day lag (0.9) but by the near-equality of all three functions for lags up to 30 days. The average period of the damped quasi-sinusoidal oscillations that dominate the functions is 11-12 days but such a period is not readily apparent from inspection of Fig. (3). It is more likely the "signature" of the three large decreases. The half-width of the central peak (~3 days) is also the approximate half-width (including precursors) of the three large decreases.

The cross-correlation function of I(t) and N(t) with P(t) (Pioneer VI daily averages) are shown in Fig. (5). They are seen to exhibit strong peaks (~0.67 ± 0.05) at a lag of +3 days, and the general similarity to the cross-correlation functions of Fig. (4) is clear. The strong peak of 0.7 at a delay of +3 days in the cross-correlation function $\langle I(t)\ P(t+\tau)\rangle$ is still present even after a removal of the contribution of the obvious co-rotating decrease of October 24 from the two species of data. This indicates that the high cross-correlation is not dictated

solely by the presence of a single well-defined co-rotating event. A shift of the main peak to τ = 4 days is expected for co-rotation, so some additional azimuthal evolution of features is implied by the observed 3-day shift. There are additional structures in Fig. (5) that are statistically significant, particularly the increase at τ = -23 days. This increase appears to be related to the increase at a corresponding lag of -27 days in $\langle I(t)\ I(t+\tau)\rangle$ depicted in Fig. (4). This may be a 27 day recurrence tendency that is more pronounced at lower energies, such as could be produced by outflow that is not completely removed from the Pioneer data by the regression technique and is also present at the higher energies detected by IMP-C. However, the presence of the feature also at τ = -24 days in $\langle N(t)\ P(t+\tau)\rangle$ suggests that the particles responsible for this 27 day recurrence tendency are more likely to be galactic cosmic rays. This discussion illustrates the ambiguity in cross-correlation analysis between recurrent solar outflow and galactic decreases, both of which give a positive cross-correlation.

CONCLUSIONS

The co-rotation of quiet-time modulations of cosmic rays from 10 MeV to 1 BeV has been established by statistical techniques. The strong correlation of the data from three observation stations implies all three are responding to galactic cosmic rays during the period under consideration here. Therefore, short-term modulation of galactic cosmic rays during undisturbed periods may, in general, be predominantly due to co-rotating magnetic structures. Since the mechanism of such modulations is not firmly established, care should be

exercised in applying current theories to short-term variations of low energy galactic cosmic rays.

This study illustrates the need to consider the role of the co-rotation effect in studies of gradient of cosmic rays in the solar system with detectors separated appreciably in the solar azimuth. Krimigis and Venkatesan (1969) discuss the inappropriateness of the inclusion of Forbush decreases in studies of the cosmic ray intensity gradient determined with detectors in orbit around the earth and carried in Mariner IV. It is clear from the results presented here that if a modulation phenomenon is observed by a detector at some point in the inner solar system, another detector separated Θ degrees in solar azimuth may also observe this modulation phenomenon. The time delay between successive observations of such a phenomenon would be given by $\sim\Theta/13.3$ days.

REFERENCES

Balasubrahmanyan, V. K., G. H. Ludwig, F. B. McDonald, and R. A. R. Palmeira, "Results From the IMP-I GM Counter Telescope Experiment," J. Geophys. Res., 70, 2005-2019, 1965.

Bartley, W. C., K. G. McCracken, and U. R. Rao, "The Pioneer 6 Detector To Measure the Degree of Anistropy of the Cosmic Radiation in the Energy Range 7.5-90 MeV/nucleon," Rev. Sci. Instr., 38, 266-272, 1967.

Bryant, D. A., T. L. Cline, U. D. Desai, and F. B. McDonald, "Continual Acceleration of Solar Protons in the MeV Range," Phys. Rev. Letters, 14, 481, 1965.

Bukata, R. P., K. G. McCracken, and U. R. Rao, "A Comparison of the Characteristics of Corotating and Flare-initiated Forbush Decreases," Can. J. Phys., 46, S994-S998, 1968.

Krimigis, S. M. and D. Venkatesan, "The Radial Gradient of Interplanetary Radiation Measured by Mariners 4 and 5," J. Geophys. Res. 74, 4129-4146, 1969.

Lin, R. P., S. W. Kahler, and E. C. Roelof, "Solar Flare Injection and Propagation of Low-Energy Protons and Electrons in the Event of 2-9 July 1966," Solar Physics 1, 338-360, 1968.

McCracken, K. G., U. R. Rao, and R. P. Bukata, "Recurrent Forbush Decreases Associated with M-Region Magnetic Storms," Phys. Rev. Letters, 17, 928-932, 1966.

McCracken, K. G., U. R. Rao, and R. P. Bukata, "Cosmic-Ray Propagation Processes, 1. A Study of the Cosmic-Ray Flare Effect," J. Geophys. Res., 72, 4293-4324, 1967.

O'Gallagher, J. J. and J. A. Simpson, "The Heliocentric Intensity Gradients of Cosmic-Ray Protons and Helium During Minimum Solar Modulation," Astrophys. J., 147, 819, 1967.

Rao, U. R., K. G. McCracken, and R. P. Bukata, "Cosmic-Ray Propagation Processes, 2. The Energetic Storm Particle Event," J. Geophys. Res., 72, 4325-4342, 1967.

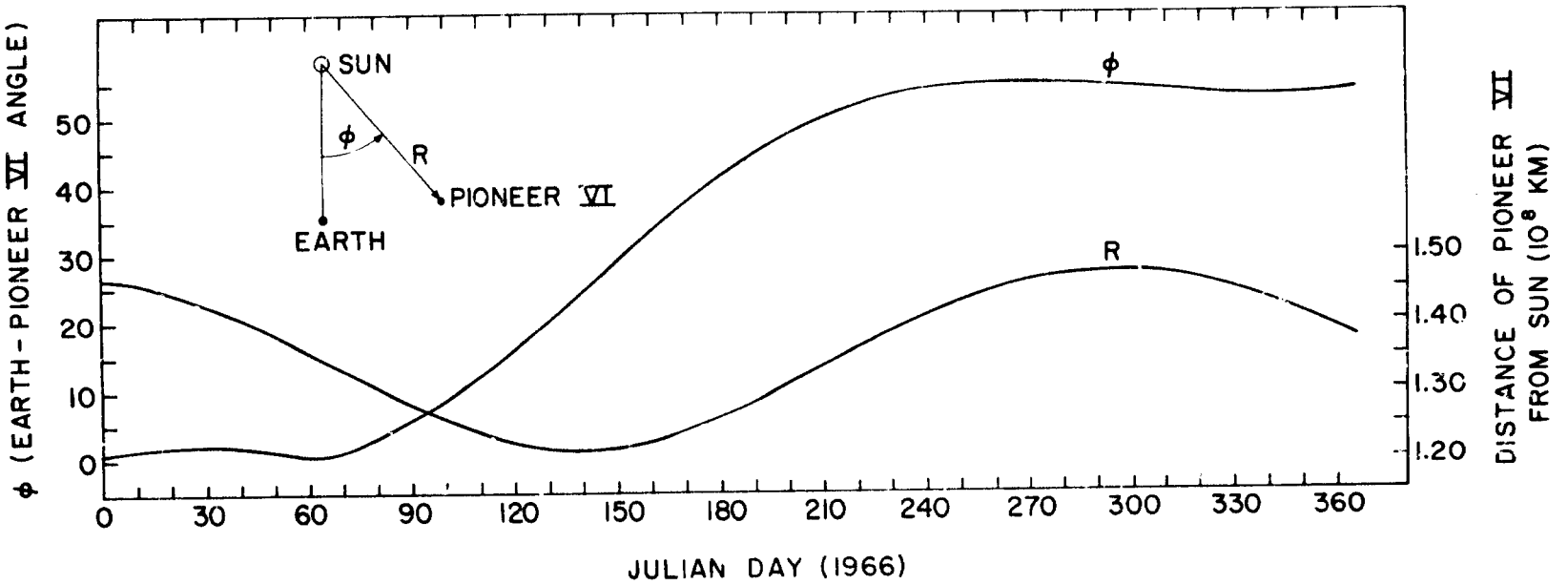

Figure 1. Solar distance (R) of Pioneer VI and angle (ϕ) westward from earth.

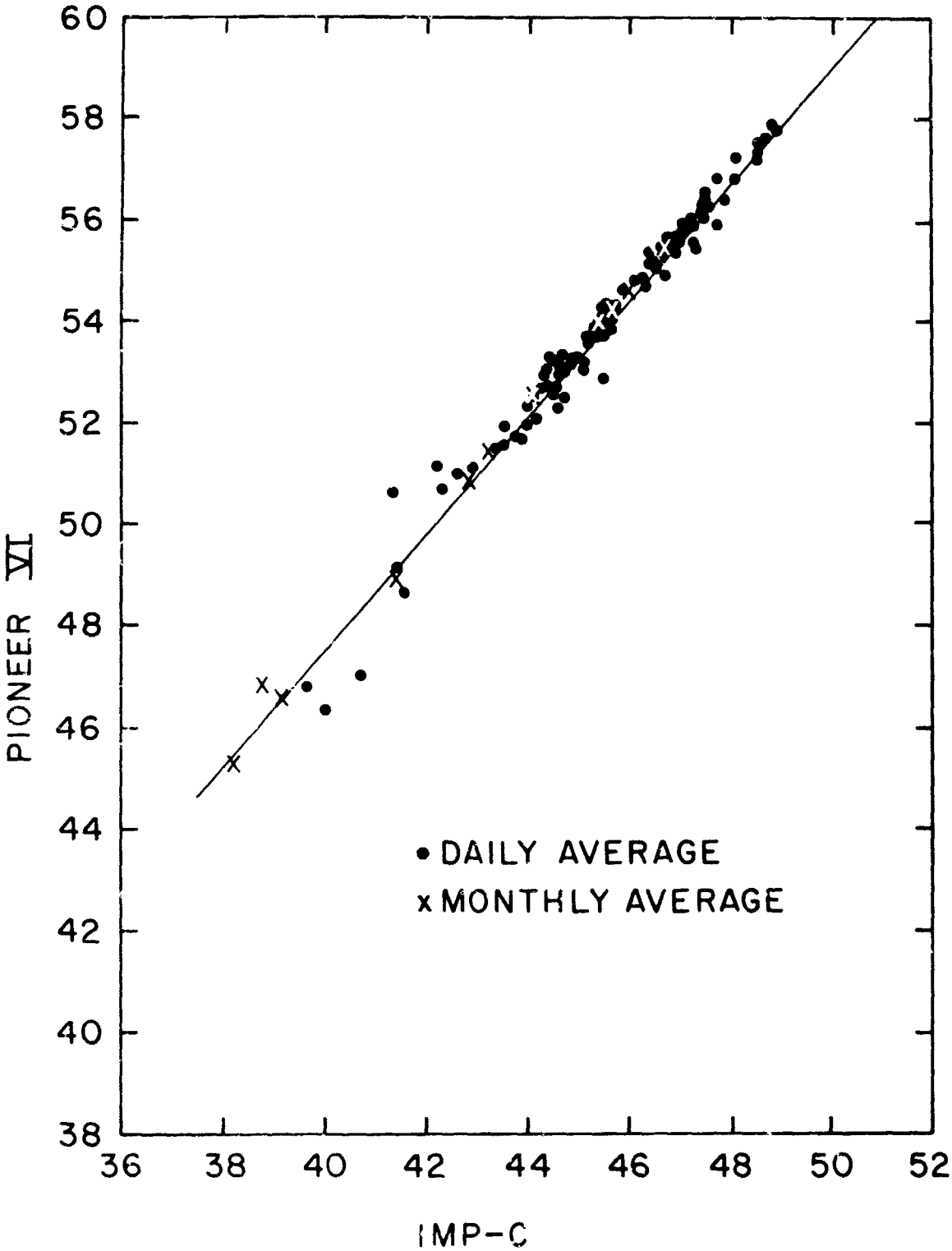

Figure 2. Regression plot of the daily average counting rates from IMP-C and Pioneer VI for days 1–85, 1966. Also plotted are monthly averages for the first 11 months of the Pioneer VI mission.

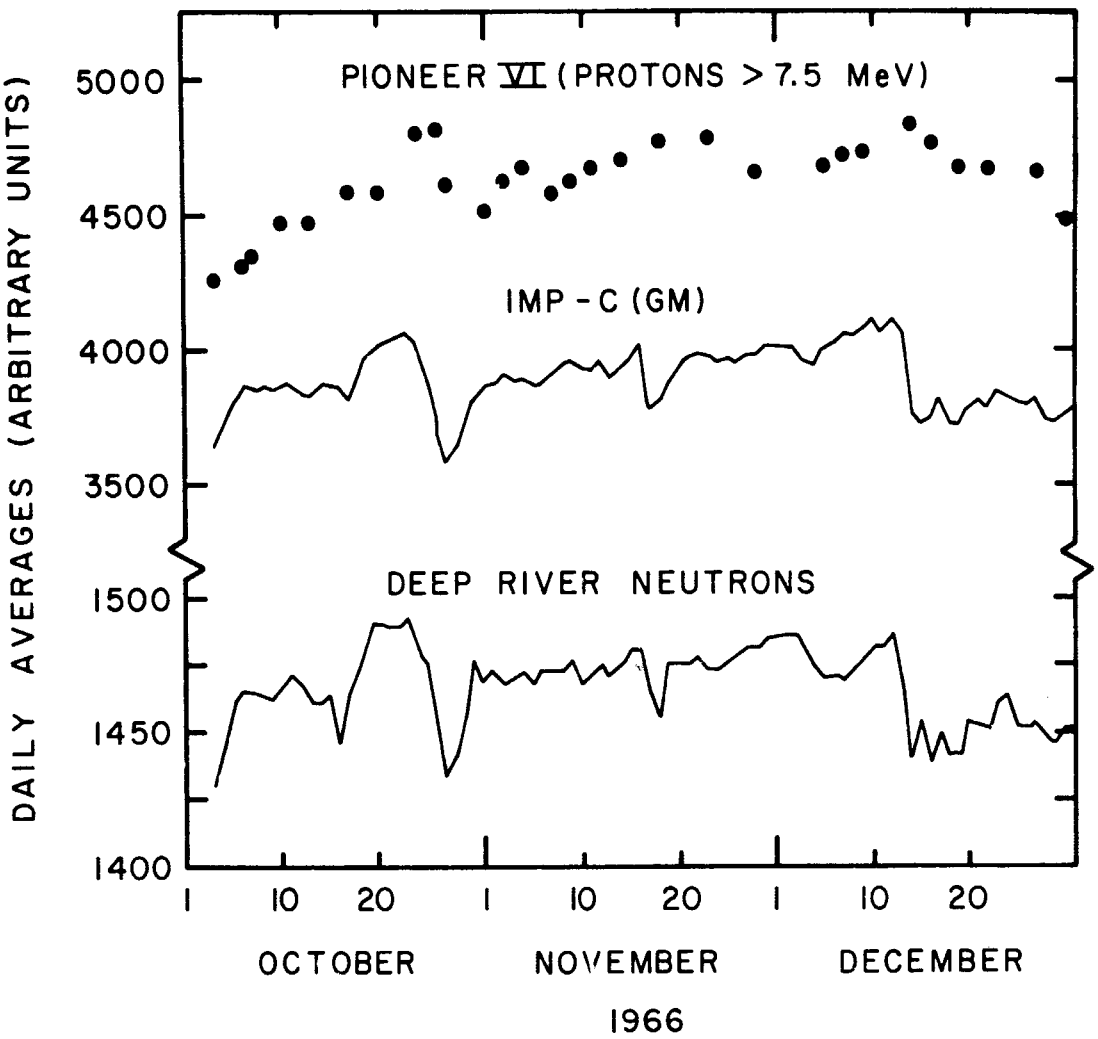

Figure 3. Daily average counting rates for the three detectors compared in this study: Pioneer VI scintillation telescope, IMP-C Geiger monitor, and Deep River neutron monitor.

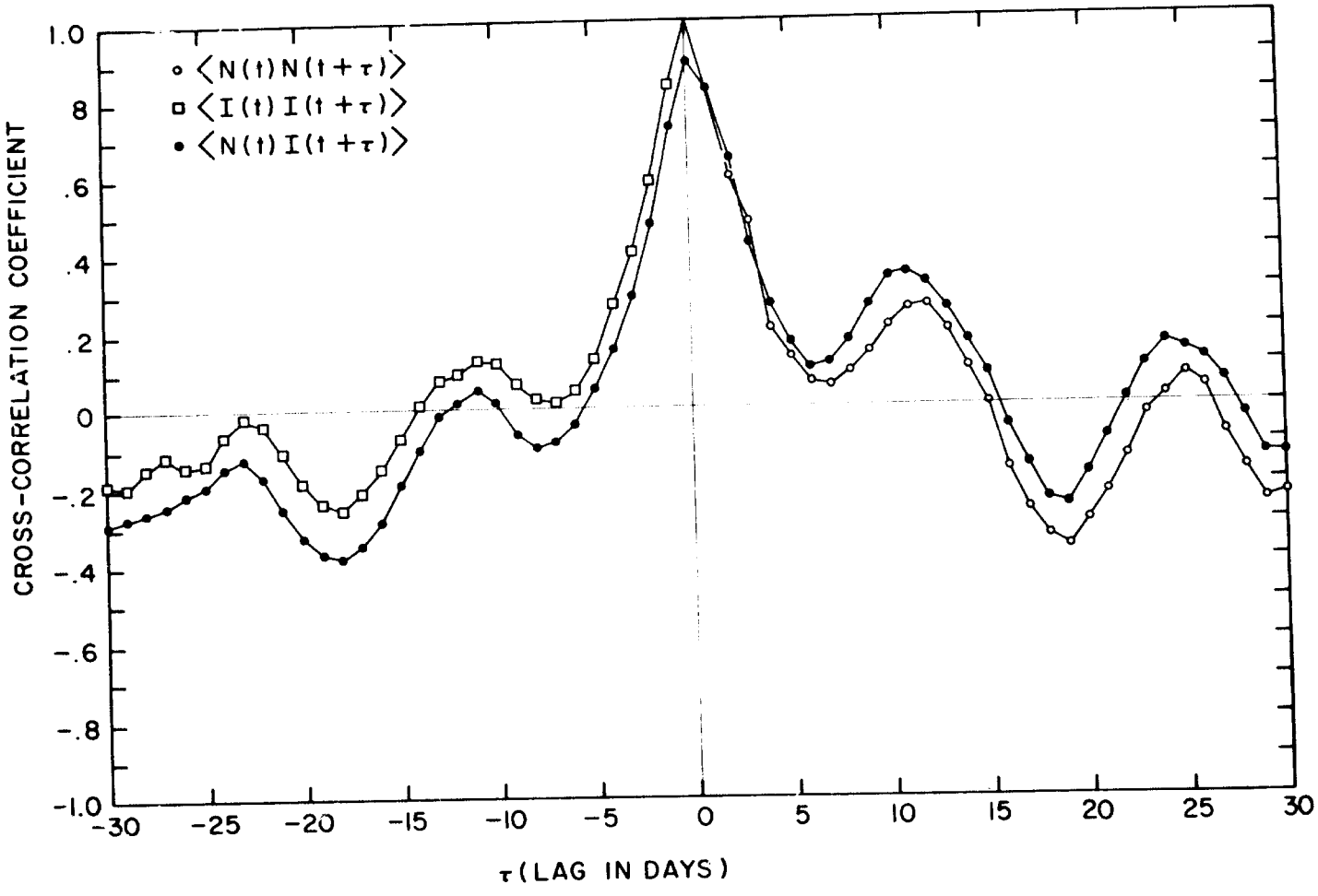

Figure 4. Auto- and cross-correlation functions for IMP-C Geiger monitor (I) and Deep River neutron monitor (M). The auto-correlation functions, being even, are plotted only for positive lags (N, open circles), and negative lags (I, open squares).

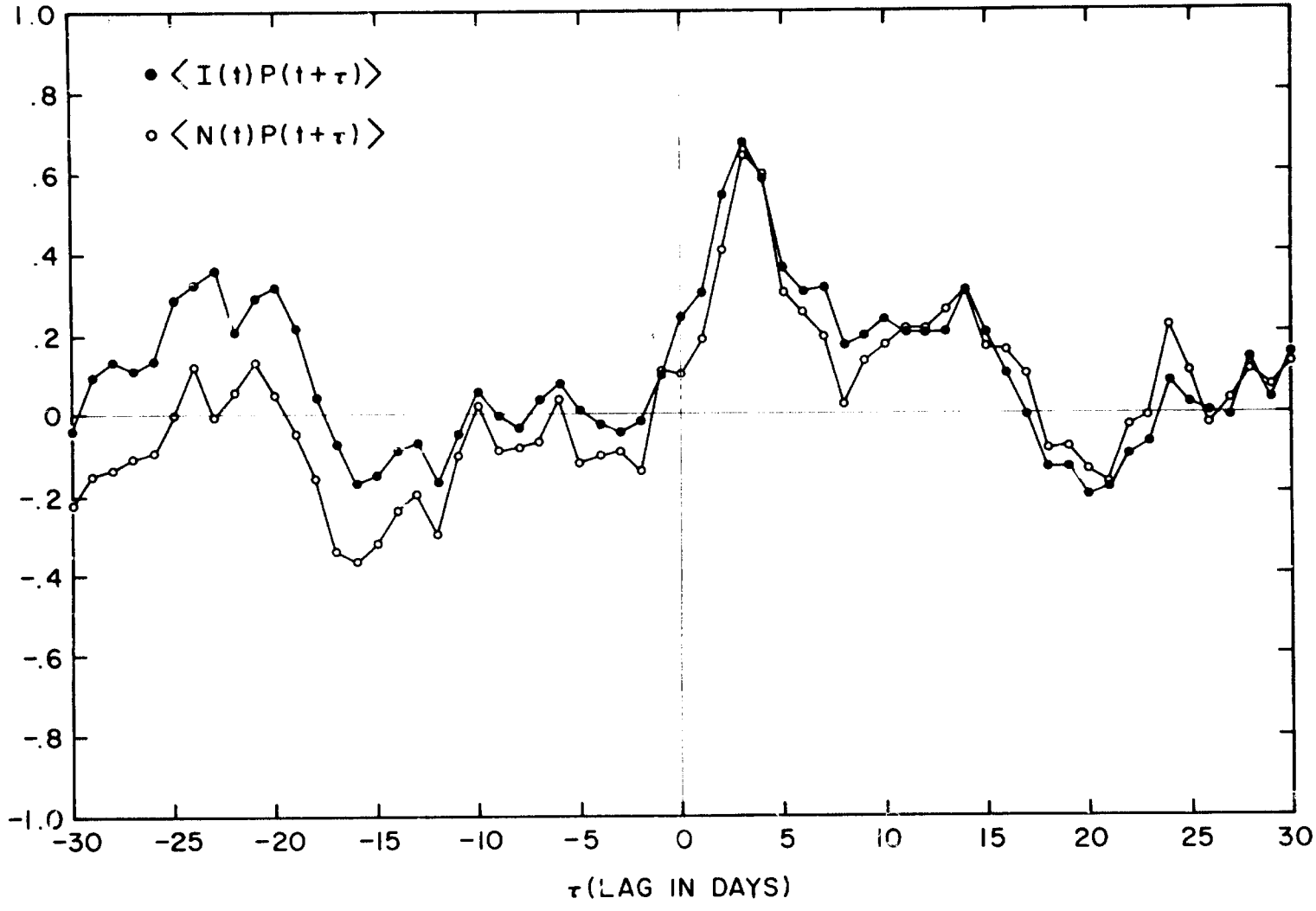

Figure 5. Cross-correlation functions for IMP-C Geiger monitor (I, closed circles) and Deep River neutron monitor (N, open circles) with the Pioneer VI scintillation telescope (P).

SPECTRAL VARIATIONS IN SHORT TERM (FORBUSH) DECREASES AND IN LONG TERM CHANGES IN COSMIC RAY INTENSITY

V. K. Balasubrahmanyan
Goddard Space Flight Center
Greenbelt, Maryland (USA)

and

D. Venkatesan*
Department of Physics
University of Calgary
Calgary, Alberta (Canada)

*On sabbatical leave; present address Goddard Space Flight Center, Greenbelt, Maryland.

ABSTRACT

Data are available from satellites IMP A, B, and C and OGO A on a continuous basis over the period November 1963—May 1967. The cosmic ray intensity registered by GM counters on these satellites, of energy $\gtrsim$50 MeV is compared with the intensities recorded by neutron monitors, at the equatorial station, Huancayo, at the high latitude station, Deep River, and at the polar station, Alert. Spectral variations during the Forbush decreases and during long term changes in cosmic ray intensity are investigated, and the results discussed in terms of current ideas.

I. INTRODUCTION

The continuous monitoring of the intensity of cosmic rays by ion chambers and neutron monitors has been instrumental in providing information on short term changes, viz., Forbush decreases and 27 day variations, and long term modulations [Sandström, 1965]. The effects of modulation are very energy dependent, with the low energy particles affected more than higher energy particles. Because of geomagnetic and/or atmospheric effects, the lower limit of energy for which neutron monitors are sensitive is $\gtrsim$400 MeV. A series of satellite borne GM counter monitors sensitive to particles of energy $\gtrsim$50 MeV have been successfully flown in the highly eccentric satellites IMP A, B, and C and OGO A. These GM counter monitors [Balasubrahmanyan et al., 1965] were of identical construction, and were designed and calibrated so that the data from the above satellites could be carefully combined to give a reliable time history of cosmic rays, almost on a continuous basis from November 1963 to May 1967. Particular care has been taken to show that a reasonably accurate time history of cosmic ray intensity is obtained by intercomparisons among the different monitors so that the effects due to long term drifts do not affect the results. The results are used to study the phenomena of short and long term modulations in this paper.

II. DESCRIPTION OF DETECTORS

Four pancake type halogen quenched counters are arrayed to form two telescopes with their axes respectively parallel ($T_{\parallel}$) and perpendicular ($T_{\perp}$) to the

main axis of the satellites. In addition to the coincidence counts due to the two telescopes, counts due to any of the four counters (referred to as omnidirectional intensity) are sampled for 40 seconds every 5 minutes. For the omnidirectional intensity the threshold energy for registration is ~50 MeV. In the case of OGO A satellite, which was not designed to be spin stabilized but to be attitude control stabilized, there were six GM counters arrayed into three telescopes along three naturally optional axes. Further counts due to any of the six counters, corresponding to the omnidirectional output, were also registered. In our study here, we are only concerned with the omnidirectional intensity.

Table I lists the details regarding the orbits of the satellites, the launch dates, and the periods for which useful data were obtained. Only data registered beyond 75,000 km from the earth are used in this study. This excludes any contamination of the results by trapped particles.

Table I

Relevant Details of the Satellites From Which the Data Used in This Analysis Have Been Taken

Satellite	Date of Launch	Apogee	Principal Data Coverage Period
IMP A	Nov. 27, 1963	31.7 Re	Nov. 1963 to May 1964 Sept. 1964 to Dec. 1966
IMP B	Oct. 4, 1964	15.9 Re	Oct. 1964 to Apr. 1965
OGO A	Sept. 4, 1964	24.3 Re	Sept. 1964 to Dec. 1966
IMP C	May 29, 1965	41.5 Re	May 1965 to May 1967

III. COMPARISON OF THE DATA FROM THE DIFFERENT SATELLITES

There was no detectable instrumental drift among the detectors from these different satellites and the maximum difference in the absolute counting rate was less than 5%. This was easily corrected by using data from periods when two or more satellites overlapped in time. An examination of Figures 1 and 2 shows that the correlation between the monitors is excellent and the dispersion in the data from the different satellites is small. Thus the average counting rate from these monitors is good approximation to an accurate time history of cosmic rays above 50 MeV.

In Figure 3 we compare the results from our monitors with the University of Minnesota ionization chamber on the OGO A satellite [Kane 1967] and the agreement between the data from these two independent measurements gives confidence in the accuracy of the data presented here.

Figure 4 shows the continuous time history of cosmic rays as measured by the GM counter monitor from the IMP and OGO satellites for the period 27 November 1963 to May 1967. The curve shows the approach to maximum intensity around May 1965 and the decline of the intensity after 1965 due to the start of the new solar cycle as evident from the many short term and large Forbush decreases.

IV. COMPARISON OF THE SATELLITE BORNE MONITOR AND GROUND BASED NEUTRON MONITORS

The comparison of the time history of the satellite cosmic ray monitor with the Deep River neutron monitor shows that the regression curve before

and after the solar minimum are different, as seen in Figure 5. There is a tendency for low energy particles to linger after May 10 suggesting a "hysteresis" type of behavior. Kane [1967] has seen a similar effect when he compared the results from the ionization chamber carried on OGO A and OGO C with the ground based neutron monitor. This type of hysteresis has been reported from a study of high latitude and low latitude neutron monitors by Simpson [1963] and Lockwood and Razdan [1963]. With the start of the new solar cycle the modulation appears to have a different energy dependence as compared to the same before the solar minimum.

During the period before May 10, 1965, the ratio of the increase in the GM rate to that of the Deep River neutron monitor is ~5.9. After the maximum intensity the corresponding ratio for the decrease of intensities becomes ~3.7, indicating that the spectrum abounds in particles which are counted by the GM counter. When a linear regression is fitted for the data from the GM counter the relationship between the neutron monitor at Deep River to the GM counter rate is given by

$1.42X - 1720.3 = Y$ for the period before the cosmic ray maximum, and

$1.16X - 1316.9 = Y$ for the period after maximum

where X and Y are the daily counting rates due to the Deep River and the GM counter monitor, respectively.

This "hysteresis" effect is shown more clearly in Figure 6 where the effect of random fluctuations is somewhat smoothed by plotting the moving averages of

the satellite monitor vs the Deep River monitor. Near the end of 1966 the "hysteresis" seems to decrease. These results indicate that the long term modulation has structural details which are not adequately covered by the theories of solar modulation. Experimental data, particularly energy spectra of the different particles, might be very useful in studying the propagation of these particles in the solar environment.

After the solar minimum, there are a number of short term Forbush decreases. A comparison of the GM counter monitor with the neutron monitor gives an idea of the spectral changes involved in these short term changes. The data used in these studies concern the short term decreases of the following dates:

1965 July 14	1966 January 1
1965 October 3	1966 March 8
1965 December 31	1966 May 25
	1966 July 22

In Figure 7 the counting rate of the GM counter monitor is plotted separately against the Deep River and Alert neutron monitor data for the above short term changes. The points corresponding to the different decreases seem to fall along a line such that the relative decreases during the different events seem to be the same within the experimental errors. Also shown in the diagram by crosses are the estimated long term changes, from the monitor long term trend observed after removing the Forbush decreases from both the monitors. The straight lines

shown in Figure 7 are the least square fit to the data shown. In the short term and the long term the data seem to correlate very well suggesting that the spectral changes for particles above 50 MeV are the same both for short term and long term modulations. A similar comparison of the satellite borne GM counter monitor with the neutron monitor at Huancayo is given in Figure 8 for the identical period. The correlation coefficient between the sets of data is 0.81, and the greater scatter in Figure 8 is indicative of that. The straight line shown is the line of least square fit. Thus this comparison also generally supports the conclusion that spectral changes for particles above 50 MeV are essentially the same for both short and long term modulations.

V. SOLAR CYCLE VARIATION IN COSMIC RAY INTENSITY

In Figure 9 we have the monthly means of R, the Zurich relative sunspot number, the cosmic ray intensity as recorded by Sulphur Mountain and Huancayo neutron monitors, for the period January 1964—December 1968. Also shown in the diagram are the monthly means of the satellite borne GM counter monitor for the period January 1964—December 1966, with a gap of three values. The cosmic ray intensities are all plotted, increasing downward for an easier comparison with solar activity.

The correlation between the monthly means of all the detectors for January 1964—December 1966 for the Sulphur Mountain-Huancayo detectors for the period January 1964—December 1968 have been found to be high, being better than 0.9.

The regression equations were determined for any two pairs. Using such a relation between the satellite detector and Sulphur Mountain, and using the observed values of the Sulphur Mountain monthly mean cosmic ray intensity, we predict the intensity of the satellite borne detector for the period January 1964—December 1968. This is shown in Figure 10 along with the observed satellite data for January 1964—December 1966.

Thus during the period May 1965—November 1968 the decrease in the integral proton intensity above 50 MeV is associated with a decrease of 57.2% in contrast to the intensity measured at Sulphur Mountain which is associated with a 17.8% and a decrease of 4.4% at Huancayo. The ratio of the first two quantities comes out to be 3.2.

It is relevant to refer to the work of Ormes and Webber [1968] where they compare the integral intensity of protons above 450 MeV against the Mt. Washington neutron monitor for a number of balloon flights, using daily values of the neutron intensity. They obtain a ratio of 16.1/5.9 or 2.7.

VI. CONCLUSIONS

1. There appears to be a "hysteresis" type of behavior on the part of low energy particles after the solar minimum. This "hysteresis" also seen during the last solar cycle by Simpson [1963] and Lockwood and Razdan [1963] by study of low and high latitude neutron monitors, may indicate the differences in propagation characteristics of cosmic ray particles at the onset of new solar activity after a period of quiet time conditions.

2. The short term decreases and long term decreases appear to have the same spectral response suggesting similar mechanisms of modulation.

3. The solar cycle variation in the integral proton intensity $\gtrsim 50$ MeV during May 1965 to November 1968 is estimated to be about 57.2% as against 17.8% for intensity for the high latitude neutron monitor at Sulphur Mountain and against 4.4% for intensity for the low altitude neutron monitor at Huancayo.

ACKNOWLEDGMENT

The work at Calgary was supported by grant A-3685 of the National Research Council, Ottawa. We are thankful to Dr. H. Carmichael for Deep River Data, Dr. B. G. Wilson for the Sulphur Mountain Data and to the World Data Center, Boulder and to Dr. J. A. Simpson for the Huancayo Neutron Monitor Data. One of us (DV) is thankful to Dr. F. B. McDonald for his hospitality during the sabbatical stay at GSFC, Greenbelt, Maryland.

REFERENCES

Balasubrahmanyan, V. K., G. H. Ludwig, F. B. McDonald, and R. A. R. Palmeira, Results from the IMP 1 GM Counter Telescope Experiment, J. Geophys. Res., 70, 2005, 1965.

Kane, Sharad R., Application of an Integrating Type Ionization Chamber to Measurements of Radiation in Space, Ph.D. Thesis, University of Minnesota, September 1967.

Lockwood, J. A., and H. Razdan, The Rigidity Dependence of the Long- and Short-Term Variations in Cosmic Radiation, Proc. of the 8th International Conference on Cosmic Rays, Jaipur, Vol. 2, 295, 1963.

Ormes, J. F., and W. R. Webber, Cosmic-Ray Proton and Helium Spectra and Solar Modulation Effects in the New Solar Cycle Measured with a Four-Element Counter Telescope [Proc. of the 10th International Conference on Cosmic Rays, Calgary], Can. J. Phys., 46, S883, 1968.

Sandström, A. E., Cosmic Ray Physics, North-Holland Publishing Co., 1965.

Simpson, J. A., The Primary Cosmic Ray Spectrum and the Transition Region between Interplanetary and Interstellar Space, Proc. of the 8th International Cosmic Ray Conference, Jaipur, Vol. 2, 155, 1963.

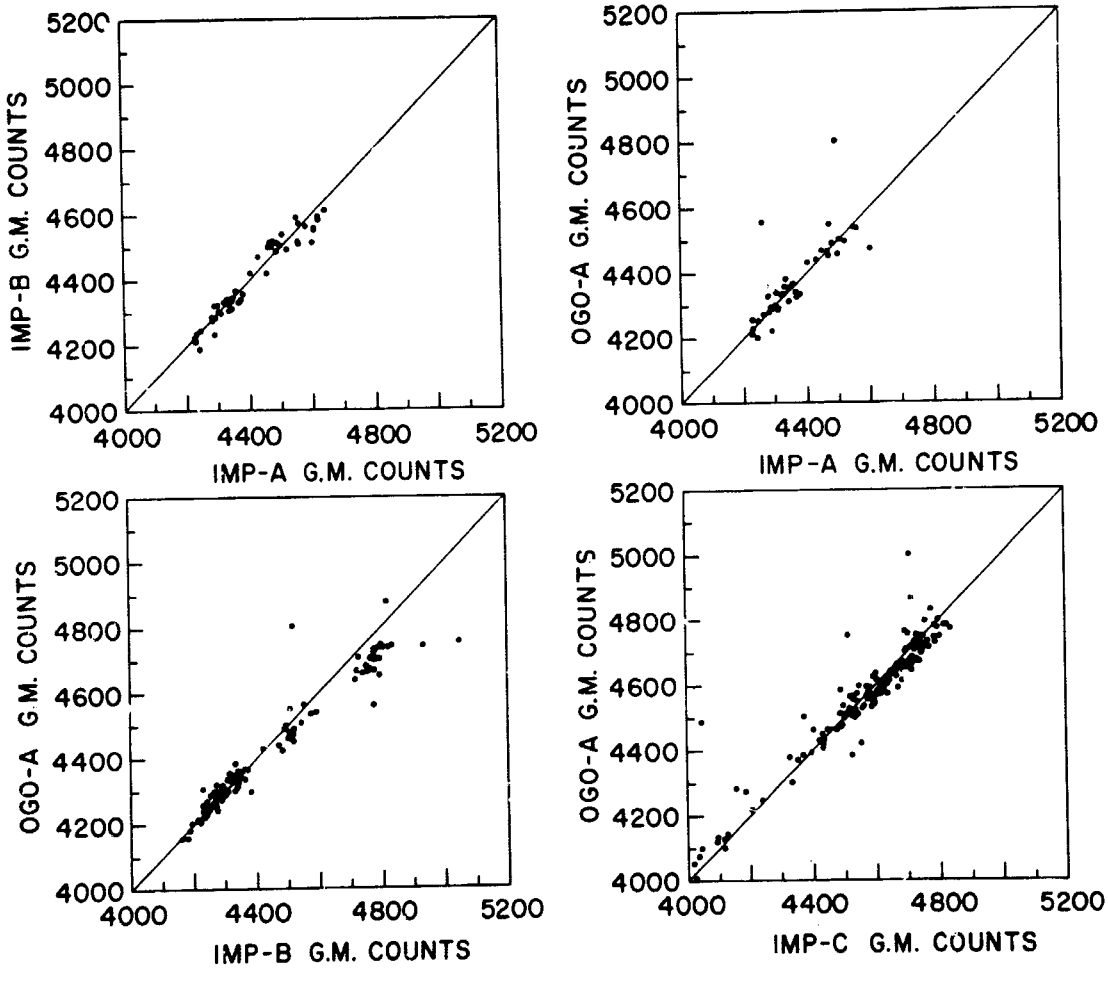

Figure 1. Crossplots of daily means of cosmic ray intensities as measured by IMP A, B, and C and OGO A monitors during common periods of functioning of any two pairs.

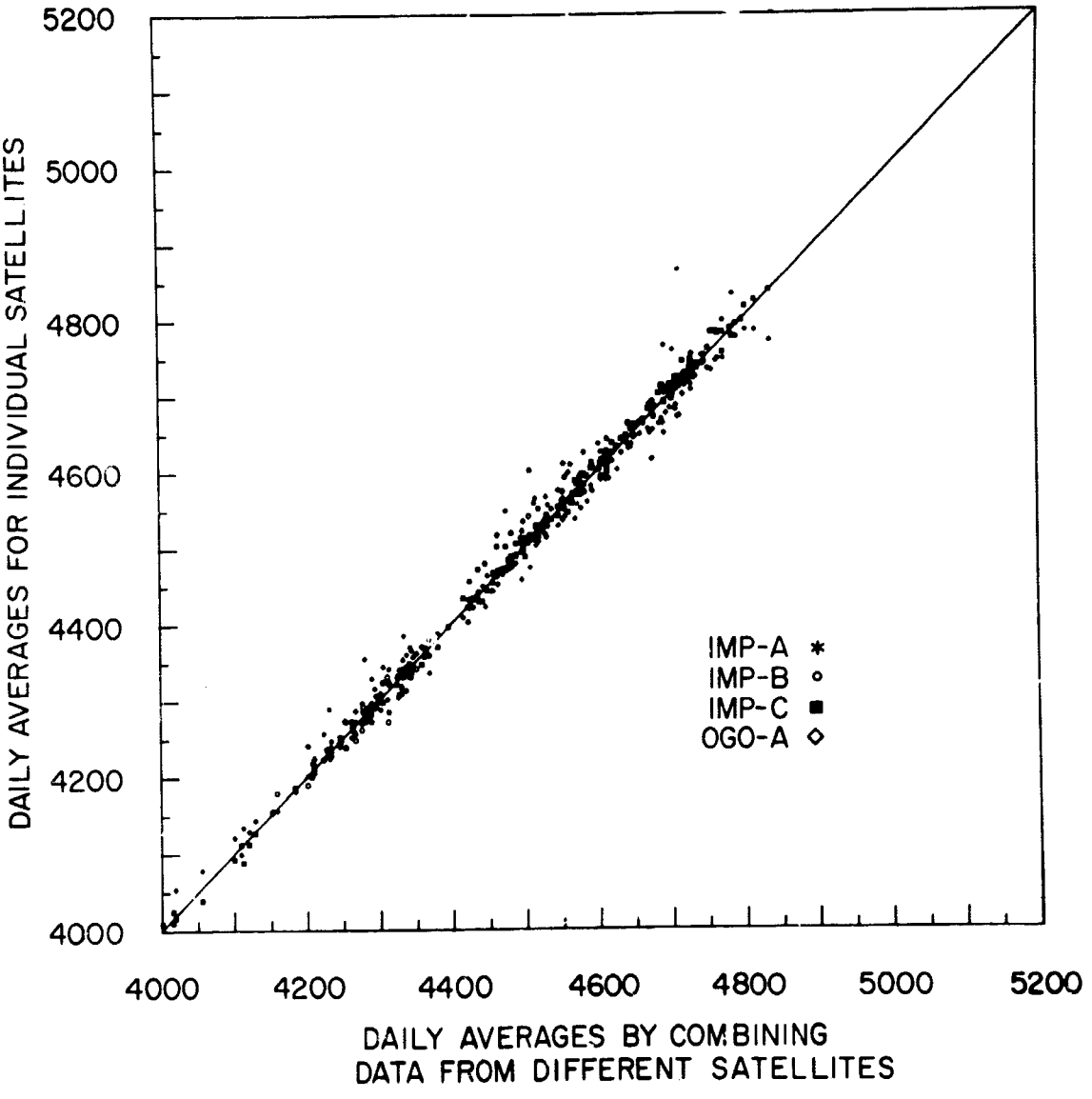

Figure 2. Crossplot of daily averages of individual IMP-OGO satellites versus daily averages obtained by combining data from different satellites.

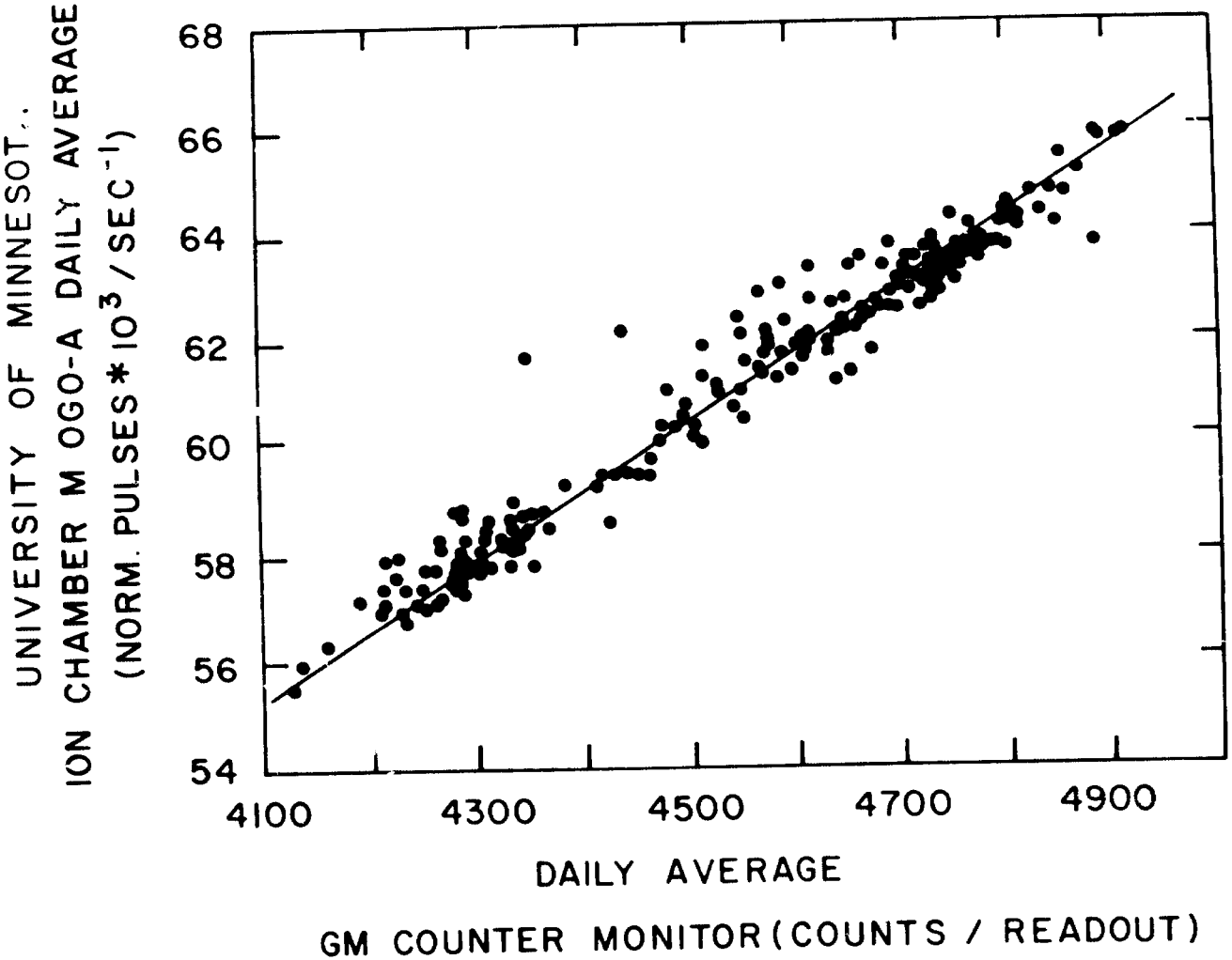

Figure 3. Crossplot of University of Minnesota ion chamber on OGO A versus Goddard Space Flight Center GM counter monitor on the same satellite.

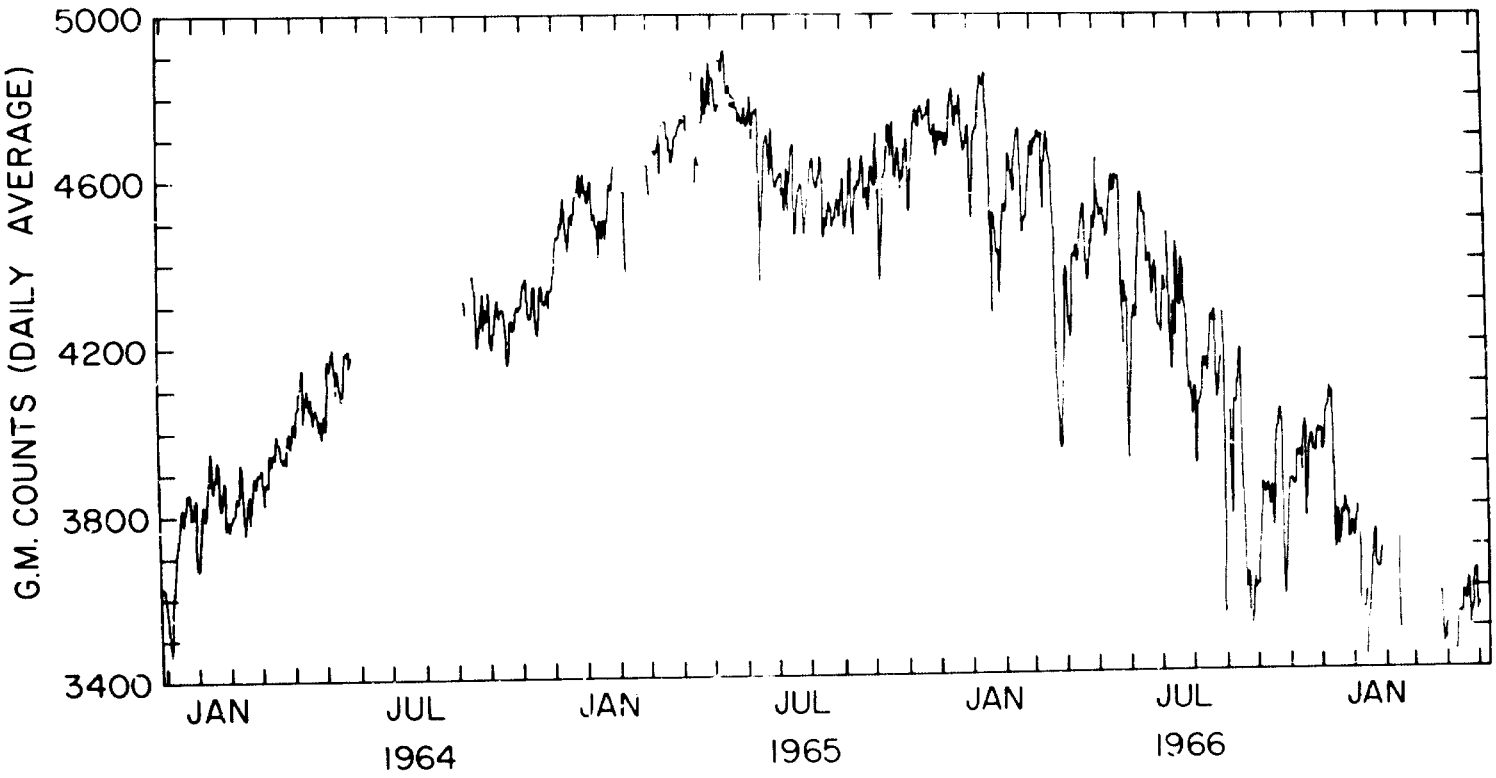

Figure 4. Daily means of cosmic ray intensity registered by the IMP-OGO satellites during November 1963–May 1967.

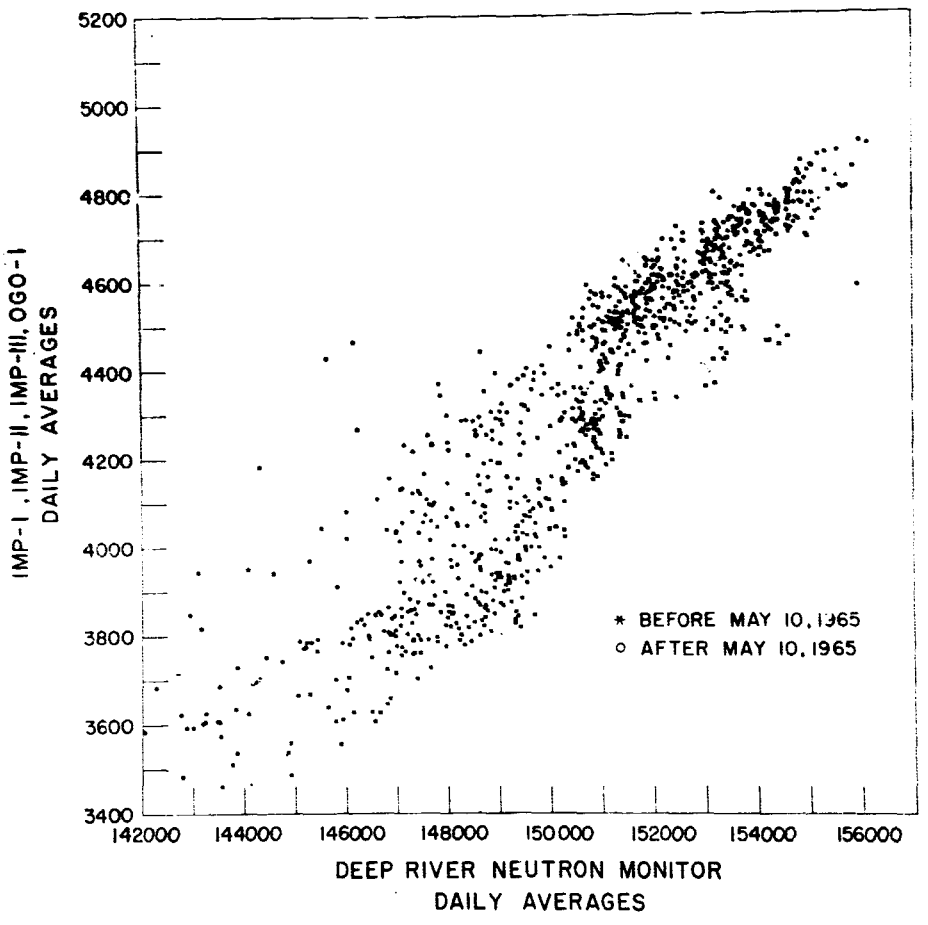

Figure 5. Crossplot of IMP-OGO daily averages versus Deep River neutron monitor daily values.

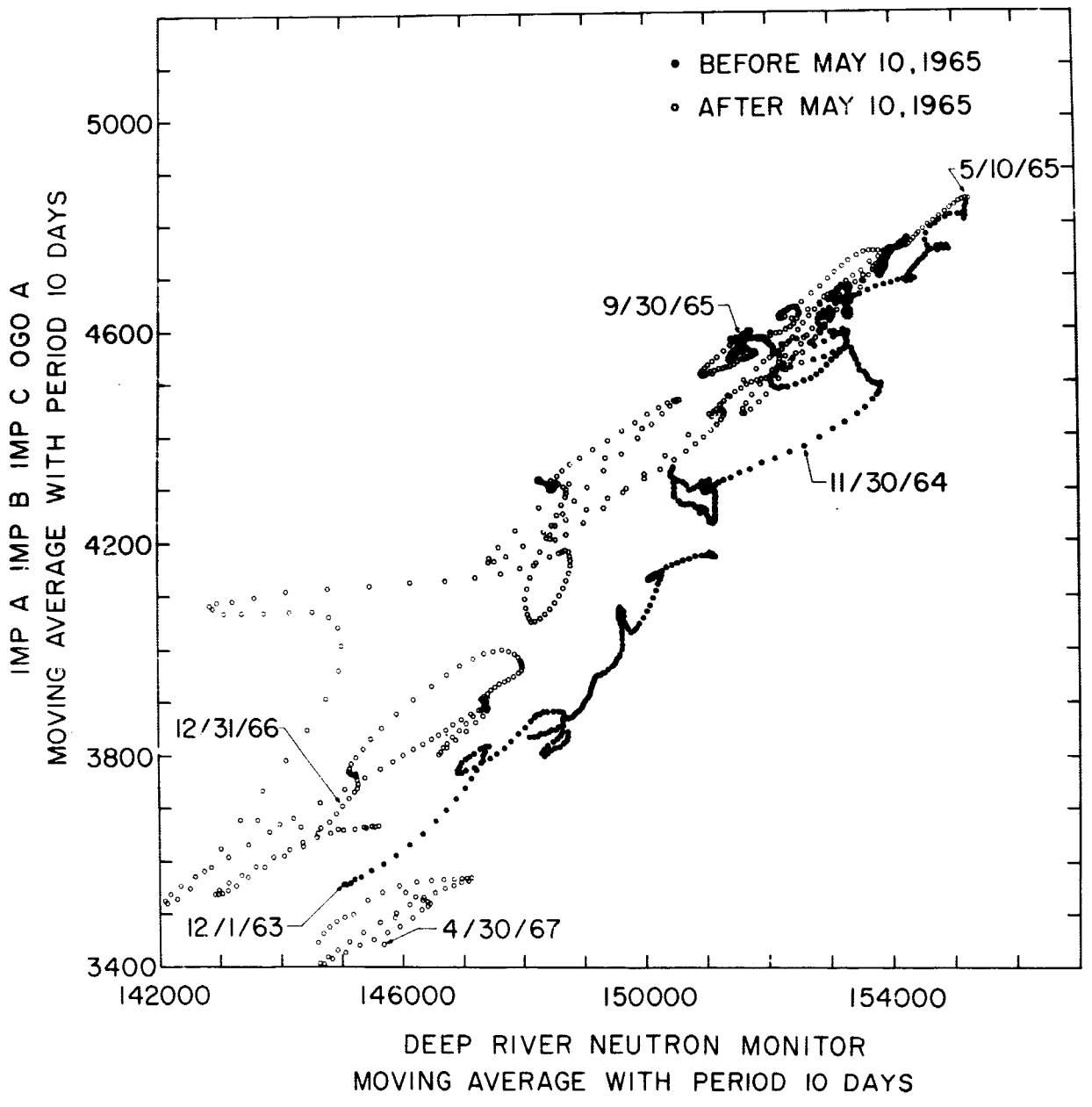

Figure 6. Crossplot of ten days moving average of IMP-OGO intensity versus ten days moving average of Deep River neutron monitor.

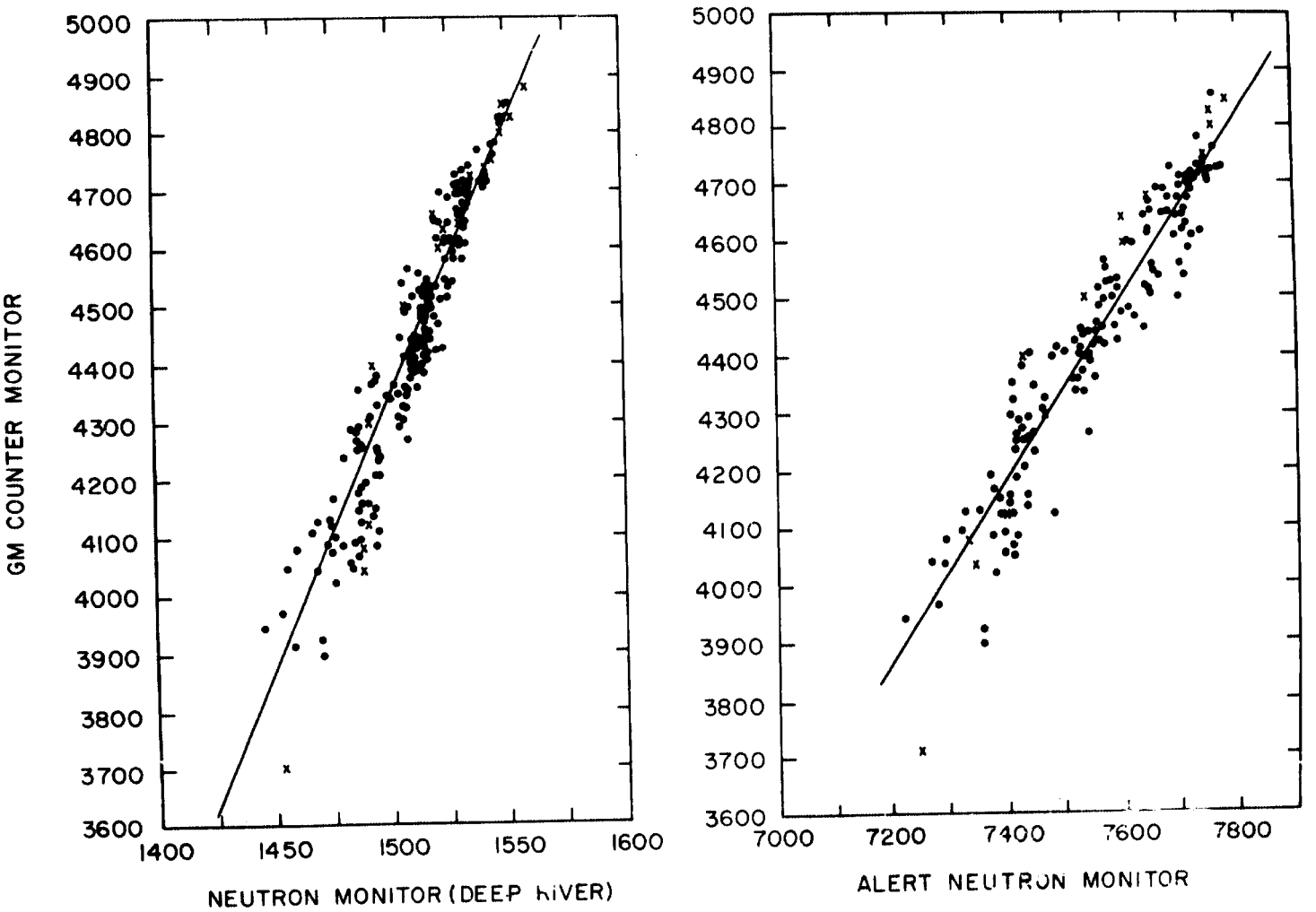

Figure 7. Crossplot of GM counter monitor on IMP-OGO satellites versus neutron monitors at Deep River and Alert, for short term and long term variations.

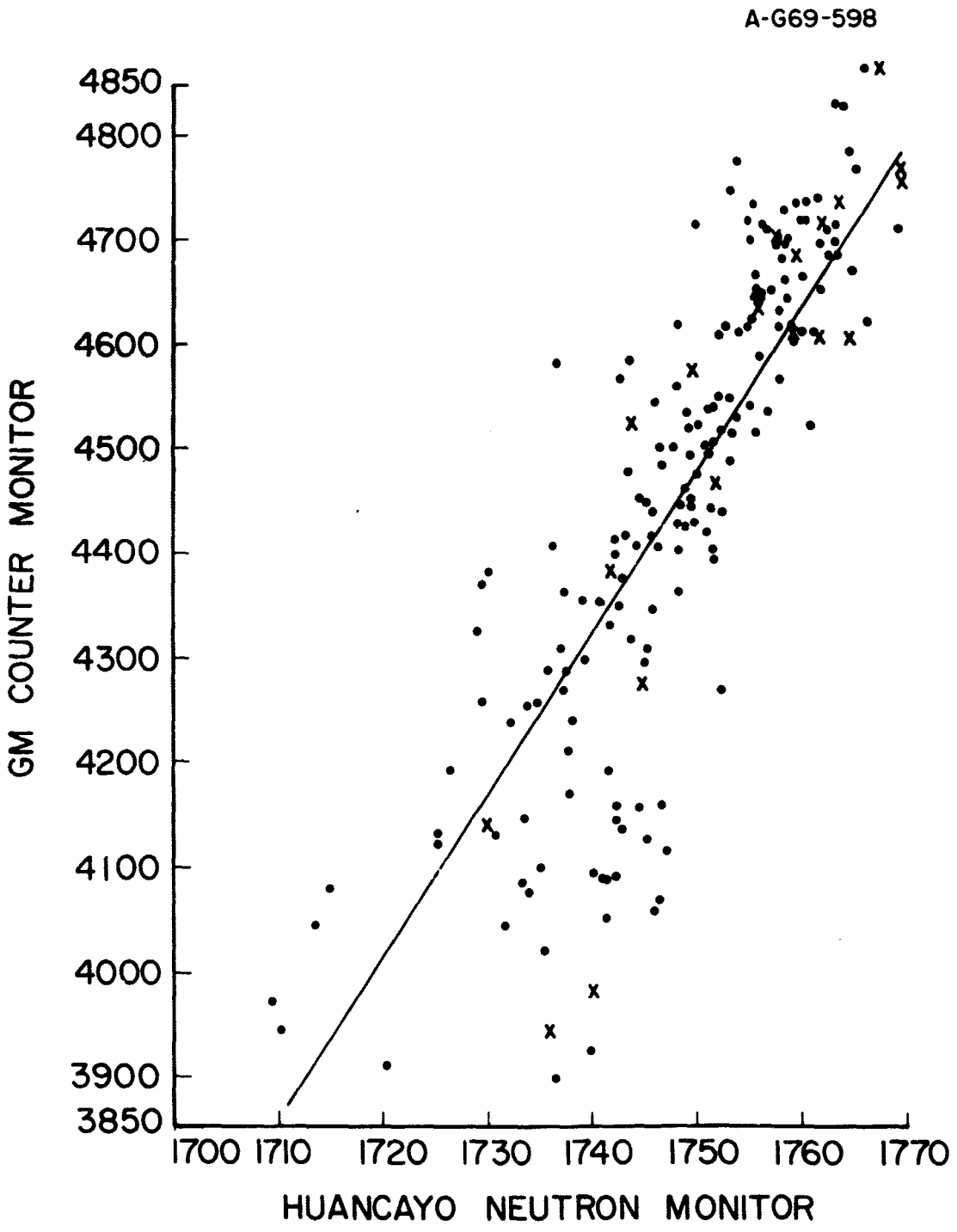

Figure 8. Crossplot of GM counter monitor on IMP-OGO satellites versus neutron monitor at Huancayo for short term and long term variations.

Figure 9. Monthly means of Zurich relative sunspot number (R); cosmic ray intensities as measured by neutron monitors at Sulphur Mountain and Huancayo; and the intensity measured by GM counter monitor on IMP-OGO satellites.

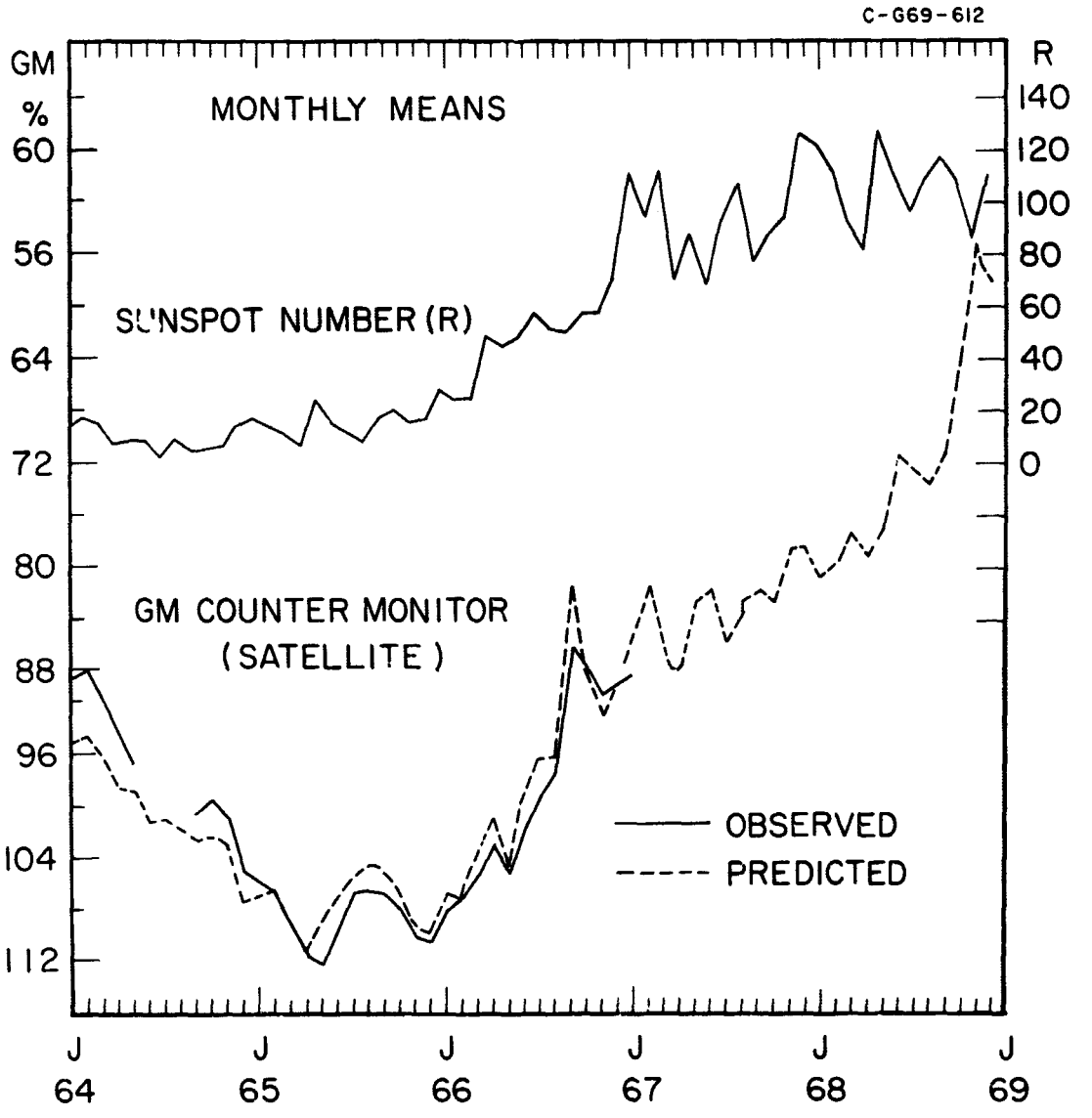

Figure 10. Monthly means of Zurich relative sunspot number (R) over the period January 1964 to December 1968; observed monthly means for the period January 1964–December 1966 of cosmic ray intensity as measured by GM detector on IMP-OGO satellites, and the predicted cosmic ray intensity for the period January 1964–December 1968 from the means of Sulphur Mountain cosmic ray intensities.

HIGH ENERGY PRIMARY COSMIC RAY PROGRAM OF GODDARD SPACE FLIGHT CENTER

J. F. Ormes and V. K. Balasubrahmanyan

Goddard Space Flight Center
Greenbelt, Maryland, USA

ABSTRACT

A status report on the high energy program of the Goddard Cosmic Ray Group is presented. This program attempts to determine the charge composition of the primary cosmic radiation in the energy range 10^{10} eV to 10^{14} eV with a series of experiments carried in balloons and satellites.

Particle charge is identified using a four element telescope containing two plastic scintillators, a lucite Cerenkov detector and a CsI(Na) mosiac, each of which is 50cm × 50cm. It has a collection factor of 2500cm^2 ster. Uniformity of response and the resolution comparable to that of much smaller detectors is obtained through use of a digitized wire spark chambers for recording particle trajectories. It also allows for identification of multiple particle background events.

Electron energy is measured through the development of the cascade shower in a tungsten scintillator sandwich 12 radiation lengths thick.

The energy measurement of protons and heavier nuclei are carried out with a total ionization spectrometer in which observations are made at every 1.5 radiation lengths of the number of traversing particles.

A successful balloon flight of 30 hours duration was achieved at 5 GV cut-off on April 28, 1969. The operating characteristics of the instrument will be discussed and future flight plans will be outlined.

A program has been initiated at Goddard Space Flight Center to study the charge composition and energy spectra of the cosmic rays in the energy range 10^{10} to 10^{14} eV. The cosmic rays in this energy range should be relatively free from perturbations by the sun. Their large radii of curvature in the galactic magnetic fields will allow one to study field regions up to the scale of the galactic arms. The charge composition data in this range is extremely interesting in terms of the production processes of cosmic rays. Also in this range important clues to the cosmic ray storage lifetime are to be found.

In order to study these astrophysical aspects of the cosmic radiation we report specifically here on an instrument designed to make the following measurements: 1) to determine the charge spectrum of the cosmic rays with accuracy of $\pm 1/2Z$ up to $Z = 30$; 2) to measure the energy spectra of the various nucleonic components above 10^{10} eV; 3) to measure the electron spectrum to beyond 10^{13} eV; and 4) to detect any anisotropies in the arrival direction of these cosmic rays.

The pioneering work of Grigorov et al. in this energy range suggests that the integral spectrum of all particles has a power law exponent of -1.74 ± 0.06. On the other hand the proton component is deduced to have a spectrum -2.6. This

implies that the heavy nuclei are becoming relatively more abundant at higher energies. On the other hand preliminary results from the "Brawley Stack" indicate that the proportion of heavy elements decreases with energy. The only other evidence for heavy nuclei at high energies comes from multiple core extensive air showers. In short, the data that exists at high energies is so sparse that it is very difficult to draw any conclusions. Direct measurements of the charge of the primary particles is essential to studies of this type.

At present the electron data extends to about 300 GeV. Various experimenters have flown detectors on balloons. Bleeker et al. have used a lead glass Cerenkov detector 7 radiation lengths thick for developing the showers. Rubtsov and Zatsepin have used a simple system consisting of three lead plates each 3 radiation lengths thick. Anand et al. have studied electromagnetic showers developing in emulsions exposed near the geomagnetic equator. These data are shown in Figure 1. While Daniel and Stephens agree fairly well with Bleeker et al., they are considerably above the results of Rubtsov and Zatsepin. From this data it is not possible to decide upon a change in slope which could be related to the electron lifetime (Ramaty and Lingenfelter).

We are of the opinion that considerably more sophisticated experiments will have to be done in order to accurately determine the cosmic ray spectra in this range. Great care will have to be taken to prevent protons from masquerading as electrons, to determine the energy reasonably accurately, to determine geometrical collection factors and to find the efficiency of detection as a function of energy. This program attempts to accomplish these aims.

The experiment which has been built and is being tested is shown schematically in Figure 2. On top is a four fold measurement of charge consisting of two plastic scintillators, a lucite Cerenkov radiator and a CsI mosaic, each 50cm × 50 cm in area. The geometry is defined by the two scintillators separated by 30cm. The collection area is 2700 ster-cm^2. This large area means that in a 10 hour balloon flight the equivalent of one year of satellite data from a typical IMF or OGO charge composition experiment can be obtained. This is essential when dealing with the extremely low fluxes present at large energy, especially for rare charges such as fluorine.

The particle trajectories through the instrument are determined using digitized wire grid spark chambers. The spark chamber provides four position measurements which determine the particle trajectory. The 50cm × 50cm area of the detector is spanned in each grid by two planes, x and y, each containing 200 wires. A high voltage pulse is applied to one of the planes upon the passage of the particle and magnetic cores are set by the spark. The coordinates of the cores specify the x and y coordinates of the particle. These wire grid spark chambers were first developed for work in gamma-ray astronomy (Ross et al., 1969).

By utilizing these direction measurements to compensate the pulse heights for differences in response due to the large opening angle of the telescope and to variations in light collection efficiencies as a function of position, resolution comparable to that of much smaller detectors can be achieved. The four fold measurement of charge should make it possible to resolve individual charges

up to Z $\approx$30. This is possible because the CsI and the Cerenkov do not suffer the same non-linearities as do the plastic scintillators in this range. The presence of the Cerenkov makes rejection of low energy background from interactions in the calorimeter much easier.

The calorimeter itself consists of two parts, an electron cascade section and a nucleonic cascade section. The former consists of a sandwich containing 12 sheets of tungsten each 3.2mm thick followed by a plastic scintillator. The pulse heights from the individual detectors are recorded yielding the details of the shower development. The nucleonic cascades are developed in a series of modules each containing 1/2 of an absorption mean free path of iron. Since, the energy of these particles goes eventually into $\pi^\circ \rightarrow 2\gamma$ decay, it is important to have sufficient samples of the ionization loss to completely record the resultant electromagnetic showers. A scintillator is placed every 1.5 radiation lengths. The pulse height from 3 samples is added and recorded, yielding a separate measurement every 1/2 mean free path.

Electrons are separated from protons primarily by their behavior in the tungsten section. Only 4% of the protons will interact per radiation length of tungsten. Those protons which do look like electromagnetic showers by producing a π° in the first radiation length will tend to interact again in the iron modules, whereas electron showers will have no secondary maxima. In addition the proton contamination is directly measured by looking for showers which start in the middle of the tungsten stack.

A version of the instrument containing 11 radiation lengths of tungsten but no iron modules was flown on a balloon on April 28, 1969 at 5 GV cutoff from southern New Mexico. This flight floated at 7 gm/cm^2 for about 30 hours. All the electronic systems worked as planned. The experiment was allowed to trigger on nuclei with $Z \geq 3$ and on electrons with energy greater than $\approx$5 GeV.

The data analysis from an instrument containing a spark chamber and sixteen pulse height analyzers each with three gain modes and a dynamic range of 10^4 does not proceed quickly. Indeed to analyze 10^5 events with 400 bits/event would be impossible without digital computers. However, the preliminary data is quite encouraging. Particle trajectories have so far been analyzed for more than 50% of the events yielding some 125,000 counts from a 12 hour period. The individual M group nuclei are clearly resolved in a two dimensional histogram utilizing the two scintillators.

The spark chamber operated at >98% efficiency for singly charged particles. The positional and directional accuracy was far greater than required for our purposes, the sparks being located to within ±7.5mm. This has given the angle to within ±1.5°. This high efficiency for singly charged particles has made the spark chamber sensitive to knockon electrons produced by high Z nuclei and to Compton electrons from 10 MeV γ-rays coming from the calorimeter. As a result VH nuclei tracks have been confused by the presence of background. In the future it is hoped to reduce the efficiency for singly charged particles when a heavy nucleus is present by delaying the application of the high voltage until some recombination has taken place.

Utilizing this spark chamber data it has been possible to find the variation in pulse height as a function of angle. This is shown in Figure 3 for a scintillator and the Cerenkov detector. The dip in the Cerenkov response at 10° is caused by the large light losses at this angle. All the Cerenkov emission is collected by total internal reflection. The Cerenkov cone lies between 45° and 48° to the particle direction for 5 GV cutoff and the angle for total internal reflection is 42° so all the light for vertically incident particles is collected. Between 3° and 6° zenith angle particles begin to loose some light. The losses increase rapidly with increasing zenith angle up to about 10° at which the losses reach a maximum. At very large angles the response is further enhanced by the increased path length through the radiator.

In the case of the scintillator response, it increases approximately like the secant of θ, but there seems to be an additional component at large zenith angles. The excess is about 3.5% at 45° and increases smoothly to about 15% at 60°. This may be due to an anisotropic component in the light produced (e.g. Cerenkov), to the decreasing probability that a knockon electron can leave the measuring device, or to a variation in collection efficiency with particle angle. In any case it is measured and can be compensated out.

The response of the detector has been calibrated in the electron beam at the Stanford linear accelerator center using a secondary positron beam containing a mean of one particle per beam pulse. Electrons ranging from 5.4 to 17.9 GeV were used. While this data is in a very preliminary analysis stage, several

things are already clear. The electron energy can be determined to within 6 to 8% using the integral of the pulse heights from the various shower detectors. The difference between one and two particles incident can be determined from the pulse height data in the charge module. In the beam of known energy one and two particle showers are easily resolved by using any counter near shower maximum. Fluctuations in the early development of the shower make measurements in the first three radiation lengths difficult to interpret.

From flight electron data it is also clear that differential information is quite important in separating electron showers from interactions. The differential information has also allowed a rather complex set of requirements to be set for triggering, thus insuring that the detector triggers only on electrons of 5 GeV or more. This could result in a serious source of background in simpler counters. In addition the spark chamber data is of extreme importance in defining the geometrical properties of each shower, and hence in checking for edge effects, etc.

Very little flight data has been examined yet, but electrons up to at least 70 GeV are clearly present.

In the future we plan to continue the balloon flight program and we hope to culminate the program with a satellite flight. In September a version will be flown containing 17 radiation lengths, 5 in the form of an iron nuclear cascade module. Next spring, a flight will be made with 5.5 absorption mean free paths, two of which will be in the form of iron filings which will be used as ballast for

controlling the balloon flight. This payload of about 7000 lbs. will be carried to about 35km by a 0.7×10^6 m^3 balloon. A satellite flight lasting one year would define any steepening of the electron spectrum up to 10^{13} eV and of the proton spectrum to 2×10^{14} eV.

REFERENCES

1. N. L. Grigorov, V. E. Nesterov, I. D. Rapoport, I. A. Savenko and G. A. Skaridin, Invited paper presented at Tenth International Conference on Cosmic Rays, Calgary, Canada, June 1967.

2. J. A. M. Bleeker, J. J. Burger, A. J. M. Deerenberg, A. Scheepmaker, B. N. Swanenburg, Y. Tanaka, Canadian Journal of Physics 46, S523, 1968.

3. K. C. Anand, R. R. Daniel and S. A. Stephens, Phys. Rev. Letters, 20, 764, 1968.

4. R. Ramaty and R. E. Lingenfelter, Phys. Rev. Letters 17, 1230, 1966.

5. R. W. Ross, C. H. Ehrmann, C. E. Fichtel, D. A. Kniffen, and H. B. Ogelman, IEEE Transactions on Nuclear Science, NS-16, 304, 1969.

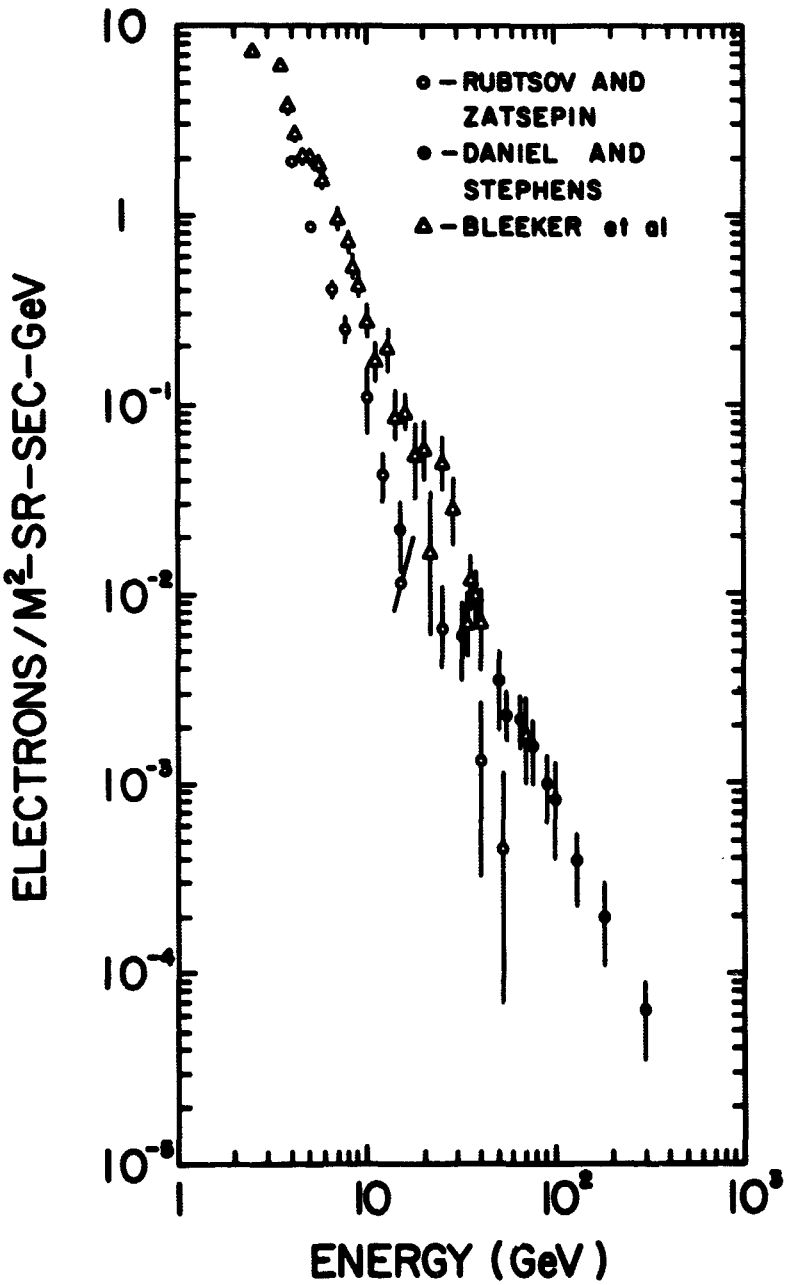

Figure 1. Differential electron energy spectrum data at high energies.

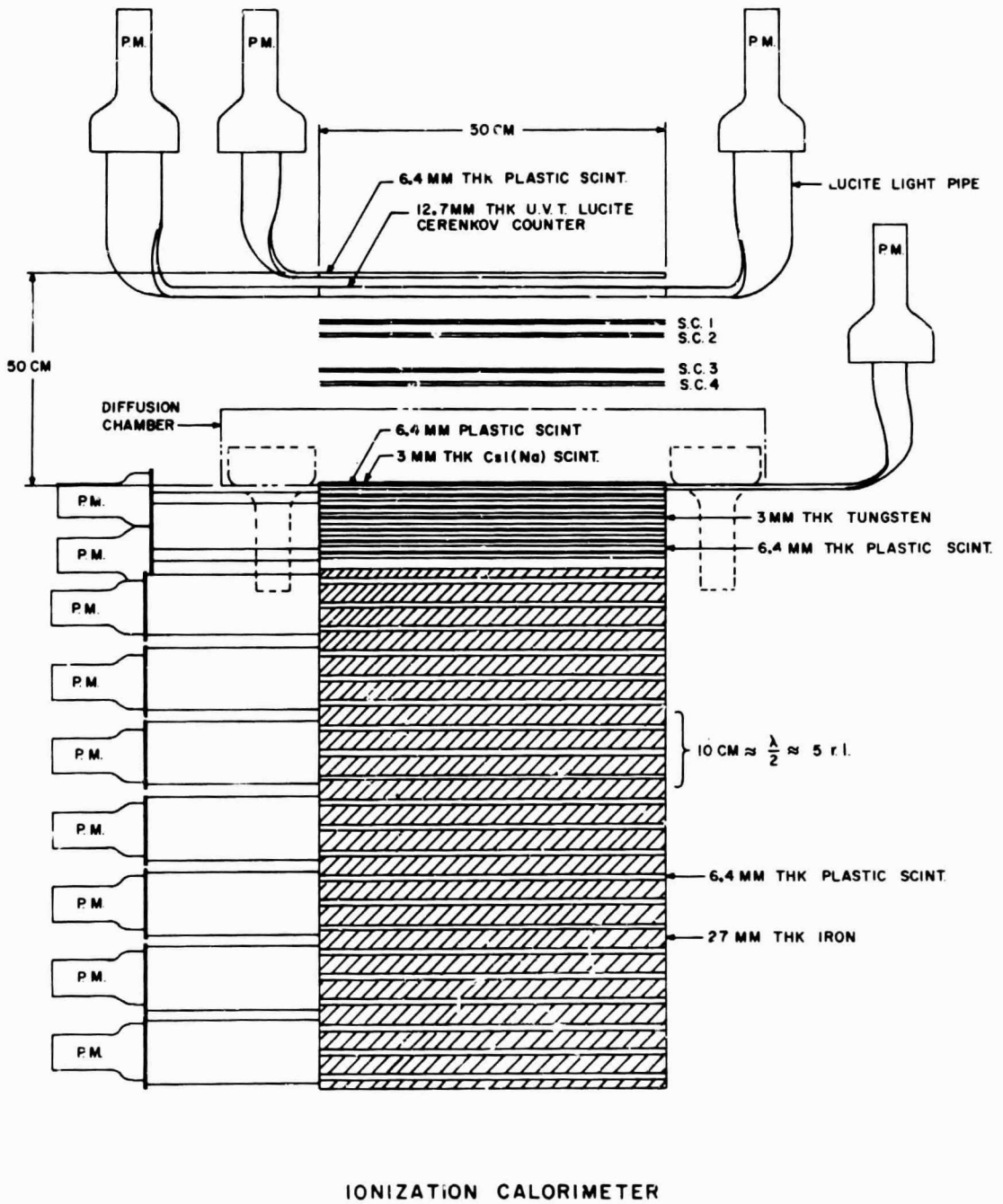

IONIZATION CALORIMETER

Figure 2. Schematic diagram of one version of the high energy cosmic ray experiment. The detectors are in order from top to bottom: plastic scintillator (S_1), Cerenkov, 4 wire grid spark chambers, CsI mosaic, plastic scintillator (S_2), 6 layers of tungsten and scintillator (5.5 radiation lengths), and 7 iron modules, each 1/2 of an absorption mean free path thick.

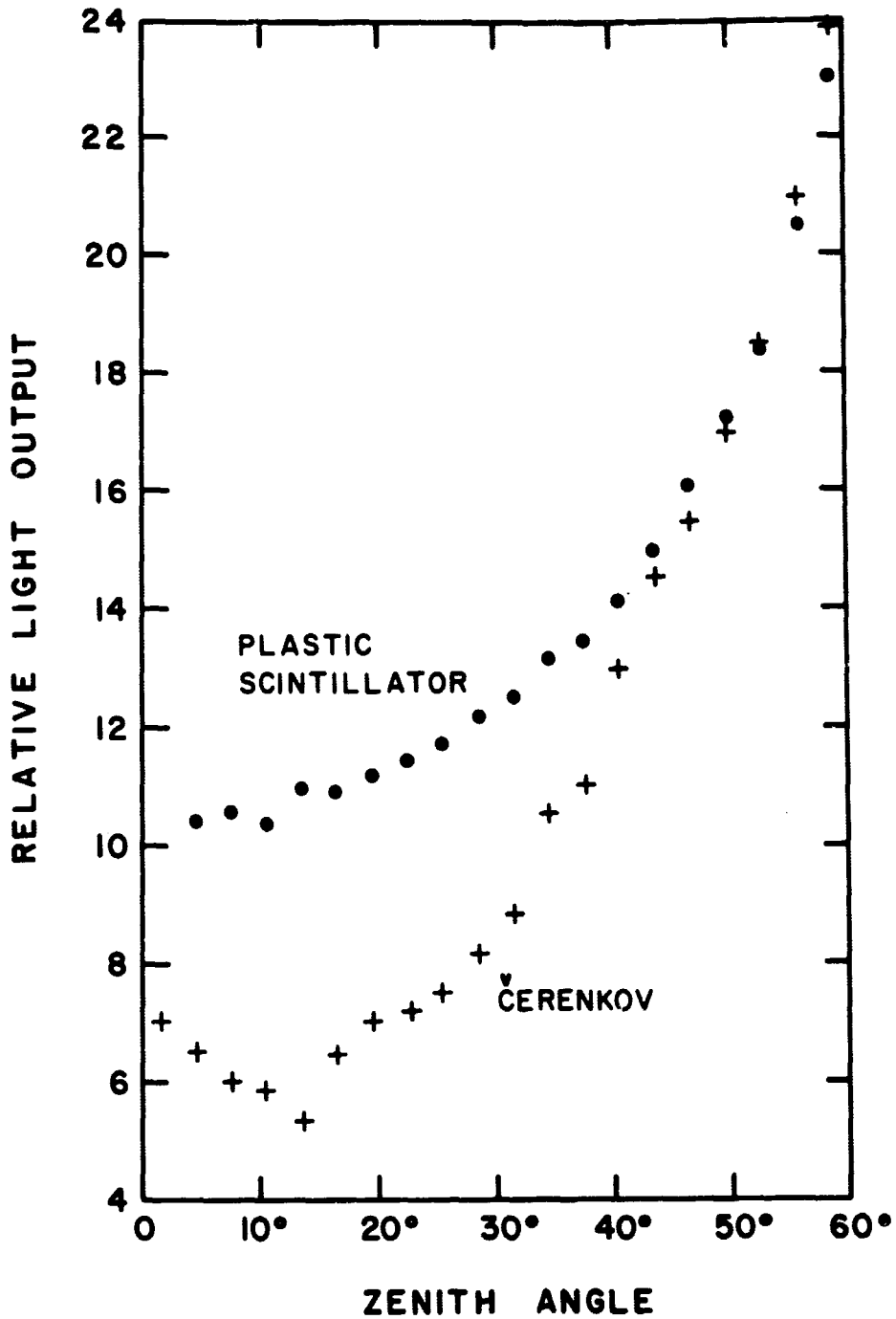

Figure 3. Most probable response of a plastic scintillator and the Cerenkov detector as a function of the zenith angle of the particles.